

## A critical review on the production and application of graphene and graphene-based materials in anti-corrosion coatings

Bohdan Kulyk, Maria A. Freitas, Nuno F. Santos, Farzin Mohseni, Alexandre F. Carvalho, Kiryl Yasakau, António J. S. Fernandes, Adriana Bernardes, Bruno Figueiredo, Rui Silva, João Tedim & Florinda M. Costa

To cite this article: Bohdan Kulyk, Maria A. Freitas, Nuno F. Santos, Farzin Mohseni, Alexandre F. Carvalho, Kiryl Yasakau, António J. S. Fernandes, Adriana Bernardes, Bruno Figueiredo, Rui Silva, João Tedim & Florinda M. Costa (2021): A critical review on the production and application of graphene and graphene-based materials in anti-corrosion coatings, Critical Reviews in Solid State and Materials Sciences, DOI: [10.1080/10408436.2021.1886046](https://doi.org/10.1080/10408436.2021.1886046)

To link to this article: <https://doi.org/10.1080/10408436.2021.1886046>



© 2021 The Author(s). Published with license by Taylor & Francis Group, LLC



Published online: 11 Mar 2021.



Submit your article to this journal



Article views: 2034



View related articles



View Crossmark data

## A critical review on the production and application of graphene and graphene-based materials in anti-corrosion coatings

Bohdan Kulyk<sup>a</sup> , Maria A. Freitas<sup>b</sup>, Nuno F. Santos<sup>a</sup>, Farzin Mohseni<sup>b</sup>, Alexandre F. Carvalho<sup>a</sup>, Kiryl Yasakau<sup>b</sup>, António J. S. Fernandes<sup>a</sup>, Adriana Bernardes<sup>c</sup>, Bruno Figueiredo<sup>c</sup>, Rui Silva<sup>c</sup>, João Tedim<sup>b</sup>, and Florinda M. Costa<sup>a</sup>

<sup>a</sup>Department of Physics, i3N, University of Aveiro, Aveiro, Portugal; <sup>b</sup>CICECO, Department of Materials and Ceramic Engineering, University of Aveiro, Aveiro, Portugal; <sup>c</sup>Graphenest, Aveiro, Portugal

### ABSTRACT

Among the many potential applications of graphene and graphene-based materials, their use as protective films or as additives in coatings for corrosion protection has seen an increased level of interest in the last decade. Much of this interest is motivated by the need to implement additional functionalities, to enhance anti-corrosion performance and to ultimately extend the service life of metallic structures. Pristine graphene films, with their impermeable nature allied to flexibility and mechanical strength, appear as particularly attractive candidates for barrier films against corrosive agents, while graphene-based materials such as graphene oxide and reduced graphene oxide offer a wide range of opportunities for their dispersion in polymeric matrices for composite anti-corrosive coatings. Simultaneously, considerable progress in the development of scalable graphene and graphene-based materials production techniques has been made during the last several years. Currently, a broad range of graphene materials with different morphologies and properties is available, making the need for an adequate fit between the production method and the desired application even more evident. This review article aims to give the reader a general overview of the recent trends in both the production of graphene and graphene-based materials, and their implementation in different anti-corrosion solutions. Moreover, the present work provides a critical look on this subject, highlighting the areas in need of further exploration.

**Abbreviations:** 2D: two-dimensional; CVD: chemical vapor deposition; DMF: dimethylformamide; DMSO: dimethylsulfoxide; EIS: electrochemical impedance spectroscopy; EPD: electro-phoretic deposition; FLG: few-layer graphene; G-NP: graphene-nanoparticle composite; GO: graphene oxide; HA<sub>p</sub>: hydroxyapatite; HOPG: highly-oriented pyrolytic graphite; LIG: laser induced graphene; NP: nanoparticle; NMP: N-methylpyrrolidone; PANI: polyaniline; PMMA: poly(methyl methacrylate); rGO: reduced graphene oxide; SEM: scanning electron microscopy; SLG: single-layer graphene; XPS: X-ray photoelectron spectroscopy; ZRC: zinc rich coating

### KEYWORDS

Graphene; graphene oxide; graphene production; composites; coatings; anti-corrosion

### Table of contents

1. Introduction .....	2
2. Production methods of graphene and graphene-based materials .....	3
2.1. Conventional high crystalline quality graphene production methods .....	3
2.2. High-throughput graphene production methods .....	5
2.2.1. Ball milling exfoliation .....	5
2.2.2. Sonication .....	7
2.2.3. Shear stress exfoliation .....	9
2.2.4. Electrochemical exfoliation .....	14
2.3. Graphene oxide and reduced graphene oxide production methods .....	20
2.4. Other production methods .....	21
3. Anti-corrosion coatings using graphene and graphene-based films .....	23

3.1. Preparation methods and corrosion resistance performance .....	23
<b>4. Anti-corrosion composites using graphene and graphene-based materials .....</b>	<b>25</b>
4.1. Dispersion in polymeric matrices.....	25
4.2. Functional incorporation in anti-corrosion composites .....	27
4.3. Composites for active corrosion protection .....	29
<b>5. Critical analysis .....</b>	<b>32</b>
5.1. Production method vs. application .....	32
5.2. Challenges and guidelines for characterization of anti-corrosion coatings using graphene .....	33
<b>Acknowledgments.....</b>	<b>34</b>
<b>Disclosure statement .....</b>	<b>34</b>
<b>References .....</b>	<b>34</b>

## 1. Introduction

With the discovery of graphene in 2004 by Geim and Novoselov<sup>[1]</sup> a whole new field in materials science, chemistry and physics has opened. Seventeen years later we are approaching a time when the industry can provide this material in quality and quantity required for its application. Graphene is known for its outstanding electron mobility,<sup>[2,3]</sup> highest thermal conductivity of all materials, on par with diamond and carbon nanotubes (CNTs) and 12 times that of copper,<sup>[4-6]</sup> a mechanical breaking strength of 42 N/m (311 times higher than that of steel), and a Young's modulus of  $1.0 \pm 0.1$  TPa.<sup>[7]</sup>

The application of graphene as a functional layer or as an additive in coatings for corrosion protection has been attracting considerable interest in the last decade. The main driving force behind this interest relies on the need to implement additional functionalities, to enhance coating performance and thus extend the service life of metallic structures under extreme conditions.<sup>[8,9]</sup> Graphene's impermeability to gases<sup>[10]</sup> provided the first indication of it being capable of acting as a physical barrier to corrosive species. Moreover, its chemical inertness with respect to oxidative etching up to temperatures of 400 °C,<sup>[11]</sup> along with the promise of an extremely lightweight coating that does not significantly affect the underlying material's optical properties, have further motivated the research efforts into graphene's application in corrosion protection.

Several recent reviews have described the breadth of research works in this area, thereby supporting the fact that graphene and graphene-based materials can and will play a central role in the protection of metallic substrates.<sup>[12-14]</sup> However, it must be said that the remarkable figures ascribed to graphene are commonly (and incorrectly) presented in the works related to *any* graphene-based material, when in reality they are only applicable to the pristine single-layer graphene (SLG). As a result, the main aim of the present review is to render a critical look on the implementation of graphene and graphene-based materials in the

field of protective coatings, combining a description of the different production methods of such materials with an overview of the recent trends in their implementation in corrosion protection, something which, to the best of our knowledge, has not yet been done.

As it will be made clear throughout this review, the range of properties of the graphene derivatives obtained by different processes is so wide that their grouping under the single word *graphene* would be scientifically inaccurate. Therefore, we will opt to follow the nomenclature for the classification of these materials according to the ISO/TS 80004-13:2017, namely:

1. Graphene, graphene layer, single-layer graphene (**SLG**), monolayer graphene: single layer of carbon atoms with each atom bound to three neighbors in a honeycomb structure.
2. Bilayer graphene (**2LG**): two-dimensional material consisting of two well-defined stacked graphene layers.
3. Few-layer graphene (**FLG**): two-dimensional material consisting of three to ten well-defined stacked graphene layers.
4. Graphene oxide (**GO**): chemically modified graphene prepared by oxidation and exfoliation of graphite, causing extensive oxidative modification of the basal plane. Graphene oxide is a single-layer material with high oxygen content, typically characterized by C/O atomic ratios of approximately 2.0, depending on the method of synthesis.
5. Reduced graphene oxide (**rGO**): reduced oxygen content form of graphene oxide.

Additionally, based on these definitions, single-layer, bilayer or few-layer graphene films or flakes will be generally grouped under the term "graphene," while any other two-dimensional carbon materials, such as GO or rGO, will be referred to as "graphene-based materials."

This review, outlined in Figure 1, is divided into four main sections. Firstly (section 2), different production methods are presented, giving particular

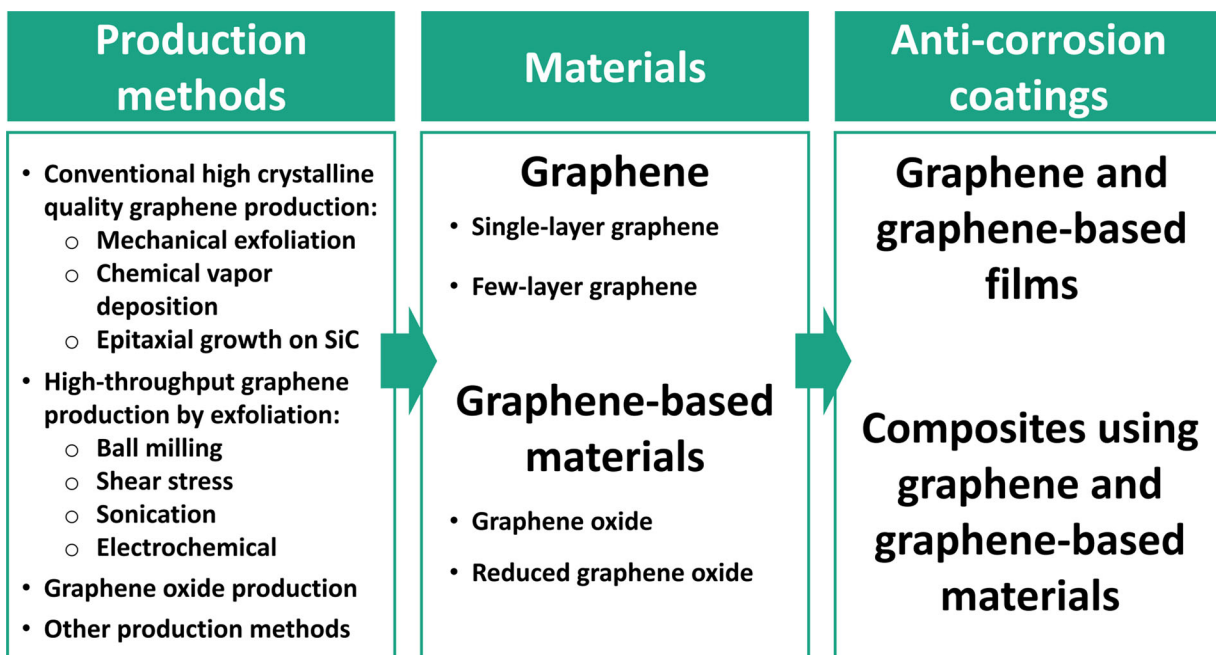


Figure 1. Outline of the review.

attention to methods to obtain high-quality graphene, high-throughput processes to produce graphene and methods to obtain graphene oxide and reduced graphene oxide. The following two sections are devoted to anti-corrosion applications, with works associated with graphene and graphene-based films (section 3) and composites using graphene (section 4) being discussed separately. The review ends with a critical overview of the field (section 5), describing not only the advantages but also challenges associated with implementation of graphene and graphene-based materials for corrosion protection.

## 2. Production methods of graphene and graphene-based materials

### 2.1. Conventional high crystalline quality graphene production methods

The first successful method to isolate graphene was through mechanical exfoliation of graphite by successive peelings using scotch tape.<sup>[1]</sup> This method produces high-quality, single crystal, one atom thick graphene flakes. However, its throughput is very low, and its upscaling is unreasonable.

One of the earliest alternative synthesis methods that emerged was that of epitaxial graphene obtained by graphitization of silicon carbide (SiC).<sup>[15]</sup> By heating up single-crystal SiC in ultrahigh vacuum conditions (or even at atmospheric pressure),<sup>[16]</sup> the Si atoms are sublimated, with the remaining C atoms

undergoing graphitization. This process can occur on both the Si-terminated face and on the C-terminated one. In the former case, a C-rich buffer layer covalently bonded to the substrate is present underneath the formed graphene, while in the latter case the interaction with the substrate is much weaker.<sup>[17]</sup> With the emergence of this synthesis approach, it was quickly established that the obtained graphene is of high quality, with charge carrier mobilities up to  $27,000 \text{ cm}^2 \text{ V}^{-1} \text{ s}^{-1}$  reported as early as 2006, for graphene obtained on the C-terminated face.<sup>[18]</sup> However, the main disadvantage of graphene synthesis from SiC remains the high price of the substrates,<sup>[19]</sup> as well as the associated limitations in terms of sizes and difficulties in micromachining of the obtained material.<sup>[20]</sup>

Alternatively, chemical vapor deposition (CVD) has been one of the most prominent graphene synthesis techniques since the early reports showing surface segregation of carbon atoms into graphene domains and continuous layers from transition metals.<sup>[21–23]</sup> Yu et al., for example, were able to form high-quality graphene layers by exposing a Ni foil to a mixture of CH<sub>4</sub>, H<sub>2</sub>, and Ar at 1000 °C (at atmospheric pressure). The process was explained on the basis of hydrocarbon gas decomposition, followed by carbon atom diffusion into the metal foil. A controlled cooling of the substrate then leads to carbon segregation, forming graphene layers at the surface. Moreover, the authors showed that this graphene can be transferred onto insulating substrates using a support layer (silicone

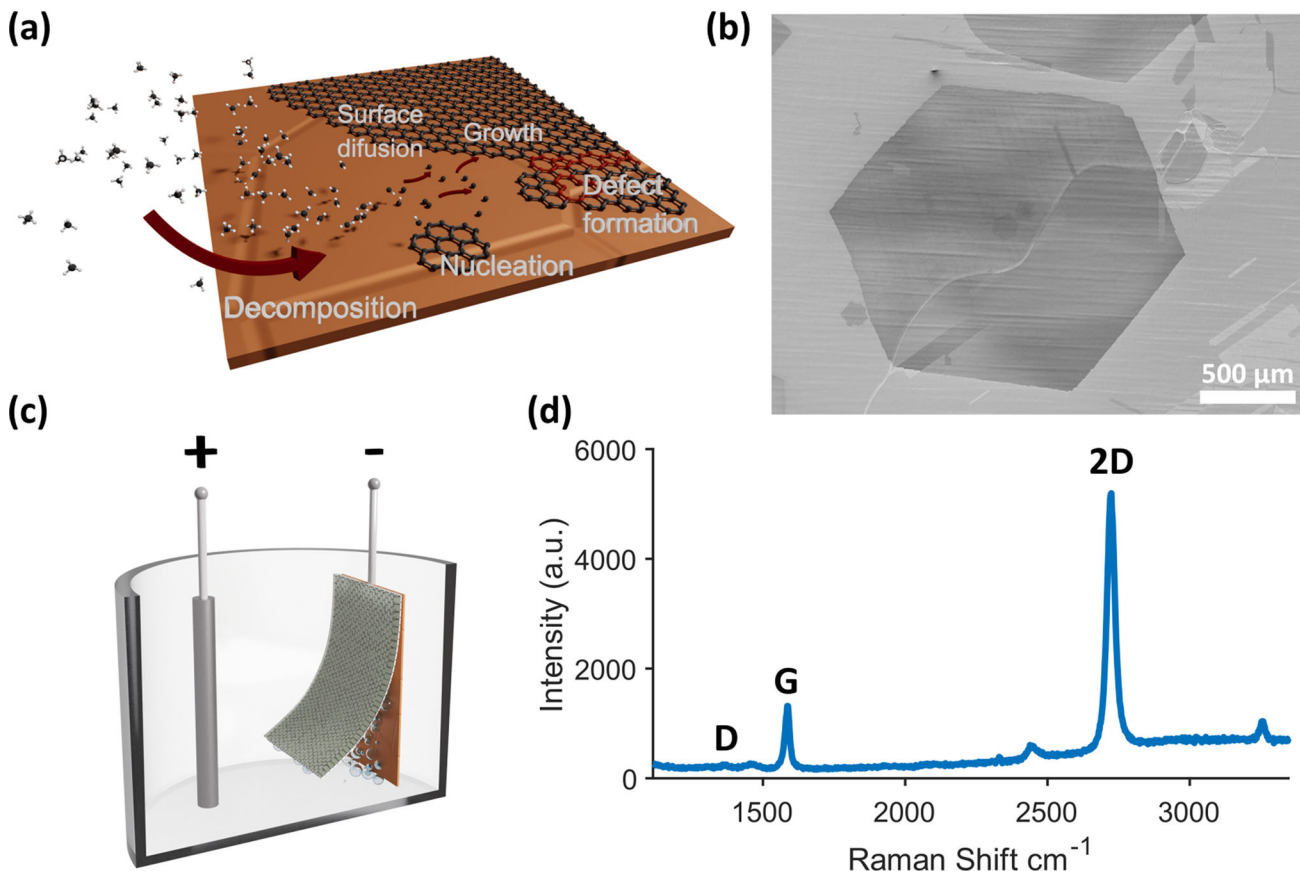


**Figure 2.** (a) Schematic representation of the CVD process of graphene growth on copper. (b) Scanning electron microscopy (SEM) image of single-layer CVD graphene domain on copper. (c) Schematic representation of the electrochemical bubbling transfer process. (d) Representative Raman spectrum of single-layer graphene on a Si/SiO<sub>2</sub> substrate.

rubber) applied to the grown film, followed by the etching of the metal and the application of the graphene/support stack onto the desired substrate.

Shortly after, copper came forth as the preferred growth substrate, thanks to its low carbon solubility and catalytic effect on the hydrocarbon precursor breakdown, allowing to grow continuous SLG films (Figure 2(a)).<sup>[24]</sup> Typical CVD graphene synthesis on copper is conducted at temperatures close to the latter's melting point. However, low-temperature (300–400 °C) growth has also been demonstrated, using microwave plasma to assist in the decomposition of the hydrocarbon precursors.<sup>[25]</sup> Currently, the CVD method allows to obtain graphene domains exceeding millimetric sizes<sup>[26]</sup> (Figure 2(b)) and arbitrarily large single-crystal films,<sup>[27]</sup> as well as graphene with charge carrier mobilities as high as 350,000 cm<sup>2</sup> V<sup>-1</sup> s<sup>-1</sup>,<sup>[3]</sup> with growth at both low and atmospheric pressures possible.<sup>[28]</sup>

Here, it should be pointed out that, in many cases, graphene grown epitaxially or using a catalyst must be transferred onto a different substrate where it can be processed or incorporated directly for the desired

application. An example of this is the transfer of graphene onto insulating substrates for lithographic fabrication of electronic devices, or onto transparent substrates for optical applications. In the case of CVD-grown graphene on copper, the copper can either be etched away,<sup>[29,30]</sup> or the graphene can be separated from the copper. The latter can be done electrochemically, by forming hydrogen gas bubbles, through hydrolysis, between graphene and copper, exfoliating the former from the latter (Figure 2(c)).<sup>[31]</sup> Alternatively, water molecules can be intercalated between the graphene and the substrate, weakening their interaction and allowing to pick up the sample using a stamp.<sup>[32]</sup> Either way, in most cases, a supporting material must be used in order to avoid the tearing or any other damage to the graphene film after its separation from the copper. The most commonly used supporting material is poly(methyl methacrylate) (PMMA), which is usually spin-coated on the as-grown graphene at the beginning of the transfer process. However, the removal of the PMMA support layer after the transfer is complete, which is typically done by placing the transferred sample in acetone,

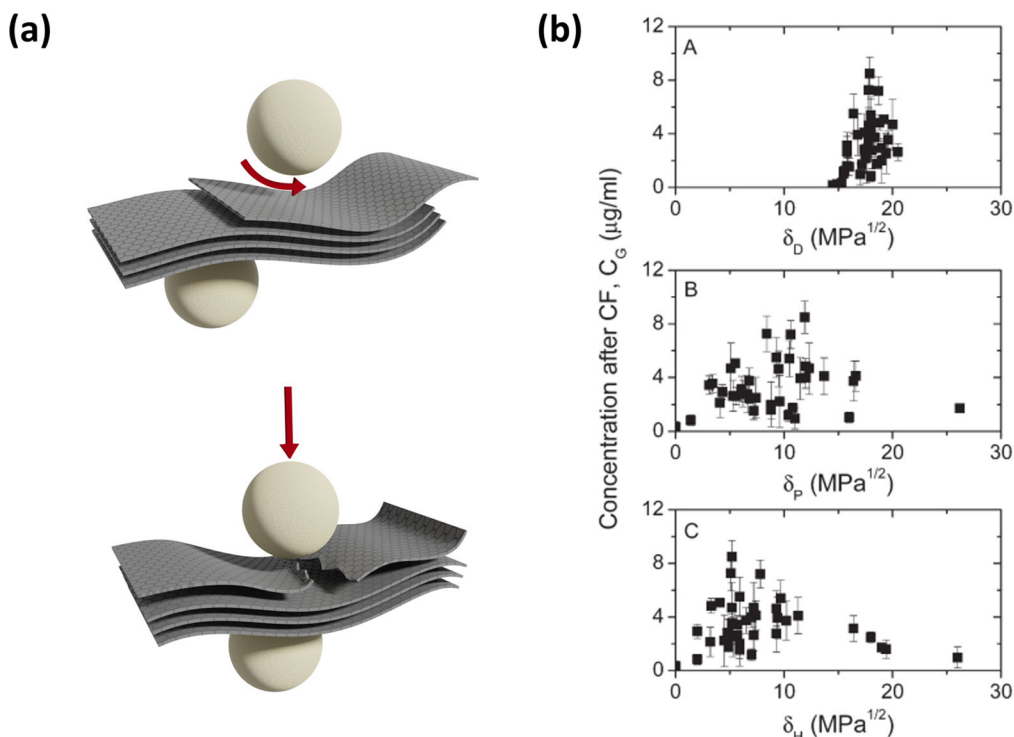


**Figure 3.** (a) Schematic illustration of the ball milling process. (b) Graphene dispersibility ( $\delta$ ) for a wide range of solvents as a function of (A) dispersive, (B) polar and (C) hydrogen-bonding Hansen solubility parameters. Reprinted with permission from ref. [51]. Copyright 2010 American Chemical Society.

leaves behind PMMA residues which are known to be difficult to eliminate completely.<sup>[33,34]</sup> These residues influence graphene's properties, mainly by giving rise to a p-type doping. Some solutions to this problem have been reported in the literature, namely by means of high-temperature annealings<sup>[35]</sup> or plasma treatments.<sup>[36]</sup> Other approaches seek to avoid PMMA altogether by exploring other supporting materials that can be removed without leaving any residues.<sup>[36–39]</sup>

Independently of the production method, high crystalline quality single-layer graphene can be characterized by narrow 2D and G characteristic Raman peaks, with a high ratio of the respective intensities, as well as by the absence (or very low intensity) of the characteristic D peak associated with structural defects (Figure 2(d)).<sup>[40]</sup>

## 2.2. High-throughput graphene production methods

For many commercial applications, a high production throughput and economic viability are still the main requirements in terms of the preferred synthesis approach. After the original mechanical exfoliation of graphite using scotch tape, other methods of

exfoliation were developed trying to follow a similar approach. The main ones are briefly reviewed below.

### 2.2.1. Ball milling exfoliation

Exfoliation of graphite by ball milling can be accomplished making use of either planetary ball mills<sup>[41–48]</sup> (in dry or wet conditions) or stirred ball mills.<sup>[49,50]</sup> In a ball milling process, the precursor material is loaded, together with the milling balls, inside the milling chamber, followed by a continuous rolling of the balls along the chamber's walls. This rolling action transfers energy to the precursor both through shear stresses due to the friction effect of the balls rolling along the chamber's walls and through direct impact of the balls on the material to be milled (Figure 3(a)). Different types of equipment can exploit this general principle, such as planetary mills, vibratory mills, and attritor mills, among others.<sup>[52]</sup> The motion of the grinding balls is typically caused by inertial forces due to the movement of the milling chamber, or, in the case of the attritor mill, due to the rotation of the impeller arms inside the chamber. The main parameters that can be controlled are thus milling speed, time, grinding medium, ball-to-precursor ratio, temperature, and milling atmosphere.<sup>[52]</sup>

For the ball milling production of graphene, the most commonly used precursor is graphite, although

helical ribbon carbon nanofibers, for instance, have also been exfoliated by this technique.<sup>[41]</sup> With graphite, the milling itself may not be sufficient for successful graphene exfoliation, as it has been shown to result in an amorphization of graphite's crystalline structure, due to the damage caused by the milling balls, which distorts the aromatic rings of the graphite.<sup>[53,54]</sup> This damage has been observed by both X-ray diffraction and Raman spectroscopy after 15 to 20 h of milling.<sup>[53]</sup>

In one of the earliest examples of graphene production by ball milling, Zhao et al.<sup>[55]</sup> milled 30 to 80 nm thick graphite nanoplatelets for 30 h in dimethylformamide (DMF), using a planetary mill. The shear forces induced by the milling process, along with the DMF-graphene interaction, allowed to exfoliate the graphite nanoplatelets into graphene sheets with up to three layers, as reported by the authors, while the low rotation speed of the rotating tray allowed to have less in-plane stress capable of damaging the graphite flakes. Other organic solvents have also been successfully employed for graphite exfoliation into graphene by ball milling, with the importance of a match between the surface tension of the solvent and that of graphene having been highlighted.<sup>[56]</sup> Sodium dodecyl sulfate has also been used as a surfactant for ball milled graphene flakes, as demonstrated by Knieke et al.<sup>[50]</sup> using a stirred media mill. As an alternative, naphthol polyoxyethylene ether (NPE), a more environmentally-friendly and more easily removable surfactant, has also been used, resulting in graphene flakes with fewer than 10 layers.<sup>[57]</sup>

A systematic study of the influence of the process conditions and parameters in wet ball milling of graphite has been performed by Damm et al.<sup>[49]</sup> The authors, besides stating that stirred media mills allow to exfoliate graphite in a relatively shorter time (few hours instead of few tens of hours) and with better temperature control than planetary mills, point out that the Hansen solubility parameters of the used solvents are some of the main factors determining their suitability for graphite exfoliation into graphene, as previously shown by Coleman's group.<sup>[51]</sup> More specifically, the parameter for the disperse interaction,  $\delta_D$ , should have a value of around 18 MPa<sup>1[N/A]2</sup> (Figure 3(b)), as is the case for N-methylpyrrolidone (NMP) and cyclohexanone (CHO). The viscosity of the solvent also plays an important role, with the more viscous ones facilitating the energy transfer from the grinding balls to the graphite while attenuating the direct impact of the balls, in order to prevent in-plane damage. In summary, wet ball milling can be

attractive for graphene production. However, it should be pointed out that, unfortunately, wet ball milling often requires additional purification steps to remove the solvents.<sup>[58]</sup>

As a way to avoid the need to remove surfactants and solvents from the obtained graphene dispersions, as well as to avoid the functionalization of the graphene sheets, which can be detrimental to its properties, Liu et al.<sup>[48]</sup> proposed a dry ball milling graphene production method. In a process taking up to 4 h, graphite was milled in the presence of ammonia borane ( $\text{NH}_3\text{BH}_3$ ). The authors claimed that ammonia borane weakens the Van de Waals forces between the graphene layers in graphite, by interacting strongly with the latter. This results in graphene flakes of 5 layers or fewer. However, a significant degree of oxidation was present, as shown via X-ray photoelectron spectroscopy (XPS), and the presented Raman and TEM analysis is insufficient to support such claims. Triazine exfoliating agents have also shown great promise in the context of graphite exfoliation by ball milling.<sup>[59]</sup> Here, melamine was identified as having the best performance, due to its aromatic nucleus capable of interfacing with graphene sheets by  $\pi$ - $\pi$  interactions, as well as due to its ability to form extended two-dimensional (2D) networks through hydrogen bonding, which lead to multipoint interactions with graphene sheets, promoting exfoliation and stabilization. Dry ball milling of graphite in the presence of certain gases and dry ice<sup>[42]</sup> has been shown to permit the production of edge-functionalized graphene flakes that can be dispersed in several solvents, including pure water. In other work, a planetary mill was used for 24 h to produce edge-carboxylated graphene from graphite precursor using dry ice.<sup>[47]</sup> The production of FLG was accomplished, but the structural quality of the products is questionable, and a significant degree of oxidation was observed. After thermal reduction, the Raman spectra show severe defect concentration, broadened vibrational modes and a near absence of 2D band, so that the product can hardly be denominated as graphene. In summary, the main advantage of the dry-milling technique resides in its simplicity and in the possibility of obtaining graphene without contaminations. However, prolonged process times (sometimes as long as 30 h), limit its throughput.

Despite the demonstrated capability of producing graphene flakes, ball milling presents some obvious disadvantages. It is a scalable process only limited by the size of the milling vessel, but it is apparent that the high degree of structural defects, including oxidation, as well as the inherent functionalization, in

many cases, restricts the spectrum of application of these graphene products. The bare impact of the balls fragments the graphene flakes into smaller flakes and induces severe structural defects to the graphene lattice, especially in basal planes.<sup>[41,42,60]</sup> This can be minimized by slowing the rotation speed at the expense of the process time, which can extend to more than one day.<sup>[45,56]</sup> Ball milling is, thus, time consuming and many thick flakes are present in the final products, despite some single- and few-layer graphene. It generally requires post sonication<sup>[43,60]</sup> or assistance by exfoliating compounds<sup>[41,45,48,59,60]</sup> in order to decrease flake thickness and increase the exfoliation yield, as well as additional purification steps to remove the solvents, in the case of wet ball milling. Table 1 summarizes the experimental conditions employed in a number of works on graphene production by ball milling.

### 2.2.2. Sonication

In sonication, ultrasonic waves produce localized compressions and rarefactions in the liquid medium, forming vacuum cavities which then collapse, generating high pressure jets. These jets are capable of peeling off graphene layers from graphite, as well as weakening the Van der Waals interaction between the layers. This facilitates the intercalation of solvent molecules between graphitic planes, allowing for further exfoliation and consequent stabilization of the dispersion. As with other graphite exfoliation approaches, attention must be paid to the choice of the dispersing solvent.

Hernandez et al.,<sup>[63]</sup> for example, noted NMP's role in successful dispersion of carbon nanotubes. The authors then went on to use it in a similar way for the dispersion of graphite powder by bath sonication, resulting in flakes of 5 or fewer graphene layers, with lateral dimensions of the order of micrometers. Similar results were also obtained with g-butyrolactone (GBL) and 1,3-dimethyl-2-imidazolidinone (DMEU) solvents, also known for their ability to disperse carbon nanotubes. A more detailed study of sonication dispersion in NMP showed that, for up to 343 h of bath sonication, the average number of layers in the flakes does not change, remaining at around 3, while the lateral size follows a  $t^{-1/2}$  dependence.<sup>[64]</sup> The authors also point out the high boiling point of NMP as a disadvantage (this issue also applies to some other solvents used in graphene production by sonication, such as benzylamine).<sup>[65]</sup> Moreover, being a polar solvent, NMP imposes some constraints on the obtained dispersions' chemistry, such as being

hygroscopic (and, thus, requiring the exclusion of water).

In an attempt to overcome the issues concerning the use of NMP as a dispersion solvent, its substitution by ethanol, by successive sonication, centrifugation, and filtering steps, has been shown to lead to stable dispersions of graphene flakes.<sup>[66]</sup> Dispersion in a nonpolar solvent was also attempted by using ortho-dichlorobenzene (ODCB).<sup>[67,68]</sup> ODCB, being aromatic, is a known reaction solvent for fullerenes and a carbon nanotube dispersant, believed to be efficient thanks to  $\pi$ - $\pi$  interactions (though it has to be noted that other aromatic solvents such as benzene, toluene, xylenes, chlorobenzene, and pyridine were unsuccessful in dispersing graphite in this study).<sup>[67]</sup> Besides, it has a surface tension of  $36.6 \text{ mJ m}^{-2}$ , which is close to the range of surface tensions that have been suggested to be good for graphite exfoliation.<sup>[63]</sup> Also in the context of aromatic molecules, but in this case perfluorinated ones, hexafluorobenzene ( $C_6F_6$ ), octafluorotoluene ( $C_6F_5CF_3$ ), pentafluorobenzonitrile ( $C_6F_5CN$ ), and pentafluoropyridine ( $C_5F_5N$ ), were shown to be successful as solvents for ultrasonication of graphite into graphene.<sup>[69]</sup> The results are explained on the basis of electron-withdrawing properties of the fluorine atoms, resulting in charge transfer through  $\pi$ - $\pi$  stacking, which promotes solubilization. Pyrene and anthracene-based compounds have also found use as dispersion agents during sonication exfoliation, as exemplified by 1-pyrenemethylamine (Py-NH<sub>2</sub>) and 1,3,6,8-pyrenetetrasulfonic acid (Py-SO<sub>3</sub>),<sup>[70]</sup> as well as by 1-pyrenecarboxylic acid (PCA)<sup>[71]</sup> and 9-anthracene carboxylic acid (9-ACA).<sup>[72]</sup> Low boiling-point solvents, such as chloroform, acetone and isopropanol, have been explored by O'Neill and coworkers.<sup>[73]</sup> Isopropanol, in particular, showed good results, both in terms of the number of layers obtained (less than 5), and in terms of stability (with 96% of graphene remaining stably dispersed for as long as 200 h after the initial dispersion). The authors claim that the Hansen solubility parameters of the solvents, particularly the dispersive parameter,  $\delta_D$ , dictate the quality of the success of the dispersion, having to match those of graphene ( $\delta_D = 18 \text{ MPa}^{1/2}$ ,  $\delta_P = 9.3 \text{ MPa}^{1/2}$ , and  $\delta_H = 7.7 \text{ MPa}^{1/2}$ ) for better results.

Despite not being suitable for graphene dispersion on its own, water has been employed for sonication exfoliation in conjunction with surfactants such as sodium dodecylbenzene sulfonate (SDBS).<sup>[74]</sup> In this example, as much as 40% of the obtained dispersion have been reported as having less than 5 layers of graphene, with 3% of obtained flakes being single-layer

**Table 1.** Summary of different ball milling approaches reported in the literature and the corresponding results.

Concentration or yield	Thickness or number of layers	Precursor	Reagents	Process time and setup	Additional steps	Ref.	Year
>0.1 mg/mL (after solvent dispersion), edge-functionalized	—	Natural graphite	H <sub>2</sub> /dry ice/SO <sub>3</sub> (each for different edge functionalization)	48 h, planetary mill, 500 rpm	Soxhlet extraction, freeze drying, dispersion in polar solvents	[42]	2013
~0.9 mg/mL (and up to 6 mg/mL by recycling the sediment)	As low as 1 layer	Graphite flakes	SDS, water	Up to 12 h, planetary mill, 100 rpm	Centrifugation, sonication (2 h, 80 W), only the supernatant used	[43]	2012
—	—	Graphite powder Graphite powder	Kerosene/2-ethylhexanol Cetyltrimethyl ammonium bromide (CTAB), water, ethanol Dry ice	60 h, planetary mill, 400 rpm Up to 16 h, planetary mill, 300 rpm	Centrifugation, heat-treatment Centrifugation, drying	[45] [46]	2017 2019
2.9 × 10 <sup>-4</sup> mg/mL	Multilayer	Graphite		24 h, planetary mill, 150 rpm revolution, 300 rpm autorotation	Sonication in HCl (20 min), freeze drying	[47]	2016
35.16 g (starting from 25 g of graphite and 20 g of dry ice), edge-functionalized ≤5 layers	4–5 layers	Graphite powder	NH <sub>3</sub> BH <sub>3</sub>	4 h, planetary mill, 150 rpm, in Ar atmosphere	Dispersion in ethanol, centrifugation	[48]	2013
~25% 1 layer		Graphite powder	N-methylpyrrolidone (NMP)/cyclonexanone (CHO)/i-propanol (IPA)	1 h, stirred media mill, 1000 rpm	Centrifugation	[49]	2015
0.43 mg/mL	Mostly 3–4 layers	Isostatic graphite	Water, sodium dodecyl sulfate (SDS)	3–5 h, stirred media mill, 1500 rpm	Centrifugation	[50]	2010
25 mg/mL	Mostly ≤ 5 layers	Synthetic graphite	N,N-dimethylformamide (DMF)	30 h, planetary mill, 300 rpm	Centrifugation, ethanol wash, only supernatant used	[55]	2010
—	≤ 3 layers	Graphite nanosheets (30–80 nm thick)	Ethanol/formamide/acetone/tetrahydrofuran (THF)/tetramethylurea(TMU)/DMF/NMP	30 h, planetary mill, 300 rpm	Sedimentation, centrifugation	[56]	2010
0.097 mg/mL (for DMF)	As low as 1 layer	Graphite nanosheets (30–80 nm thick, from expanded graphite)	Naphthal polyoxyethylene ether (NPE)	12 h, planetary mill, 400 rpm	Transfer to water, centrifugation, vacuum filtering, ethanol rinsing, water redispersion	[57]	2010
0.5–1.2 mg/mL (~10 wt% of the initial graphite)	Mostly <10 layers (as low as 1 layer)	Graphite powder	NaCl	2 h or 5 h, planetary ball mill, 350 rpm, in Ar atmosphere (0.4 MPa)	Ultrasonication in water, centrifugation, vacuum drying	[61]	2017
0.37 mg/mL (for melamine)	—	Graphite powder	2,4,6-triamino-1,3,5-triazine (melamine), 2,4,6-tri(N,N-diethylamino)-1,3,5-triazine (TNE-T), 2,4,6-trihydroxy-1,3,5-triazine (TOH-T), 2,4,6-trimethoxy-1,3,5-triazine (TOC-T), 2,4,6-trihydroxybenzene (TOH-B)	30 min, planetary mill, 100 rpm, in air atmosphere	Redispersing in water or DMF, sonication (1 min), sedimentation	[59]	2014
—	As low as 2 layers	Graphite powder	Na <sub>2</sub> SO <sub>4</sub>	24 h, 150 rpm	Water wash, filtering, drying (90 °C, 3 h)	[62]	2014

graphene. As an alternative to SDBS, sodium deoxycholate (SDC) has also been used.<sup>[75]</sup>

Guardia and coworkers compared a wide range of different aqueous surfactants for bath sonication exfoliation of graphite.<sup>[76]</sup> Among these, the commercial nonionic surfactant Pluronic P-123 was identified as being particularly effective for the preparation of graphene dispersions, allowing to achieve concentrations as high as 1.5 mg/mL after 5 h of sonication. Tween 80 gave similarly good results. Dispersions obtained using P-123 were identified, by AFM profiles, to mostly have no more than 5 graphene layers, with 10% to 15% of flakes being single-layer graphene.

Nuvoli et al.<sup>[77]</sup> dispersed graphite, by bath sonication, in an ionic liquid (1-hexyl-3-methylimidazolium hexafluorophosphate, HMIH). This approach yielded graphene flake concentrations of 5.33 mg/mL, after 24 h of sonication and using an optimized concentration of the starting material (5.0 wt% of graphite flakes in HMIH).

As an alternative to bath sonication, horn ultrasonication has also been employed to exfoliate naturally occurring graphite flakes in the presence of a sodium cholate amphiphilic surfactant.<sup>[78]</sup> Supplemented by density gradient ultracentrifugation, this approach yielded flakes with an average thickness as low as 1.1 nm, with lateral sizes ranging from 50 to several hundred nanometers. The use of biomolecules, such as silk fibroin nanofibers, for sonication exfoliation has also been shown.<sup>[79]</sup> Also in an attempt to overcome the use of NMP, Sun and coworkers dispersed graphite, by 1 hr of tip-sonication, in amine-based solvents.<sup>[80]</sup> Namely, 3,3'-iminobis(N,N-dimethylpropylamine) (DMPA), N-[3-(dimethylamino)-propyl]methacrylamide (DMAPMA), 2-(tert-butylamino)ethyl methacrylate (BAEMA) and 2-(dimethylamino)ethyl methacrylate (MAEMA) were employed. DMPA, in particular, allowed to obtain dispersions with concentrations of up to 15 mg/mL, superior to those obtained for NMP in control experiments. Among aromatic molecules, tetrasodium 1,3,6,8-pyrene-tetrasulfonic acid (TPA) was shown to be capable of exfoliating graphite by probe sonication (in a pulsed mode in an ice bath, with a power of 70 W, for 2 h).<sup>[81]</sup> Here, ~90 % of the obtained flakes were identified as single-layer graphene.

When dealing with surfactants, their depletion from the solution during sonication should be taken into account, as pointed out in a report where step-wise or even continuous addition of fresh surfactant was shown to result in considerably higher yields compared to the conventional process.<sup>[82]</sup> This was explained by the variation in the surface tension of

the solution throughout the process due to the depletion of the available surfactant as it adsorbs on the surface of the graphene sheets. This shifts the surface tension from the optimum value for graphite exfoliation (around 41 mJ/m<sup>2</sup>, according to the report). A continuous addition of Pluronic F108 surfactant, for example, to a graphite dispersion in water during tip-sonication resulted in yields of up to 1.5 wt%. Increases in obtained yields were also observed with the continuous addition method for a range of ionic surfactants, including SDS.

Polymers based on aromatic molecules have also found use as stabilizing agents in graphite sonication, as shown by Zheng et al.<sup>[83]</sup> Here, graphite powder and pyrene-polyethylene glycol (pyrene-PEG) or pyrene-polycaprolactone (pyrene-PCL) were bath sonicated for 3 h in dimethylsulfoxide (DMSO). The obtained dispersion was then transferred to supercritical CO<sub>2</sub>, where it remained for 6 h, followed by a further period of sonication for 2 h. After centrifugation, the supernatant was extracted and re-dispersed either in water (in the case of pyrene-PEG as the stabilizing agent) or in DMSO (for pyrene-PCL). Concentrations of up to 0.518 mg/mL were obtained (for the dispersion obtained using pyrene-PCL with 19 repeat units of caprolactone), higher than for the dispersion obtained using PCA in an equivalent control experiment.

In summary, sonication is an attractive technique for liquid-phase exfoliation, but, much like the other liquid-phase exfoliation approaches, it relies on the choice of an appropriate dispersant or stabilizing agent. The obtained yields are relatively low, and the long processing times, with continuous energy input, are a drawback of sonication exfoliation. Table 2 presents the conditions employed in a number of works on graphene production by sonication.

### 2.2.3. Shear stress exfoliation

**Shear stress exfoliation of graphite** can be accomplished in liquids using different types of apparatus, **relying purely on fluid dynamics** considerations in laminar or turbulent flow regimes. In particular, some authors<sup>[91,92]</sup> employed a rotating tube at sufficiently **high rotating speeds to produce vortex fluidic films** (e.g., 7000 rpm),<sup>[91]</sup> which are capable of producing enough **shear forces to overcome Van der Waals interactions**. The graphite precursors are mixed with organic or aqueous media and exfoliation takes place at the tube wall via combined lifting and slippage of graphene sheets.<sup>[58,91]</sup> The inclination of the tube was found to play a vital role in exfoliation, inducing

turbulence via combined centrifugal and gravitational interactions, which are crucial for the lifting/slippage process. Centrifugal forces hold the graphite precursors against the tube wall and allow for the slippage of graphene sheets. Despite the principle being successfully demonstrated for the production of good quality graphene, the shear stresses capable of graphene exfoliation are localized only at the tube surface, severely limiting the yield rate. This means that very high surface area fast rotating tubes are needed to improve the yield to satisfactory levels, which poses many technological challenges at increased costs. It was thus apparent that higher energy shear stress systems were needed to obtain graphene in a faster way and to increase the production yield.

In this sense, it was found that pressurized fluids containing graphite precursors inserted in constriction channels also lead to the successful exfoliation of graphene and other 2D materials via fluid dynamics mechanisms (Figure 4(a)).<sup>[93–96]</sup> This type of exfoliation was the subject of theoretical simulations showing several mechanisms contributing to exfoliation besides shear stresses, namely collision, cavitation, and pressure release, the latter two mechanisms exerting normal forces aiding exfoliation. Among those producing shear forces are the turbulence-induced (Reynolds) stresses, velocity gradient stresses, and inter-flake collisions. Remarkable yields of 15% of mainly FLG with little oxidation have been demonstrated using high pressure pumps and closed circulation loops.<sup>[96]</sup> Interestingly, although constriction tubes are usually constructed in a straight geometry, recent theoretical simulations<sup>[95]</sup> have shown that helical tubes allow higher shear stresses, and thus more efficient exfoliation, despite turbulence being present in both cases.

Whilst most of the previous strategies use compressed fluids to obtain the desired shear rates, an alternative approach using compressed air-driven graphite suspensions through a tube was proposed in order to decrease the defects in the produced graphene because of the milder conditions compared to pressurized fluid approaches. An extreme shear rate of up to  $3.3 \times 10^7 \text{ s}^{-1}$  was inferred at working pressures as low as 0.5 MPa.<sup>[97]</sup> Nevertheless, the calculated yield is still low, about 1.5%. The low yield is likely due to the fact that the extreme shear rates were found to be concentrated at the edges of the tube at the outlet. Indeed, by smoothing those edges the shear rates decreased by 3 orders of magnitude, barely above  $\sim 10^4 \text{ s}^{-1}$ . Authors claimed the production of unoxidized graphene, and that up to 62% and 35% of

the flakes were monolayer and bilayer, respectively, via statistical analysis of AFM measurements. However, Raman measurements show a spectrum more attributable to FLG.

The most common and efficient approaches using fluid dynamics rely on rotor-stator<sup>[60,98–100]</sup> or rotating blades<sup>[101,102]</sup> immersed in a fluid containing the graphite precursor and suitable surfactants, commonly denominated by high-shear exfoliation (Figure 4(b)). The authors introducing the rotor-stator technique successfully produced highly concentrated graphene flake dispersions in sodium cholate and NMP, having no oxidation and low density of basal defects, judging by the low  $I_D/I_G$  Raman band ratio.<sup>[98]</sup> Exfoliation rates exceeding 5 g/h were demonstrated using a 300 L system and exfoliating rates of 100 g/h were extrapolated to  $10^4$  L high shear apparatus. Through several combinations of diameters and rotor speeds, it was noted that graphene flakes could be produced at relevant concentrations/yields if a minimum of  $10^4 \text{ s}^{-1}$  shear rate is attained, independently if the regime is laminar or turbulent (discriminated by a Reynolds number of  $10^4$ ). Hence, the exfoliation mechanism should be similar in both cases; nevertheless, turbulent regimes characterized by higher Reynolds numbers should in principle produce higher magnitude shear stresses, thus in principle allowing for enhanced yields.

An apparent disadvantage of high-shear exfoliation using rotor/stator is that the desired high shear rates are not uniformly distributed in all regions of the exfoliating media, being rather concentrated near the stator orifices and rotor-stator gap.<sup>[60,103]</sup> In this sense, high Reynolds numbers within the fluid are desirable because the developed turbulence homogenizes shear stresses within the exfoliation container. An obvious and easily accessible choice for this purpose are kitchen blenders equipped with rotating blades, as explored by some authors.<sup>[101,102,104]</sup> Commonly to ball stirring, shear force is not the only mechanism responsible for exfoliation in rotor-stator and rotating blade apparatus; it is aided by inter-flake collisions, as well as interactions with the rotor/blade such as flake edge collisions and cavitation,<sup>[103]</sup> with a possible contribution from pressure differences induced by turbulence.<sup>[101]</sup> The high-speed rotating blade apparatus can produce enough shear stress for graphene exfoliation in all volume of the container, despite an obvious decrease of these stresses as the distance from the blade increases. Hence, using rotating blades seemingly ensures that shear stresses will dominate exfoliation at larger regions of the system

**Table 2.** Summary of different sonication exfoliation approaches reported in the literature and the corresponding results.

Concentration or yield	Thickness or number of layers	Precursor	Solvent	Surfactant	Sonication time	Sonication setup	Additional steps	Ref. Year
1.2 mg/mL 3.18 ng/mL 0.5 mg/mL 0.04 ng/mL	Mostly 2–4 layers 28% monolayers — Mostly <10 nm	Natural graphite powder Graphite powder Graphite flakes Graphite flakes	NMP NMP Benzylamine NMP, progressively replaced with ethanol	— — — —	270 h 30 min 2–4 h >2 h	23 W, bath Bath Bath Bath	Centrifugation Centrifugation Centrifugation Several centrifugation, solvent exchange and sonication steps	[64] 2010 [63] 2008 [65] 2010 [66] 2010
0.02 mg/mL	Mostly <5 layers	Synthetic graphite	ODCB	—	30 min	Horn	Prior homogenization in a high-shear mixer, centrifugation	[67] 2009
0.18 ng/mL	26% monolayers, 22% bilayers, 28% monolayers, 19% bilayers	Graphite flakes	Water	SDC	3 h	Bath	Centrifugation	[68] 2010
0.1 mg/mL	—	—	NMP	—	6–9 h	—	—	—
0.06 ng/mL 0.1 mg/mL (for pentfluorobenzenonitrile)	— 0.5–1 nm on average	Graphite powder	ODCB Hexafluorobenzene, octafluorobenzene, pentfluoronitrobenzene, pentfluorobenzonitrile, pentfluoropyridine, or pyridine	— —	6–9 h 1 h	135 W, bath	—	[69] 2009
—	0.9 ± 0.3 nm on average	Graphite powder	Water	Py-NH <sub>2</sub> or Py-SO <sub>3</sub>	Up to 2 h	130 W, probe	Centrifugation, dialysis to remove surfactant	[70] 2010
—	<10% monolayers	Graphite powder	Methanol and water	PCA	—	Bath	Centrifugation and additional sonication	[71] 2010
0.5 mg/mL (for isopropanol)	≤5 layers for isopropanol	Graphite powder	Acetone, chloroform, isopropanol, cyclohexanone, NMP, DMF	—	48 h	16 W, bath	Centrifugation	[73] 2011
0.05 ng/mL	~3% monolayers, 40% with <5 layers	Graphite powder	Water	SDBS	30 min	Bath	Centrifugation	[74] 2009
— 0.5 mg/mL —	~60% monolayers Mostly 2–4 layers Mostly 0.5–2 nm	Kish graphite Graphite powder Graphite powder	Water Water Water solution of Phosphate Buffer Saline	SDC MP•ZCl Perylene-based bolaamphiphile detergent	90 min 30 min 40 min + 5 × 45 min	Bath — Bath	Centrifugation — —	[75] 2010 [84] 2013 [85] 2009
1 mg/mL	~10%–15% of monolayers	Natural graphite powder	Water	Wide range of ionic and nonionic surfactants, with the best one being Pluronic® P-123	2 h	Bath	Centrifugation	[76] 2011
5.33 ng/mL 0.09 ng/mL	2 nm on average 80% with a thickness of ≤1.2 nm	Graphite flakes Natural graphite flakes	1-hexyl-3-methylimidazolium hexafluorophosphate Water	— Sodium cholate	24 h —	0.55 kW, bath —	Centrifugation Centrifugation, density gradient centrifugation	[77] 2011 [78] 2009
1.92 ng/mL	2 nm on average	Graphite powder	Water	Silk nanofiber	1 h	51–52 W, horn	Centrifugation	[79] 2018
—	0.696–0.870 nm	Natural graphite	Water	Ethylene glycol	50 min	195 W, 5 s/2 s working pulse, probe 20 kHz, 1 kW, pressurized reactor, horn	—	[86] 2012
~0.24 mg/mL	—	Graphite flakes	DMPA, DMApMA, BAEMA, and MAEMA, among others	—	1 h	20 kHz, 100 W, tip	Centrifugation	[80] 2014
—	~1.4 nm on average	Graphite powder	Deuterated water	TPA	2 h	70 W, probe	—	[81] 2009

(Continued)

**Table 2.** Continued.

Concentration or yield	Thickness or number of layers	Precursor	Solvent	Surfactant	Sonication time	Sonication setup	Additional steps	Ref. Year
15 mg/mL	—	Synthetic or natural graphite	Water	Pluronic® F108 or F127	5 min	60 W, probe, with stepwise or continuous surfactant addition	Dialysis, centrifugation	[82] 2012
12 wt%	2–3 nm on average	Microwave expanded graphite flakes	N,N-dimethylacetamide aqueous solution	Rose bengal	6–10 h	250 W, bath	Several centrifugation and short sonication steps	[87] 2012
0.1–0.2 mg/mL 1.02 mg/mL	<1 nm on average Thickness distribution peaking at 1.6–1.8 nm <5 layers	Graphite powder Graphite flakes Graphite powder	Water Ethanol DMSO, followed by supercritical CO <sub>2</sub>	PVP Ethyl cellulose Pyrene-polyethylene glycol or pyrene-polycaprolactone Alkali lignin	9 h 3 h 3 h + 2 h	135 W, bath 40 kHz, 100 W, bath 40 kHz, 120 W, bath	— Centrifugation, solvent exchange with terpineol to iteratively increase concentration Several centrifugation and short sonication steps	[88] 2009 [89] 2010 [83] 2012
0.5 mg/mL	~22% monolayers	Natural graphite flakes	Water		15 h	20 kHz, 750 W, horn	Sedimentation, centrifugation, vacuum filtration, washing, bath sonication, additional centrifugation	[90] 2015
0.65 ± 0.03 mg/mL								

when compared to stator-rotor arrangements. This means that high yield rates are feasible using these simple systems that are readily scalable to mass production.

A more recent approach makes use of Taylor vortex flows to promote high-shear stress exfoliation of graphene,<sup>[105]</sup> denominated as Taylor–Couette flow. The apparatus comprises two concentric cylinders that are able to rotate independently and a graphite dispersion in an appropriate fluid contained between them (Figure 4(c)). If the inner cylinder rotation speed reaches a critical value whilst the outer one is held at rest, this special type of flow pattern can form, resulting in steady state axisymmetric toroidal vortices. These vortices pose strong shear forces and pressure gradients to the graphite precursors, leading to FLG production at yields of up to 5%. The authors have claimed a low oxidation degree and a low defect concentration of graphene via XPS and Raman spectroscopy. Nevertheless, the method used for inferring oxidation is not unequivocal. More studies are needed on this type of exfoliation, namely on the quality and characteristics of the produced graphene and on the possible limitations of scaling up to industrial production.

Advantageously, no compound intercalating steps are needed for high shear exfoliation, such as in electrochemical (described below) or some ball milling exfoliation routes, despite some attempts to combine both, using electrochemical intercalation of tetrabutylammonium tetrafluoroborate, resulting in stable graphene dispersions in NMP with yields of up to 16%.<sup>[106]</sup> In addition, this type of shear exfoliation provides higher yields compared to ball milling because the graphite precursors move within the exfoliating media and can be continuously exposed to the shear forces, thus increasing exfoliation efficiency.<sup>[60]</sup> As a result, exfoliation rates are enhanced and processing times are significantly decreased, typically down to a few hours or less. Additionally, final product concentrations of up to about 1 g/L were reported, e.g., in aqueous solutions of PVP and sodium cholate surfactant<sup>[107]</sup> or even in household dishwashing liquids at a rate of up to 0.15 g/h.<sup>[102]</sup> It is also significant that, for similar exfoliation energy density, the exfoliation yield of shear stress using fluid dynamics can be about one order of magnitude larger when compared to purely sonication routes.<sup>[58,60,91,98]</sup> Finally, an increase of the processing time in shear stress leads to a linearly proportional increase in graphene product formation,<sup>[98,108]</sup> whilst in sonication routes a saturation tendency is observed.<sup>[64,109]</sup> Unsurprisingly, high-shear

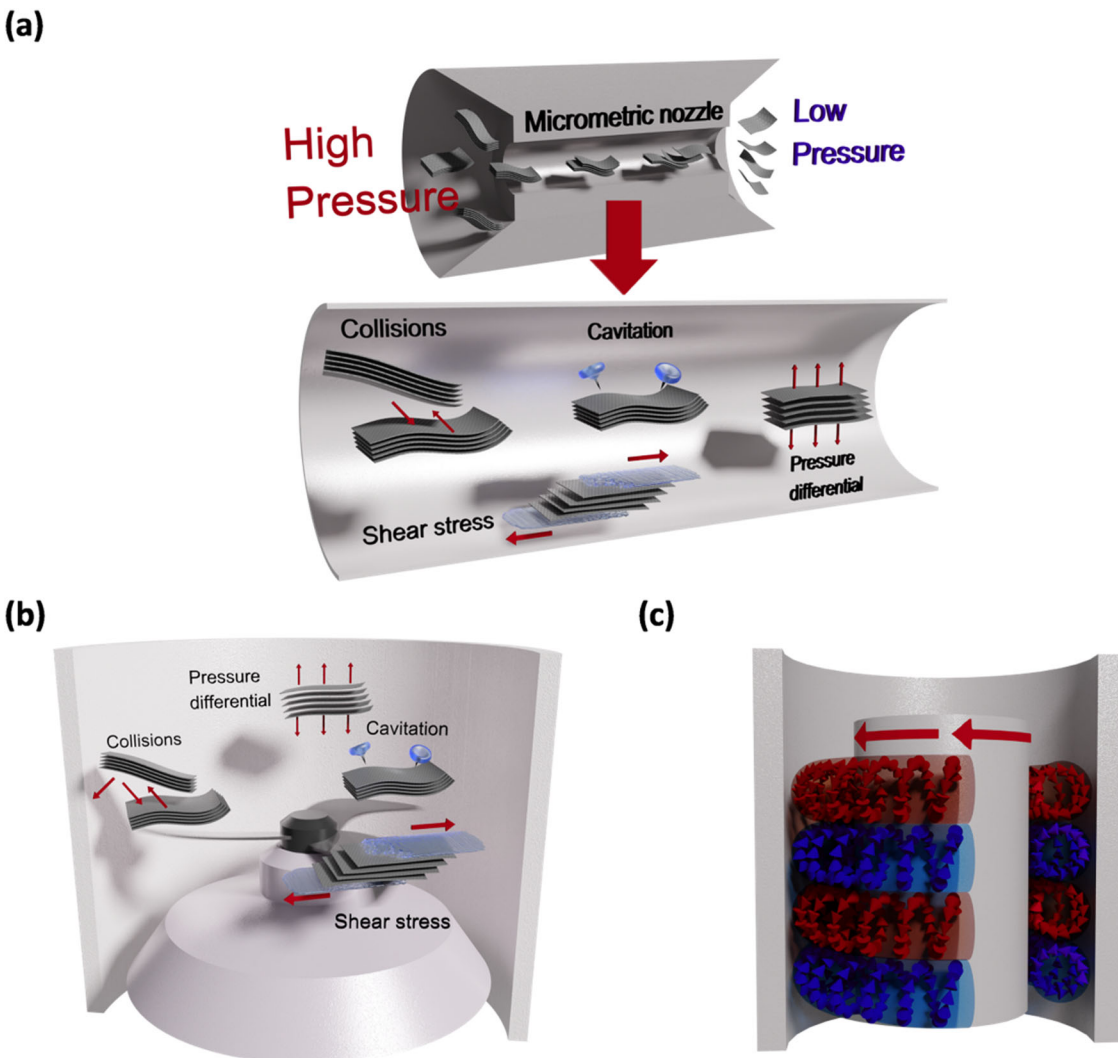


**Figure 4.** (a) Schematic illustration of the high shear stress exfoliation process in a constriction channel. (b) Schematic illustration of the high shear stress exfoliation process in a rotating blade system. (c) High shear stress exfoliation relying on Taylor–Couette flow.

exfoliation is reported to provide the same amount of FLG as obtained via sonication routes in about one tenth to one hundredth of the time.<sup>[107]</sup>

On the other hand, similarly to other liquid-phase exfoliation approaches, the graphene products by shear exfoliation generally suffer from size and thickness polydispersity,<sup>[107]</sup> and require centrifugation for separating larger flakes. Additionally, only very recently the effect of the viscosity of the exfoliating media on the produced graphene characteristics and yield was more systematically addressed,<sup>[110]</sup> despite some older studies using solvents/surfactants with different viscosities.<sup>[103]</sup> This is an example demonstrating that many features of the process are still lacking optimization. Furthermore, it is important to check if high yields, quality, and fast production times of graphene flakes are maintained in very large containers. Moreover, similarly to other liquid-phase exfoliation

techniques, it matters to demonstrate the production of stable graphene dispersions using nontoxic and cheaper solvents at similar figures of merit compared to strong organic solvents (e.g., NMP, DMSO, and DMF, among others), ionic liquids or common surfactant aqueous solutions (e.g., SDS, SDBS and PVP).<sup>[99]</sup> Pure water would be the optimal solution, due to its nontoxicity and low cost, but this is hindered by the hydrophobic nature of graphene. In this sense,<sup>[103]</sup> the use of IPA aqueous solutions yielding graphene dispersions of up to 0.27 g/L in one hour high-shear processing has been reported, which tended to be stable for up to 25 days after initial dispersion. Nevertheless, the stability is found to be highly dependent on the size and thickness of the graphene flakes. Other types of nontoxic dispersants are being unveiled for liquid-phase exfoliation of graphene and other 2D materials, such as nontoxic, cost-effective nonionic polymers,<sup>[107]</sup>

or the so-called green dispersants (e.g., black tea,<sup>[104]</sup> alkaline lignin,<sup>[90]</sup> black liquor).<sup>[108]</sup> The latter, for example, resulted in FLG dispersions of up to 10 g/L, via shear stress mixing, providing a yield of about 18% after 10 h of process time.<sup>[108]</sup> More studies within these approaches are needed to pave the way toward the environmental-friendly and cost-effective industrial production of graphene flakes using shear stress exfoliation. Table 3 summarizes some of the shear stress exfoliation approaches reported in the literature.

#### 2.2.4. Electrochemical exfoliation

The production of graphene via electrochemical exfoliation is based on the physical deformation of a graphitic working electrode immersed in an appropriate electrolyte, via the exchange of an electric current. The experimental setup also comprises a counter (auxiliary) electrode against which the potential of the working electrode is applied, ideally providing a large surface area and low electrical resistance. The counter electrode should also be chemically inert (e.g., platinum) in order to avoid the production of species that could interfere with the graphene exfoliation process, but some recent approaches rely on the exfoliation of both electrodes in order to improve the yield.<sup>[113–115]</sup>

In terms of industrial production, electrochemical exfoliation of graphene provides several advantages over other exfoliation types such as sonication or purely chemical procedures. In general, it encompasses simple, economically viable processes requiring no extreme temperature/pressure conditions. Furthermore, it permits obtaining graphene with lateral sizes of tens of micrometers,<sup>[116,117]</sup> yields larger than 50 wt% and quantities up to a few grams in relatively short production times (e.g., a few hours versus days in chemical exfoliation and sonication).<sup>[64,109,117]</sup> It has been shown that the applied potential is a critical parameter, through which it is possible to tune not only the quantity of the produced graphene, but also its quality. For instance, it has a profound impact on the degree of oxidation of the products.<sup>[58,118,119]</sup> Hence, a third (reference or pseudo-reference) electrode is often employed (Figure 5(a)), through which negligible current is withdrawn, providing a stable potential to accurately and stably control the potential applied to the working electrode. Finally, it is a versatile technique that can be combined with other approaches such as sonication,<sup>[117,121]</sup> microwave processing,<sup>[118]</sup> and shear stress<sup>[122]</sup> to increase the yield, although this poses some restrictions in terms of production scale-up and industrialization. The main

disadvantages are common to sonication and high shear stress exfoliation, such as the lack of widely available, cheap, and “green” solvents needed to efficiently perform exfoliation and properly disperse the products. In this sense, NaOH/H<sub>2</sub>O<sub>2</sub>/H<sub>2</sub>O solutions are promising in terms of exfoliation efficiency, but the products still need to be posteriorly stabilized in surfactants.<sup>[123]</sup> Finally, electrochemical exfoliation also suffers from a high degree of size polydispersity, requiring posterior purification or separation.<sup>[117,124,125]</sup>

The general exfoliation principle is that the applied voltage promotes the intercalation of ionic species present in the electrolyte in between the graphite layers, leading to physical deformation and an increase in the interlayer distance, thus weakening the Van der Walls forces and culminating with the separation of graphene layers (Figure 5(a)).<sup>[117]</sup> Two main types of electrochemical exfoliation of graphene exist depending on whether the electrode is anodically or cathodically driven. In anodic (cathodic) exfoliation the graphite electrode is positively (negatively) charged, promoting the intercalation of anions (cations). Anodic exfoliation provides faster and higher-yield graphene exfoliation at lower applied potentials when compared to cathodic exfoliation. In general, anodic exfoliation makes use of a variety of aqueous or organic solutions<sup>[113,116,119,123,126–132]</sup> or ionic liquids.<sup>[133]</sup> In particular, the usage of both organic and inorganic salts as intercalating agents has been attracting great attention, and recent studies<sup>[134]</sup> point out sodium pyrophosphate and sodium phosphate as better exfoliating agents than sodium citrate, the former greatly enhancing the yield and allowing to obtain graphene with a reduced number of layers, but also with increased defect content. However, organic salts such as sodium citrate are also promising due to better solubility in NMP compared to inorganic salts.<sup>[135]</sup>

In many cases, intercalation and exfoliation is attained using a constant voltage, the magnitude of which varies greatly among the literature, mainly influenced by the electrolyte properties and the desired characteristics of the graphene (see Table 4). The intercalated ions can undergo a change into the gas state, which enhances the exfoliation process by increasing structural deformation, e.g., via the formation of O<sub>2</sub>/CO<sub>2</sub><sup>[137]</sup> or propylene gas.<sup>[153]</sup> In this sense, a commonly employed strategy is to use aqueous solutions of sulfates.<sup>[116,137]</sup> Parvez et al.<sup>[137]</sup> analyzed several sulfate compounds in the exfoliation process and found up to 85% of graphene having three or less layers. According to the authors,

**Table 3.** Summary of different shear stress exfoliation approaches reported in the literature and the corresponding results.

Yield or yield rate	Flake size	Thickness or number of layers	C/O ratio	Raman $I_0/I_c$ ratio	Precursor	Media	Process time and setup	Additional steps or conditions	Ref.	Year
<1 wt%	~1 μm	0.7 to 1.3 nm	—	—	Graphite flakes (0.1 mg/mL)	NMP	Vortex fluidic film, 7000 rpm, 30 min	—	[91]	2012
5 wt%	<~2 μm	<1.5 nm	~20 to ~27	~0.4	Graphite flakes (1 mg/mL)	DI Water:IPA (1:1)	Pressurized fluid, 2 h	Centrifugation	[93]	2014
594 g/h	Mostly <1 μm <sup>2</sup>	<100 nm	—	—	Thermally expanded graphite flakes (20 mg/mL)	2 wt% polyacrylic acid aqueous solution	Pressurized fluid, 10 passes	—	[95]	2019
15 ± 0.3 wt%	<~2 μm	<12 layers	~25	~0.5 to ~0.6	Graphite flakes (10 mg/mL)	NMP	Pressurized fluid, 2 h	Centrifugation	[96]	2018
~1.5 wt%	0.5–2.6 /μm	<1.5 nm	~24	0.13	Graphite powder (40 mg/mL)	NMP	Pressurized gas-driven, 90 min	Centrifugation	[97]	2019
5.3 g/h	Mostly <1 μm	Mostly <10 layers	No oxidation	0.17 to 0.37	Graphite flakes (50 mg/mL)	NMP, sodium cholate solution	Rotor-stator, 20 min	Centrifugation	[98]	2014
7.3 wt%	~0.1 μm <sup>2</sup>	~1.5 nm (~20% <1 nm) <10 layers	~21	~0.12	Graphite flakes (3 mg/mL)	DMF	Kitchen blender, 8 h	Centrifugation	[101]	2014
1 wt%, ~0.15 g/h	Mostly <1 μm	Mostly <3 nm	—	0.3–0.7	Graphite flakes (50 mg/mL)	Household dishwashing	Kitchen blender, 4 h	Centrifugation	[102]	2014
~1 to 5 wt%	Mostly <2 μm	Mostly 4–6 layers	Residual O content	0.24±0.10	Graphite powder (1 to 5 mg/mL)	NMP	Taylor-Couette flow, 1 h	Centrifugation	[105]	2016
16.0 ± 0.2 wt%	<1.5 μm	Mostly <1 μm	—	—	Graphite flakes (1 mg/mL)	NMP	Rotor-stator, 1 h	Electrochemical intercalation; Centrifugation	[106]	2017
—	Mostly <1 μm	Mostly <2 nm	—	0.14–0.18	Graphite powder (10 mg/mL)	40 vol% IPA aqueous solution	Rotor-stator (variable sizes), 1 h	Centrifugation	[103]	2014
—	200 nm to 1 μm	2 to 8 layers, average of 4	~4	0.17	Graphite flakes, (~17 mg/mL)	Black tea solution	Kitchen blender, 15 min	Centrifugation	[104]	2017
—	Mostly <1 μm	Mostly <20 nm	—	~0.2 to ~0.3	Graphite flakes (40 mg/mL)	PVP and sodium cholate aqueous solutions	Rotor-stator, 2 h	Centrifugation	[107]	2017
Up to 18 wt%	<3.5 μm	Mostly <5 nm	—	—	Graphite powder	Black liquor/water solution (2:1)	Rotor-stator, 0.5 to 10 h	Sonication; Centrifugation	[108]	2018
—	~1 to 5 μm	1 to 5 layers (qualitative measurement)	—	0.1	Graphite flakes (50 mg/mL)	NMP with zeolite particles	Cappuccino mixer, 6 h	Centrifugation	[111]	2019
Up to 65 wt%	<~10 μm	<~3 nm	—	—	Mildly oxidized graphite (1 mg/mL)	Aqueous solution	Millstone, 45 min	Centrifugation	[112]	2018

**Table 4.** Summary of different electrochemical exfoliation approaches reported in the literature and the corresponding results.

Yield or yield rate	Flake size	Thickness or number of layers	C/O ratio	Raman I <sub>D</sub> /I <sub>G</sub> ratio	Electrode	Applied signal	Complementary steps or conditions <sup>a</sup>	Ref. Year
—	Tens to hundreds $\mu\text{m}$	— 2–6 nm	—	~1 ~1	Graphite rod Graphite rod	0.05 M and 0.1 M SDSBS 10 mg/mL copper phthalocyanine	25 V DC (anodic) 12 V DC (anodic)	— Sonication [136] 2013 [137] 2014
~15 wt%	<1 $\mu\text{m}$	Mono and few layer —	<1	Graphite rod	1 mM sodium-4-styrenesulfonate	5 V DC (anodic)	—	[130] 2009
5 to 8 wt%	1–40 $\mu\text{m}$	<3 nm	—	Graphite flakes or HOPG	2.4 g of 98% $\text{H}_2\text{SO}_4$ in 100 mL of DI water plus 11 mL of 30% KOH	Alternating 10 V (anodic) and -10 V (cathodic)	Preliminary intercalation step at 2.5 V (anodic)	[138] 2011
60 to 77 wt%	50–230 $\mu\text{m}^2$	<5 layers	~21	Graphite rod or HOPG	0.1 M $(\text{NH}_4)_2\text{SO}_4$ to 10 V (anodic)	LSV <sup>b</sup> or sinusoidal, <sup>c</sup> 7 to 10 V (anodic)	Posterior deintercalation at -0.5 V (cathodic); Sonication	[127] 2019
65 wt%	>30 $\mu\text{m}$	2–7 nm	~5	0.9–1.2	Graphite flakes	0.1 M $(\text{NH}_4)_2\text{SO}_4$	10 V DC (anodic)	Physical compression [116] 2018 of graphite; Shear mixing at 800 rpm
2.29 $\text{L}^{-1} \text{h}^{-1}$ 1.6 mg $\text{cm}^{-2} \text{h}^{-1}$	— <10 $\mu\text{m}$	2–5 layers 1–3 layers	~8 —	0.7 0.2 to 0.3	Graphite rod HOPG	Glycine in $\text{HSO}_4/\text{H}_2\text{O}$ 0.1 M $\text{H}_2\text{SO}_4$	1 V and 3 V DC (anodic) 1 to 10 V DC (Anodic)	Sonication [139] 2015 Shear stress field ( $\sim 74,000 \text{s}^{-1}$ ) [122] 2016
—	—	Mono and few layer	~27	0.05	Graphite foil	0.5 M $\text{Na}_2\text{SO}_4$	20 V DC (anodic)	Several transition metal compound additives [140] 2018
56 wt%	~2 $\mu\text{m}$ 0.2–0.6 $\mu\text{m}$	2–4 layers 1–2 nm	11 ~27	~0.3 ~0.4	Graphite foil Graphite foil, powder and flakes, HOPG	0.5 M $\text{H}_2\text{SO}_4$ 0.1 M $\text{K}_2\text{SO}_4$	10 V DC (Anodic) 10 V DC (Anodic)	1 M NaOH pretreatment [141] 2015 Sonication or shear mixing [142] 2015
—	0.6 $\mu\text{m}$	2–3 nm	~17	0.8	Graphite foil	Sodium halides (0.05 M $\text{NaCl}$ , 0.1 M $\text{NaBr}$ , 0.1 M $\text{NaI}$ )	10 V DC (Anodic)	Sonication [143] 2017
42 ± 7 wt%	Average of 12 $\mu\text{m}$	Average of 10 nm	~14	1	HOPG	0.1 M $(\text{NH}_4)_2\text{SO}_4$	12 V DC (Anodic)	Thermal treatments up to 800 °C [144] 2016
90 wt%	10 to 30 $\mu\text{m}$	85% <7 layers	7.5	0.3	Pre-expanded graphite foil	10 M $\text{H}_2\text{SO}_4$	2 V DC (Anodic)	Preliminary 1 V DC intercalation step [145] 2014
~77 wt%	—	5–15 nm	—	~0.3	Graphite foil	0.25 M $\text{H}_2\text{SO}_4$ plus 11 mM KOH (30%)	10 V DC (anodic)	80 °C [146] 2015
~30 wt%	0.5–1 $\mu\text{m}$	Mostly 2 layers	~12	~1.8	Graphite rod	0.2 M $(\text{NH}_4)_2\text{SO}_4$	2 V DC (Anodic)	2 V DC preliminary step; sonication; thermal reduction [147] 2016
75 wt%	Mostly 1–5 $\mu\text{m}$	Mostly 1–3	~21	0.16	Graphite sheet	0.1 M TBA- $\text{HSO}_4$ , NaOH (pH adjustment)	10 V AC, 0.1 Hz (both anodic and cathodic)	— [114] 2017

—	18–37 μm	—	—	0.06–0.14	Graphite foil	0.1M (NH <sub>4</sub> ) <sub>2</sub> SO <sub>4</sub> , varying amounts of CH <sub>4</sub> N <sub>2</sub> S	10 V DC (anodic) and –10 V DC (cathodic)	Sonication	[113] 2018
25 wt%, 1.5 g h <sup>-1</sup>	18 μm	Mostly 1 to 3	~26	0.2–0.54	Graphite powder	65 g/L H <sub>2</sub> SO <sub>4</sub> in H <sub>2</sub> O, varying amounts of melamine	20 V DC (anodic) and 20 V DC (cathodic) —20 V DC	Intercalation step	[148] 2015
63 ± 4% (cathodic), 45 ± 3% (anodic)	0.5–0.8 μm	~5 layers	~9 (anodic) ~23.5 (cathodic)	—	Graphite rod	0.1 M of ionic liquids in acetonitrile	10 to 20 V DC (anodic and cathodic) 3 V DC (Anodic)	Hydrogen cell apparatus; Sonication Spark	[149] 2015
—	~25 μm	Mono and bilayer	~25	0.16	Graphite foil	1.0 M H <sub>2</sub> SO <sub>4</sub>	—	—	[150] 2017
13 wt% 25 wt%	~33–50 μm —	1–5 layers Mostly 2–5 layers	~30–50 ~36	~0.2 <0.05	Graphite Foil HOPG, graphite rod	0.1 M Na <sub>2</sub> SO <sub>4</sub> , 0.1 M NaCl BMPT-F2N	10 V DC (anodic) —15 to –30 V DC (cathodic)	plasma treatment Sonication —	[126] 2018 [151] 2013
0.5–2 g h <sup>-1</sup>	Mostly 1–50 μm	<5 nm	~12	90% <0.5	Graphite /polyvinylidene fluoride pellets or rods	Lithium chloride and/or Triethylamine hydrochloride in dimethyl sulfoxide	LSV, –1.7 to –5 V DC, plus step at –5 V	Preliminary step at –1.7 V DC	[152] 2014
Up to 70 wt%	Mostly < 5 μm	70 % < 5 layers	—	<0.1	HOPG and graphite powder	30 mg/mL LiClO <sub>4</sub> in propylene carbonate	DC (cathodic) –15 V (cathodic)	Sonication	[153] 2011
—	Few μm	Mono, few and multilayer	—	—	Graphite foil	1.0 M HClO <sub>4</sub>	–0.6 to –1.5 V DC (cathodic)	Thermal treatment via MW radiation; sonication	[118] 2011
85 wt% (cathodic) and 48 wt% (anodic) 25 g h <sup>-1</sup>	70% of 1–5 μm	70% of 1–3 layers	~18 (anodic); ~21 (cathodic)	<0.1	Graphite rod and graphite flakes	0.1 M TBAClO <sub>4</sub> in propylene carbonate	5 V DC (both anodic and cathodic)	Thermal treatment at 800 °C in Ar; Sonication	[115] 2019
80 wt%	—	2–4 nm	~8.6	~0.3	Graphite rod	Molten LiOH	Constant current 15 A current	600 °C	[154] 2012
—	100–200 nm	~2 nm	11.5	—	HOPG and graphite rod	0.1 M TMA ClO <sub>4</sub> , TEA BF <sub>4</sub> or TBA BF <sub>4</sub>	–5 V DC (cathodic)	Sonication (for HOPG)	[120] 2014
—	—	~3 nm	12.5	~0.1	Graphite rod	NaCl, DMSO, and thionin acetate salt	–5 V DC (Cathodic)	Sonication	[121] 2013

<sup>a</sup>Similarly to other production routes, centrifugation is also used in almost all the works listed in this table and is excluded from this entry for practicality.

<sup>b</sup>Linear sweep voltammetry.

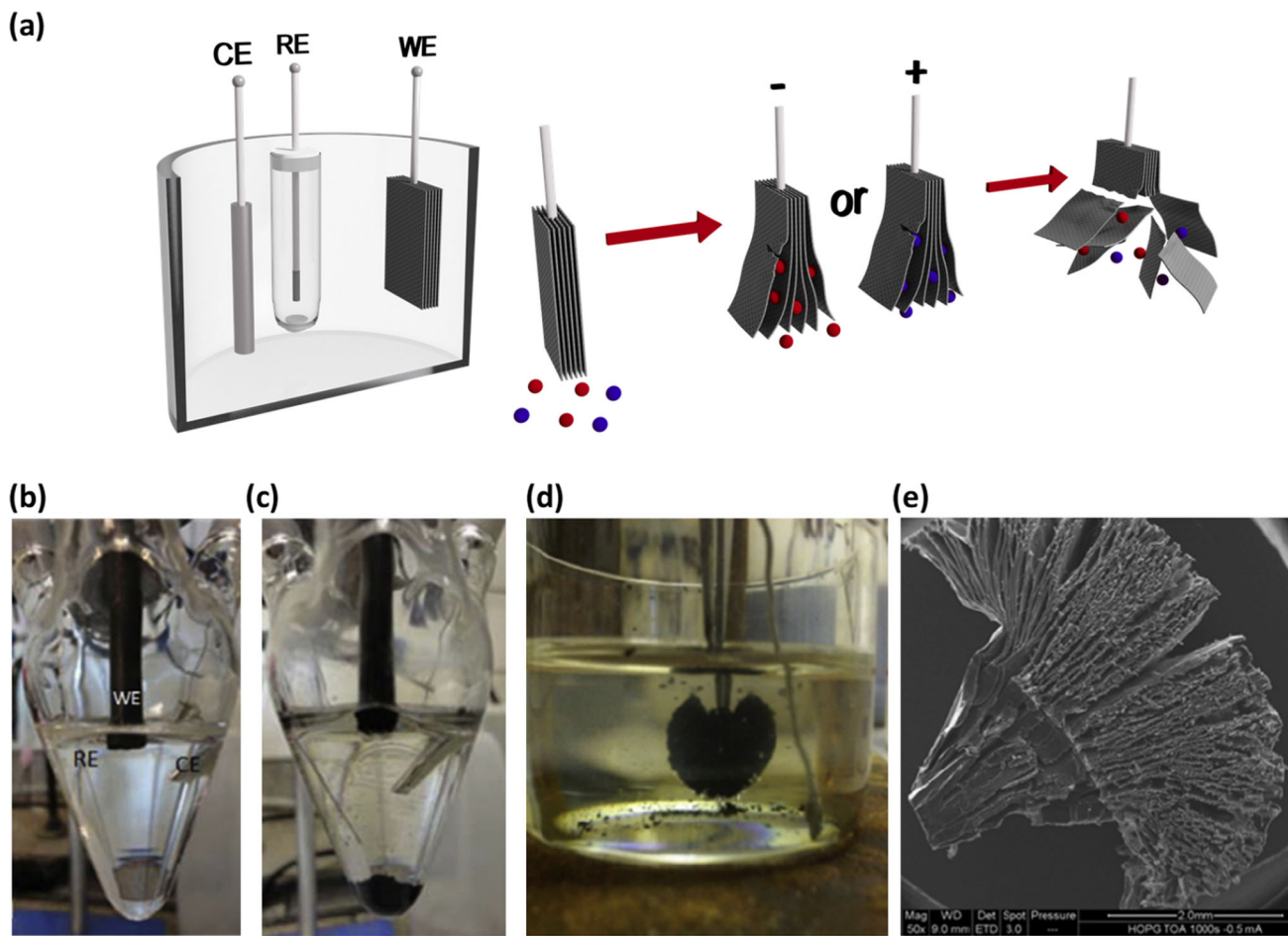


**Figure 5.** (a) Schematic illustration of the electrochemical exfoliation process. WE, RE and CE labels correspond to the working, reference and counter electrodes. Photograph of a graphite rod (b) before and (c) after electrochemical exfoliation by tetraethylammonium intercalation. Adapted from ref. [120] under the Creative Commons CC-BY license. (d) Photograph and (e) SEM image of HOPG expanded after tetrabutylammonium intercalation. Adapted from ref. [120] under the Creative Commons CC-BY license.

hydroxyl ions from water reduction attack preferentially the graphite edges and grain boundaries, where expansion starts promoting the intercalation of sulfate ions and  $\text{H}_2\text{O}$ . Afterwards, sulfate ions and water molecules undergo reduction and oxidation, leading to the production of  $\text{SO}_2$  and  $\text{O}_2$  that assist the exfoliation process.

The major obstacle often observed using bulky graphite electrodes lies in the inherent mechanism of exfoliation. Since the electrode is physically deformed during intercalation, it may start disintegrating, creating thick graphite flakes that are no longer electrochemically active by lack of electrical contact with the electrode. This is the main reason justifying the need for posterior thinning of the graphitic products via sonication.<sup>[116,129,137,155,156]</sup> A potential breakthrough to solve this problem whilst maintaining good scalability prospects is the use of physical compression of the graphite,<sup>[116]</sup> taking place within a permeable and

compressible container. Authors have shown appreciable yields of 38%, which could theoretically be improved to 65%, but the large-scale production with this figure of merit is yet to be demonstrated.

The formation of thick flakes occurs especially when employing acid electrolytes, because of the higher anion intercalation rate in such conditions.<sup>[156]</sup> Moreover, the products often denote an important degree of overoxidation.<sup>[117,156,157]</sup> In this sense, the usage of inorganic salts at neutral pH<sup>[137]</sup> has been also proposed in order to control anion intercalation, seemingly allowing the production of good quality and thin exfoliated graphene. The addition of antioxidant species to the electrolyte also enhances carbon to oxygen content ratio.<sup>[140,158]</sup> Nevertheless, the major issue is that, in general, anodic-based processes using aqueous solutions at the potentials required for successful anion intercalation also lead to water hydrolysis. This culminates with low yields, severe oxidation

defects and/or other undesired functionalization, the extent of which depends mainly on the applied potential and on the pH of the electrolyte.

An alternative approach relies on the application of multi-potential programs, as opposed to the traditional constant potential process.<sup>[117,123,127,138,139]</sup> A better control in the intercalation process leading to the formation of thinner graphene flakes (e.g., <3 nm)<sup>[138]</sup> was reported. Recently, Chen et al.<sup>[127]</sup> employed different potential sweep profiles between 7 and 10 V, followed by deintercalation steps at -0.5 V, in 0.1 M  $(\text{NH}_4)_2\text{SO}_4$  solutions. A sinusoidal profile more than doubled the average area of the products, and an increase of 9% up to 96% of graphene with less than 5 layers was also obtained. Without the -0.5 V step, that percentage decreased to about 60%. Authors claimed that the potential sweeps, especially sinusoidal ones, greatly reduced the oxidative breaking of the graphite basal C=C bonds and promoted  $\text{SO}_4^{2-}$  intercalation in comparison with fixed potential approaches, by equilibrating these two kinetically dissimilar processes. On the other hand, at -0.5 V the basal plane disruption and anion intercalation is hindered, and anion release from in between the graphite layers is promoted. This allows a more controlled interlayer expansion and exfoliation, yielding higher surface area graphene with fewer layers and less defects. Despite the merits, the final optimized products still denote a considerable degree of oxidation as shown via XPS.

Despite the above-mentioned efforts to control the anodic exfoliation, cathodically-driven exfoliation is conceptually preferable to obtain higher structural quality graphene, mainly because cathodic processes avoid the formation of graphene oxide.<sup>[118]</sup> Cathodic exfoliation is, in general, achieved using organic solvents or ionic liquids, because the insertion of aqueous cations into graphite is a slow and inefficient process,<sup>[118]</sup> limited at higher potentials by the hydrogen evolution reaction.<sup>[115]</sup> Ionic liquids are an interesting approach because of their tunable miscibility and viscosity, recyclability, high electrical conductivity, large electrochemical windows and surface energies compatible with graphene.<sup>[124,159]</sup>

On the other hand, Li ions have been known for decades to intercalate graphite, and this fact was used to promote cathodic exfoliation of graphene. Nevertheless, Li ion insertion is a slow, inhomogeneous process<sup>[117,160]</sup> that limits the yield, in most cases also requiring post-sonication to obtain a satisfactory exfoliation of graphene. The sluggish kinetics can be sped up by increasing the applied voltage magnitude,

such as -30 V,<sup>[151]</sup> versus 1 to 10 V in anodic exfoliation (although reports exist using higher potentials, see Table 4). Nevertheless, this comes at the expense of energy efficiency via competing decomposition of solvent cations,<sup>[152,161]</sup> lack of control over the characteristics of the produced graphene, with increased defect content and unwanted contaminations. There are, however, other compounds that can be cathodically intercalated into graphite.  $\text{Na}^+/\text{DMSO}$  complexes with the aid of thionin acetate salt in aqueous solutions were shown to be viable intercalants, but still post-sonication was necessary.<sup>[121]</sup> Cathodic exfoliation at low potentials (-4 V to -5 V) using tetraalkylammonium salts has been shown to yield few layer graphene products with minimal oxygen content and without the need for any subsequent exfoliation steps,<sup>[120]</sup> which is one of the most impressive results in the literature on cathodic exfoliation (Figure 5(b-e)). Interestingly, little to none graphite expansion is seen using Li-based electrolyte as a comparison.

Some authors have put efforts to combine both anodic and cathodic exfoliation of graphite electrodes in the same run, either through application of alternating positive/negative DC pulses,<sup>[113]</sup> AC pulses<sup>[114]</sup> or employing electrolytes allowing both anionic and cationic intercalation,<sup>[115]</sup> including ionic liquids.<sup>[149]</sup> Contrarily to purely anodic or cathodic exfoliation, these strategies allow for exfoliation of both the working and counter (graphite) electrodes. Using the latter approach, graphene was produced in tetrabutylammonium perchlorate ( $\text{TBAClO}_4$ ) in propylene carbonate, which provides a potential window large enough for electrochemical anion ( $\text{ClO}_4^-$ ) and cation ( $\text{TBA}^+$ ) intercalation at the graphite anode and cathode, respectively.<sup>[115]</sup> A posterior thermal treatment enhances interlayer expansion via transition of the intercalated ions to gas state. The obtained yield is admirable (see Table 4), but extensive temperature treatments, post sonication and repeated wash by vacuum filtration and centrifugation were necessary, so that the process is hardly two-step. In addition, the influence of the sonication on the final product quality and yield is unclear.

AC signals ( $\pm 10 \text{ V}, 0.1 \text{ Hz}$ ) in 0.1 M tetra-n-butylammonium bisulfate ( $\text{TBA}\cdot\text{HSO}_4$ ) have been proposed to achieve simultaneous cathodic and anodic exfoliation.<sup>[114]</sup> The authors claimed outstanding yields (see Table 4) and the low defect density of the products was attributed to both the higher intrinsic quality of cathodic exfoliation and the reduction of anodic graphene via the AC signal. The mechanism involves the initial oxygen radicals formation during the anodic process, which

attack graphite grain boundaries and defects preferentially, opening gaps for the consequent intercalation of sulfate ions. The sulfate ions are reduced at the cathodic counterpart forming  $\text{SO}_2$  gas bubbles, which expand the graphite and allow the bigger  $\text{TBA}^+$  ions to intercalate, expanding the graphite even further. Interestingly, little exfoliation at the cathode was observed when using ammonium sulfate. However, in other work, exfoliation could be accomplished simultaneously at both graphite electrodes using alternating DC pulses of  $\pm 10\text{ V}$  in ammonium sulfate-based aqueous solutions.<sup>[113]</sup> The pulses were shown to promote anion ( $\text{SO}_4^{2-}$ ) and cation ( $\text{NH}_4^+$ ) intercalation and bubbling, thereby increasing the exfoliation efficiency.

Despite the recent progress, further studies are needed in order to establish electrochemical exfoliation as a definite alternative for scalable graphene production, preferentially without the aid of post-sonication or other co-assisting routes. Such should be accomplished using cheap, environmental-friendly, and widely available chemicals, which still remains a challenge.

### 2.3. Graphene oxide and reduced graphene oxide production methods

Graphene Oxide (GO) is another important member of the graphene-graphite family, which is a single layer of graphite oxide discovered in mid-19<sup>th</sup> century.<sup>[162]</sup>

There are multiple routes to prepare GO, most commonly by oxidizing graphite, followed by an exfoliation process. As a result of these chemical methods, a stable colloidal suspension of GO is achieved. The first example of oxidizing graphite came when Brodie employed a combination of potassium chlorate ( $\text{KClO}_3$ ) and nitric acid ( $\text{HNO}_3$ ) in his investigations to study the chemistry of graphite.<sup>[162]</sup> As a result of these studies, a new material was developed, dispersible in pure or regular water, which he named “graphic acid.” In the late 19th century, Staudenmaier improved Brodie’s process by adding  $\text{H}_2\text{SO}_4$  to the combination and by adding  $\text{KClO}_3$  throughout the reaction rather than in a single addition.<sup>[163]</sup> Nearly 60 years later, Hummers used a combination of potassium permanganate ( $\text{KMnO}_4$ ), sodium nitrate ( $\text{NaNO}_3$ ) and  $\text{H}_2\text{SO}_4$  to oxidize graphite,<sup>[164]</sup> while Hofmann’s method involved oxidation of graphite with  $\text{KClO}_3$  and  $\text{HNO}_3$ .<sup>[165]</sup> Tour’s group used a combination of  $\text{KMnO}_4$ ,  $\text{H}_2\text{SO}_4$  and phosphoric acid ( $\text{H}_3\text{PO}_4$ ) as the oxidants.<sup>[166]</sup> As a result of oxidizing with different combinations of

compounds and reaction conditions, the carbon to oxygen ratio would vary from 1.17 to 0.74 in Staudenmaier to Tour methods, respectively.<sup>[167]</sup> The most common source of graphite used for these chemical methods is flake graphite. The localized defects in the  $\pi$ -structure may serve as starting sites of the oxidation process.<sup>[168]</sup> Depending on the oxidation process, different oxygen-containing functional groups, such as carboxyl ( $\text{C}=\text{O}$ ), hydroxyl ( $\text{C}-\text{OH}$ ) and epoxide ( $\text{C}-\text{O}$ ), form on the surface and around the edges of the graphene layers, making them hydrophilic and reducing the interlayer forces. Depending on the relative humidity within the stacked GO sheets, the interlayer spacing varies from 0.6 nm to 1.2 nm.<sup>[169]</sup> These interlayer spacings weaken the interactions between the GO sheets and facilitate the exfoliation process. The GO is then exfoliated in the aqueous media via mechanical stirring, rapid heating or sonification to separate the layers of GO.<sup>[170]</sup> Currently, the Hummers method and its modified versions<sup>[166,171,172]</sup> are the most commonly employed methods to synthesize GO.

The less common methods of preparing GO involve direct oxidation of graphene layers via atomic oxygen in ultrahigh vacuum conditions,<sup>[173]</sup> photochemical reaction in ultraviolet light and oxygen,<sup>[174]</sup> or oxidation in nitric acid under potentiostatic conditions.<sup>[175]</sup>

Due to its disrupted  $\text{sp}^2$  bonding network, GO is an electrical insulator (with electrical conductivity  $<1\ \mu\text{S}/\text{m}$ ). This disruption is also reflected in the Raman spectra of GO, which present broadened characteristic peaks, low  $I_{2\text{D}}/I_{\text{G}}$  intensity ratios and a prominent D peak (Figure 6(a)). In order to increase the electrical conductivity of these 2D nanomaterials, GO can be reduced by a strong chemical reductant<sup>[176]</sup> or thermal reduction,<sup>[177]</sup> which results in the formation of rGO (Figure 6(b)). As a result of the deoxygenation process, the  $\pi$ -network is partially restored and recovers most of the electrical conductivity. The thermal properties are also improved as a result of the reduction process.<sup>[178]</sup> However, due to the residual oxygen functional groups, rGO does not exhibit the same electrical properties as those of pure graphene. Although the reduction process can bring GO’s optical and electrical properties closer to those of pristine graphene, it is still not enough to heal the vacancy defects.<sup>[179]</sup> One should note, however, that certain application can benefit from the presence of oxygen-containing functional groups. In the context of water purification, a prominent example of a potential practical application of GO, the oxygen-

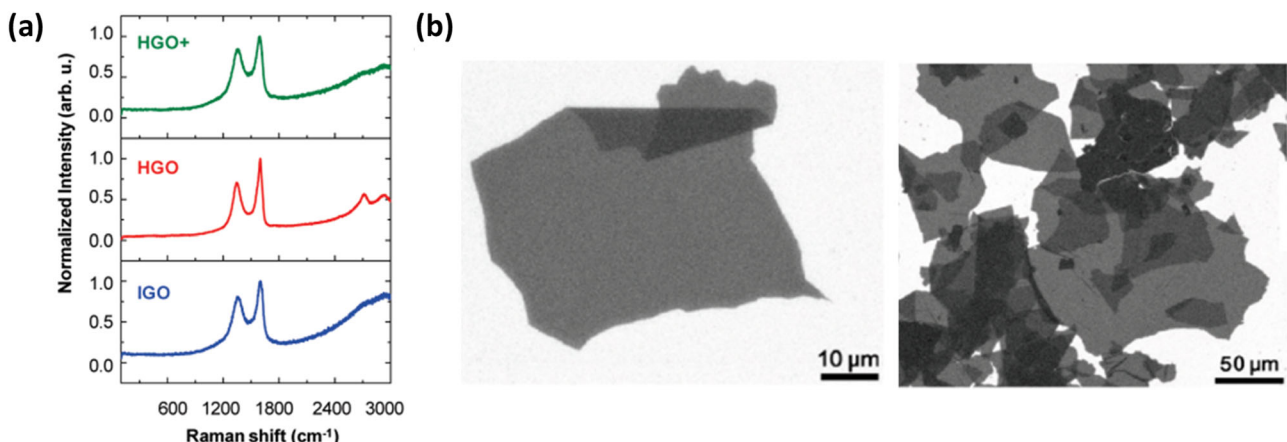


**Figure 6.** (a) Raman spectra of GO obtained by the Hummers method with additional KMnO<sub>4</sub> (HGO+), the conventional Hummers method (HGO) and the Hummers method utilizing H<sub>3</sub>PO<sub>4</sub> (IGO). Reprinted with permission from ref. [166]. Copyright 2010 American Chemical Society. (b) SEM images of chemically reduced GO (on a Si/SiO<sub>2</sub> substrate) obtained by the Hummers method utilizing H<sub>3</sub>PO<sub>4</sub>. Reprinted with permission from ref. [166]. Copyright 2010 American Chemical Society.

containing functional groups ensure sufficient inter-layer spacing in GO membranes, allowing capillary permeation of water through two-dimensional channels formed between the layers while maintaining impermeability toward gases such as He.<sup>[180]</sup> Such behavior has led to an increased interest in the use of GO membranes not only in water purification, but also in gas separation applications.<sup>[181]</sup>

#### 2.4. Other production methods

A method with potential to produce graphene with medium to high quality in moderate quantities relies on the atmospheric synthesis by microwave-sustained plasmas. This method was reported for the first time by Dato et al.<sup>[182]</sup> In this approach, the use of a substrate or a catalyst is not necessary, as the nucleation and growth of the graphene flakes take place within the gas phase. Complicated vacuum fixtures are also avoided in this open-air graphene synthesis alternative. The principle of the synthesis consists in the decomposition of the carbon precursor organic compounds (ex. ethanol) in a dense microwave argon plasma and the subsequent radical rearrangement into sp<sup>2</sup> coordinated carbon, along with CO and H<sub>2</sub> gaseous by-products. The material thus obtained is a ‘fluffy’ dark powder constituted by graphene sheets that show good structural quality when characterized by Raman, XPS and electron microscopy techniques, matching or even exceeding the best grade quality of liquid-phase exfoliated graphene.<sup>[183]</sup>

Although the yield of the process is pointed out as its major disadvantage, growth rates as high as 2 mg/min have been reported in a surface wave induced based reactor (surfatron) assisted with IR/UV

radiation excitation applied at the “cold” outlet gas flow section.<sup>[184]</sup> In fact, this does not scale as well as much higher throughput methods like liquid-phase exfoliation, but considering the higher structural quality of the atmospheric plasma graphene deposits, this technique may become an option.

Alternatively to the standard atmospheric microwave plasma torch set up in the seminal work by Dato et al.,<sup>[183]</sup> there are at least three types of reactors capable of depositing graphene, mainly differing in terms of the configuration through which the microwave plasma is sustained.

- i. Surfatron: a surfatron-based setup consists in creating a surface wave induced microwave configuration that enables maintaining a stable plasma in atmospheric pressure conditions.
- ii. TIAGO: a device constituted by a waveguide, whose central section is reduced in height, and a cylindrical hollow metallic rod placed perpendicularly, producing a jet conical flame plasma surrounded by the air around it.
- iii. Microwave slot antenna: a simple set up that allows initiating and maintaining atmospheric plasmas in H<sub>2</sub>/Ar mixtures.

Since this approach to produce graphene is relatively new, in the last years more groups have been devoting their workforce to the development of this technique.<sup>[185–187]</sup> Therefore, its full potential is not yet disclosed, and it is expected that graphene produced by microwave atmospheric plasmas will be soon reported embodying different applications, ranging from nanocomposites and energy storage devices to water purification or drug delivery systems.<sup>[183]</sup>

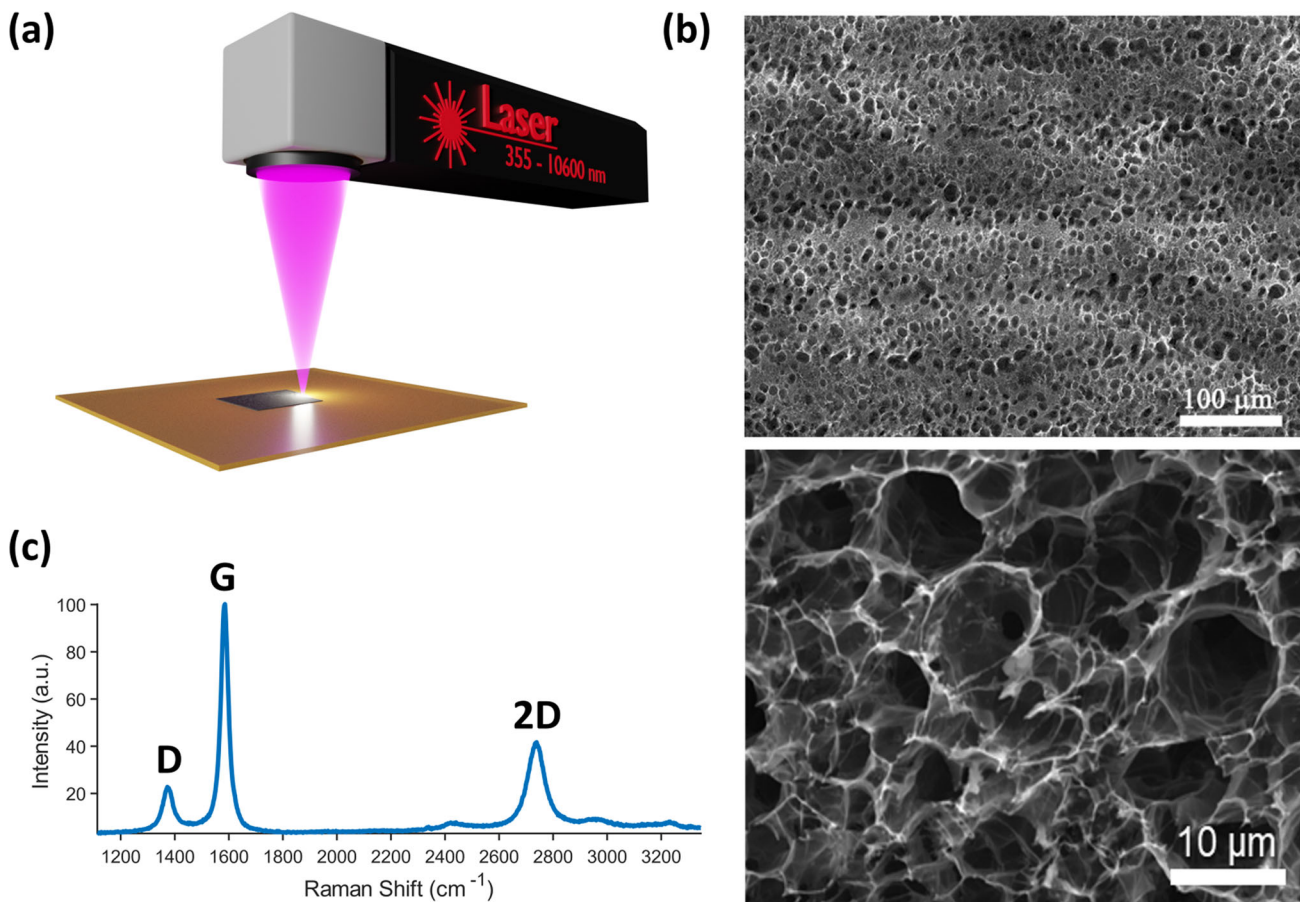


**Figure 7.** (a) Schematic illustration of the direct laser writing process for the synthesis of laser-induced graphene (LIG). (b) Secondary electron SEM images of LIG. (c) Typical Raman spectrum of LIG.

Laser processing is a powerful tool explored in different processes, since it is a rapid and efficient method to produce complex structures at different scales. Thus, nowadays, laser technology is being used to produce graphene-based materials, since there is a strong demand for cost-effective fabrication of graphene patterns with low energy consumption in a short fabrication time (Figure 7(a)). This novel one-step process was developed, in 2014, by Tour's group, and allows to obtain porous graphene-based structures through the incidence of a laser beam on a polymeric sheet at atmospheric conditions<sup>[188]</sup> (Figure 7(b)). The laser-induced graphene (LIG) technique enables to transform  $\text{sp}^3$  carbon present in the polymeric substrate into  $\text{sp}^2$  carbon<sup>[188]</sup> (Figure 7(c)). Laser irradiation can cause the increase of local temperature to produce LIG due to local decomposition and rearrangement of the precursor's structure.<sup>[189]</sup> Moreover, gas release during the reaction creates a 3D porous graphitic material. This photothermal effect was firstly produced by the incidence of an infrared  $\text{CO}_2$  laser beam on a commercial polymer polyimide

sheet,<sup>[188]</sup> but was further pursued by other authors using different laser sources (UV laser,<sup>[190]</sup> visible laser<sup>[191]</sup> and carbon precursor materials (wood, food, cork, paper, among others).<sup>[192,193]</sup>

Figure 7(b) shows that LIG has the appearance of a foam with a percolation network of porous multi-layer graphenes, which is associated with the localized high temperature and pressure produced by laser irradiation. The image puts in evidence the very high surface area of this material, comparable to that of the wet-chemistry derived 3D graphene.<sup>[192]</sup>

This direct laser writing process has emerged as a facile method enabling the synthesis of flexible, patternable and scalable graphene-based structures, and has many advantages, such as nontoxicity and controllability, envisioning large-scale catalyst free non-contact production and maskless patterning. In fact, LIG has become a multifunctional graphene foam, with many applications having been explored since it was discovered in 2014, such as: supercapacitors for energy storage devices,<sup>[188]</sup> electrochemical biosensors,<sup>[194,195]</sup> piezoresistive sensors,<sup>[190,196]</sup> water treatment

devices,<sup>[192]</sup> touch screens and antennas,<sup>[197]</sup> among others.

In another example of graphene production by laser, graphene films were obtained by coating a Ni substrate with graphite nanoparticles, followed by laser irradiation of the coated surface.<sup>[198]</sup> Carbon atoms from the graphite particles dissolve into Ni bulk under the action of laser-induced heating, and, subsequently, precipitate onto the surface, where the graphene film is formed. The obtained material presents Raman spectra characteristic of high crystalline quality graphene, with SLG accounting for 25% of the overall area of the film.

Novel and innovative ways of producing graphene are still arising in the literature. One outstanding example is that of Tour's group, who used a technique similar to flash sintering to produce graphene from organic waste in a fast and inexpensive way, with yields of 1 g per batch.<sup>[199]</sup>

### **3. Anti-corrosion coatings using graphene and graphene-based films**

Corrosion, the gradual degradation of metals and alloys as a result of chemical and/or electrochemical reactions with the surrounding environment, has an undeniable impact in terms of ecological health and economic loss. Material deteriorates, appearance is significantly altered, mechanical properties are lost and eventually the affected metallic parts end up losing their functionality. Protecting such structures is, therefore, of utmost importance.<sup>[14]</sup> Coating technology is among the plethora of approaches developed to provide protection to metallic surfaces and improve their quality. In addition to passive barrier properties and esthetic appearance, coating formulations can serve other functional purposes, such as an active self-healing action triggered by specific stimuli. When it comes to corrosion prevention, the key requirements of an ideal barrier coating system include an inherent resistance to degradation in hostile conditions, an effective resistance toward the permeation of corrosive agents and mechanical integrity over the desired life of the coated components. Conventional anti-corrosion coating technologies that involve, for instance, the use of hexavalent chromium connote a negative environmental impact given the carcinogenic risk of such compounds.<sup>[200]</sup> Furthermore, traditional approaches reveal several limitations, such as susceptibility to damage by heat, limited chemical stability, potentially high cost and the possibility of altering the physical properties of the metals being protected. Hence, there is a need for a disruptive eco-

friendly alternative in order to overcome the aforementioned roadblocks and achieve long-lasting corrosion mitigation.<sup>[200–202]</sup>

Graphene has emerged as a promising candidate due to its remarkable set of properties arisen from its unique structure. Being the barrier effect one of the most relevant characteristics in a multilayer system, much attention has been devoted to such material by virtue of its impermeability to fluids and gases. Apart from preventing the transport of corrosive or oxidative species toward the underlying substrate without notably altering its thermal conductivity and optical properties, graphene-based films enable a reduction of the applied layer in terms of quantity and volume. Besides, because of its chemical inertness, particularly regarding oxidation, **graphene is highly resistant** to corrosion in conditions under which other substances would undergo chemical transformations. However, despite this exceptional combination of features, the application of graphene in corrosion science appeared inconceivable, at first, since it was exclusively obtained via mechanical exfoliation, a low throughput, non-scalable method that renders graphene flakes smaller than 0.1 mm. Nonetheless, the discovery that not even the smallest atoms of helium can penetrate the dense lattice structure of graphene,<sup>[10]</sup> along with the first large-area syntheses of such material on copper substrates through CVD,<sup>[24]</sup> significantly altered this scenario. The seminal research conducted by Chen et al.,<sup>[203]</sup> in turn, can be considered the major turning point in the application of graphene as an anti-corrosive coating. Chen and coworkers unequivocally demonstrated, for the first time, the ability of CVD-grown graphene layers to protect refined metals in hostile environments over relatively short periods. Even though the early studies on the utilization of graphene in the field of corrosion prevention emerged later than those in other engineering fields, the number of citations is increasing at an accelerating pace, reflecting the quickly growing interest of corrosion scientists and engineers in this multipurpose material.<sup>[12,14,202,204]</sup> Research on graphene-based anti-corrosion technologies can be split into two generalized groups, pure graphene anti-corrosive coatings and composite graphene anti-corrosive coatings. The achievements regarding both types were reviewed by Tong et al.,<sup>[204]</sup> for example.

#### **3.1. Preparation methods and corrosion resistance performance**

The studies of Chen et al.<sup>[203]</sup> in 2011, on the ability of graphene films to protect metals from reactive

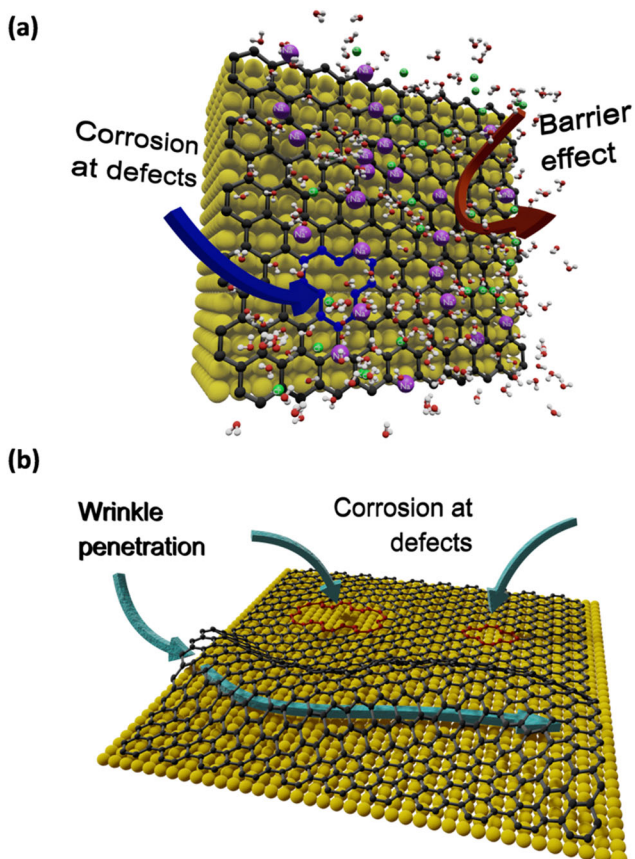


**Figure 8.** Schematic illustration of (a) the corrosion protection mechanism through barrier effect and (b) possible reasons for its failure.

environments, attracted considerable attention to applying both graphene and graphene oxide films as a protective layer due to their barrier effect. Several studies showed the benefit of applying graphene layers on the surface of metals, such as nickel alloys, copper alloys and steel.<sup>[205–207]</sup> The protective graphene layer could be prepared directly on the metal surface via methods such as CVD, electrophoretic deposition (EPD) and laser fabrication methods,<sup>[198]</sup> or could be transferred to the surface using a mechanical transfer technology. Among all the preparation techniques, CVD is the most commonly used method due to its simplicity, quality of the film and the ability to coat large areas.<sup>[13]</sup> The distance between the graphene film and the metal substrate largely affects the bonding strength between the graphene and the metal, and the graphene films prepared on different metals show different structures. It has been reported that the strength between the carbon atoms and copper, nickel and cobalt is weaker compared to gold, silver, and palladium.<sup>[208]</sup> Therefore, other techniques such as mechanical transfer have been reported to be applied to coat any metal materials with high-quality graphene films.

Anisur et al.<sup>[209]</sup> prepared graphene films on the surface of nickel via a CVD method and investigated the role of hydrogen flow and the cooling rate during graphene growth on the barrier properties and defect density of the film. Electrochemical impedance spectroscopy (EIS) and potentiodynamic tests on the samples immersed in a 0.1 M NaCl solution showed that graphene coatings prepared on Ni in an environment without H<sub>2</sub> flow offer nearly one order of magnitude superior corrosion resistance than that of uncoated Ni. SEM revealed that the hydrogen flow during the graphene growth facilitated wrinkle formation, resulting in a similar corrosion resistance to the uncoated Ni. Ye et al.<sup>[198]</sup> prepared graphene on Ni substrates, using a laser fabrication method at room temperature, showing the possibility of fabrication of large-area graphene films with superior anti-corrosion performance compared to the bare substrate.

In the study of Pu et al.,<sup>[207]</sup> a CVD method was used to coat stainless steel and nickel-plated stainless steel with graphene films. The SEM analysis showed 100% graphitization of the nickel-plated stainless steel, while for the stainless steel sample the SEM images showed a poor coverage of the graphene film on the substrate surface. The polarization curves also showed that the corrosion currents of the graphene coated nickel-plated stainless steel sample were one fifth of the bare nickel-plated stainless steel. In order to eliminate the complications of transferring grown graphene films to another substrate, different preparation techniques were applied in other studies. Ye et al.<sup>[210]</sup> employed a laser alloying process to form a Ni/Fe layer on the surface of carbon steel, followed by the growth of graphene films via laser irradiation. Anti-corrosion performance, including the results of polarization and EIS in 3.5% NaCl (aq) solutions, showed a significant improvement in the corrosion resistance of carbon steel, which is even superior to stainless steel. In another study, Quezada-Rentería et al.<sup>[211]</sup> applied the EPD technique to grow rGO films as an anti-corrosive coating on carbon steel, which showed a reduction of up to three times in the corrosion rate compared to the bared carbon steel.

Tiwari et al.<sup>[212]</sup> prepared graphene films on a copper surface using the CVD method. In order to increase the corrosion protection ability of the graphene films, a multilayer graphene coating was prepared. In this study a significant corrosion resistance in a 0.1 M NaCl solution was observed and the corrosion resistance was sustained for longer durations. This study showed that multilayer graphene could be effective in blocking the pathways of corrosive species to the metal surface. Raza

et al.<sup>[213]</sup> prepared GO films on copper substrates via an EPD method. The results showed control of coating thickness by varying the GO/water suspension concentrations and the voltage in the EPD process. EIS results also showed that the corrosion rate of GO film covered copper was six times lower than that of bare copper in 0.6 M NaCl solution. Hsieh et al.<sup>[214]</sup> applied the atomic layer deposition (ALD) technique to grow graphene films on copper to eliminate the structural defects in CVD-grown graphene, which resulted in an inhibition efficiency of more than 99%.

The main mechanism which allows graphene and graphene-based films and coatings to significantly reduce the corrosion rate of copper, nickel, and steel in aggressive solutions is the barrier effect (Figure 8(a)). The contact between the graphene film and the metal substrate makes it difficult for reactive agents such as oxygen and water to reach the metal surface. Thus, in order to have a long-lasting corrosion resistance and a high-quality film with a complete barrier effect, the film needs to fully cover the metal surface. There should also be a good adhesion between the graphene film and the substrate, with high resistance to wear and friction.

Nonetheless, although there are several reports showing promising results on the corrosion resistance of graphene-coated metals, recent studies have shown that graphene-coated metals could corrode at even greater rates than bare metals.<sup>[215]</sup> These considerable variations in results arise due to the lack of complete surface coverage, the presence of defects including wrinkles and cracks.<sup>[216,217]</sup> These defects are also the main reason for poor corrosion resistance in long-lasting applications (Figure 8(b)). Therefore, many researchers proposed that it was not practical to consider graphene films as a corrosion protective layer for long-term applications due to the difficulties in avoiding defects in the preparation process.<sup>[218]</sup> There are other studies that tried to improve the protective ability of the graphene films by repairing the defects via an atomic layer precipitation technology.<sup>[214]</sup> Some researchers have also shown that due to the high electrical conductivity of graphene it promotes electrochemical corrosion of metals.<sup>[215]</sup> It has been shown that in the damaged regions, graphene and metal form corrosion microcells. In such cases, metals such as copper, nickel, aluminum, magnesium, iron, or steel, act as the anode, promoting galvanic corrosion. In addition, the as-grown graphene layers are characterized by low adherence to the subjacent metal as a consequence of weak interaction.<sup>[200,202]</sup> Although some surface treatments and graphene

functionalization routes can improve the quality of coating adhesion, such measures may not be considered good enough for long term durability.

#### 4. Anti-corrosion composites using graphene and graphene-based materials

When performance is the absolute priority, the development of graphene-based nanocomposites is a promising route to trigger the commercialization of graphene-based coatings. The first studies of graphene-based composite coatings date from around 2012,<sup>[219]</sup> and since then such films have been applied to a broad range of substrates, such as aluminum, steel, brass and copper. The preparation methodology and coating procedure of such materials can be established based on the traditional coating production processes with controllable workability. The most relevant coating methodologies include lamination,<sup>[220]</sup> physical deposition or dispersion and subsequent curing,<sup>[221,222]</sup> self-assembly, layer-by-layer (LbL) deposition and the sol-gel method.<sup>[200]</sup>

##### 4.1. Dispersion in polymeric matrices

In coating applications, graphene and its derivatives have stood out as efficient fillers in polymer matrices to form hybrid films. Polymer nanocomposites provide superior features at a relatively low cost and the processing procedure is less complex when compared to multilayer coating systems. Moreover, polymer/graphene hybrids address other problematic issues, such as galvanic corrosion.<sup>[14,204]</sup> By utilizing graphene or its derivatives as nanometric fillers in the polymeric matrix, it is possible to lengthen the diffusion pathway of the corrosion medium in the coatings by taking advantage of its chemical inertness and barrier properties.<sup>[13]</sup> Graphene has heretofore been combined with a wide variety of polymeric materials, such as epoxy (EP),<sup>[223–253]</sup> polyurethane (PU),<sup>[254–259]</sup> polyaniline (PANI),<sup>[227,233,260–262]</sup> alkyd,<sup>[263]</sup> polystyrene (PS),<sup>[264]</sup> PMMA,<sup>[265,266]</sup> polyvinyl butyral (PVB) and<sup>[267,268]</sup> polydimethylsiloxane (PDMS).<sup>[269]</sup>

The lack of functional groups on the surface of pure graphene, its high surface area (and, consequently, high surface energy) and the Van der Waals interactions pose major challenges for the dispersion of graphene as filler particles in coating matrices, resulting in poor compatibility. Such factors contribute to the agglomeration of graphene sheets in aqueous media and organic matter, which in turn compromises the overall coating performance and

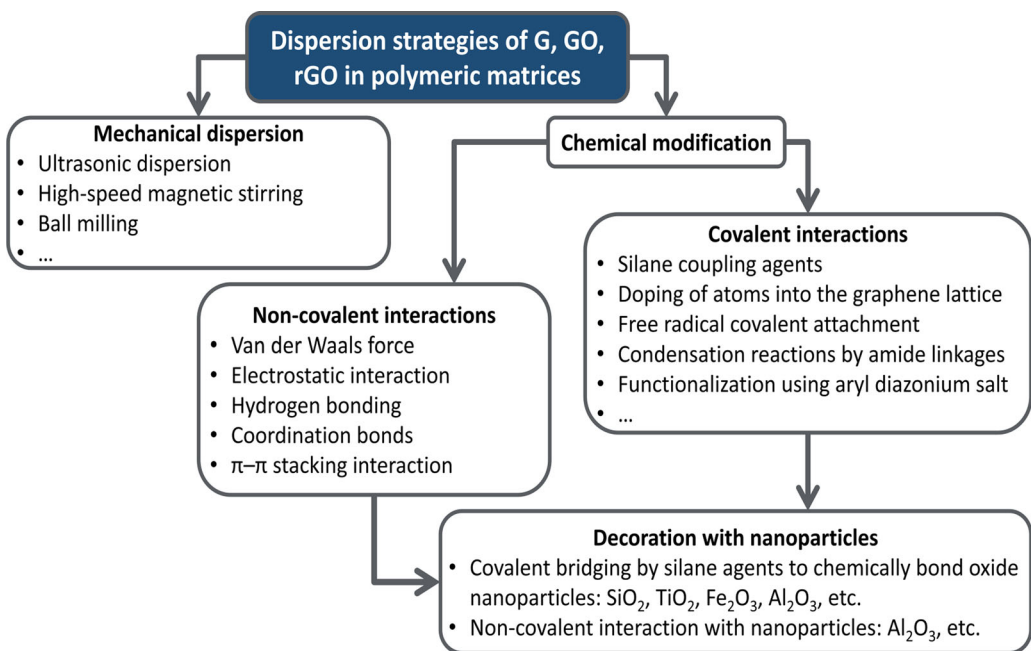


**Figure 9.** Different approaches for the dispersion of graphene and graphene-related materials in polymeric matrices.

undermines its corrosion resistance. The inclusion of graphene fillers in polymer matrices aims at hampering the diffusion of corrosive species through the coating, thus enhancing its barrier effect. However, their agglomeration has quite the opposite effect by providing direct diffusion pathways through the matrix. Thus, improving the dispersibility of graphene must be an utmost priority when developing graphene/polymer nanocomposites. And even though some researchers have simply incorporated unmodified graphene in polymeric matrices by way of physical means<sup>[224]</sup> or in situ polymerization,<sup>[270]</sup> the results were not considered ideal and such methods have proven suitable only for GO and rGO, due to the presence of epoxy and carboxyl groups on its surface.<sup>[271]</sup> To achieve improved dispersibility, two main (often complementary) approaches can be identified (Figure 9): mechanical dispersion and dispersion through chemical modification. The latter aims to affect the interaction between graphene or graphene-based materials and the polymeric matrix. These interactions can be either covalent or non-covalent. Moreover, decoration with nanoparticles is also common, often taking advantage of the modified interactions. In the context of mechanical dispersion, Chang et al.,<sup>[266]</sup> for example, prepared thermally reduced graphene oxides with varying carboxylic-group content, and found that higher amounts of carboxyl groups appeared to enhance the compatibility of these rGOs with the acrylic resin, thus improving their dispersion in the PMMA matrix. On the other hand, the

simple mechanical dispersion of unmodified single-layered GO in epoxy resin required vigorous mechanical mixing and intense sonication processes in order to effectively deagglomerate the GO sheets.<sup>[235]</sup>

The structural and chemical modification of graphene and graphene-based materials is among the most commonly used approaches to stabilize suspensions of such material in complex environments without agglomeration taking place. Surface functionalization can play an important role in achieving good interfacial bonding between graphene sheets and the surrounding matrices. Graphane, the fully hydrogenated analogue of graphene, was one of the first chemically modified graphene derivatives.<sup>[272,273]</sup> Aside from hydrogenation, the controlled oxidation of graphite flakes to generate hydrophilic GO and its selective reduction into hydrophobic rGO are also among the simplest routes to introduce surface functional groups onto graphene layers.<sup>[200]</sup> The chemical modification of graphene usually involves the use of coupling agents, such as silanes<sup>[239,240,244,246,252,256,257]</sup> and other common dispersants.<sup>[219,225–231,241,242,253,255,258,260,264,269]</sup> Generally, such additives contain both hydrophilic and organophilic functional groups, which can be combined with inorganic filler particles and organic coating matrices respectively. As a result, these compounds are able to improve the quality of the matrix/filler interactions and, consequently, enhance the overall performance of graphene/polymer composites.<sup>[12]</sup> The anti-corrosion properties of protective hybrid systems benefit from the incorporation of functionalized graphene and graphene-based nanostructures, given their ability to retard

**Table 5.** Chemical modification of graphene and graphene-based materials dispersed in polymer matrices.

Anti-corrosion system

Filler	Dispersing agent	Polymer matrix	Substrate	Ref.	Year
Graphene oxide	(3-Aminopropyl) triethoxysilane (APTES)	Epoxy resin	Steel	[246]	2017
Graphene oxide	g-(2,3-epoxypropoxy) propytrimethoxysilane (EPTES)	Epoxy resin	Carbon steel	[252]	2016
Graphene oxide	(3-Aminopropyl) triethoxysilane (APTES) and 3-glycidyloxypropyl trimethoxysilane (GPTMS)	Epoxy resin	Steel	[239]	2017
Graphene quantum dots	APTES	Epoxy resin	Steel	[240]	2018
Graphene-tannic acid	$\gamma$ -(2,3-epoxypropoxy)propytrimethoxysilane (KH560)	Epoxy resin	—	[244]	2019
Graphene and graphene oxide	APTES	PU	Iron	[256]	2015
Graphene	APTES	PU	Iron	[257]	2016
Graphene	4-aminobenzoic acid (ABA)	Polyaniline	Steel	[219]	2012
Reduced graphene oxide	PVP	Epoxy resin	Zinc	[253]	2015
Carbon nanotubes and graphene oxide	3-aminophenoxyphthalonitrile	Epoxy resin	Steel	[225]	2017
Graphene	Furan diepoxide (FdE)	Epoxy resin	Steel	[226]	2018
Graphene oxide	Polyaniline	Epoxy resin	Steel	[227]	2018
Graphene	Hydroxyl epoxy phosphate monomer (PGHEP)	Epoxy resin	Steel	[228]	2018
Graphene oxide	Polydopamine (PDA)	Epoxy resin	Steel	[229]	2018
Graphene oxide	p-phenylenediamine (PPDA)	Epoxy resin	Steel	[230]	2018
Graphene	Poly(2-butylaniline) (P2BA)	Epoxy resin	Steel	[241]	2017
Graphene oxide	N-(3-aminopropyl)-3-decylimidazole ionic liquid	Epoxy resin	Steel	[242]	2018
Reduced graphene oxide	Titanate coupling agent (TGO)	PU	Steel	[255]	2014
Reduced graphene oxide	Pernigraniline	Polyvinylbutyral	Copper	[260]	2014
Graphene oxide	p-phenylenediamine (PPD) and 4-vinylbenzoic acid	Polystyrene	Steel	[264]	2014
Graphene oxide	PPDA	Epoxy resin	Steel	[231]	2016
Graphene oxide	Polyisocyanate (PI)	PU	Steel	[258]	2015
Graphene	PDMS	Epoxy resin	Brass	[269]	2018

corrosion processes by restraining the diffusion of corrosive species. Table 5 compiles some of the most relevant research studies on the surface modification of graphene and its derivatives, either by coupling agents or other chemical reagents, over the past few years.

The synthesis of graphene-nanoparticle composites (G-NPs) is another route to improve the dispersibility of graphene-based materials in polymeric matrices and ensure the integrity of their structure. Several nanoparticles have been utilized for such purpose, as summarized in Table 6. In addition to their availability, mechanical properties and photo and thermal stability—among other appealing characteristics—these nanostructures increase the interlayer spacing between GO sheets, preventing their aggregation,<sup>[248,250]</sup> and may be employed to impart new functionalities to graphene-based nanocomposites, as will be covered in the following section. By taking advantage of the synergistic effects arising from the combination of both materials, it is possible to develop high-quality coatings with excellent properties. The three main strategies to fabricate G-NPs nanohybrids are the following: pre-graphenization, post-graphenization and syn-graphenization.<sup>[204]</sup> Pre-graphenization involves mixing the pre-synthesized graphene or its derivatives with the desired nanoparticles. In post-graphenization, the composite (graphene precursor and nanoparticles) is pre-prepared and the precursor is then converted to chemically reduced graphene. In syn-graphenization, the two components are synthesized simultaneously in a one-pot system.

#### 4.2. Functional incorporation in anti-corrosion composites

Nearly all the above-mentioned works have reached a unanimous conclusion: the superior performance of the obtained graphene-based composite coatings is unquestionably associated with the barrier effect provided by graphene or its derivatives. As previously noted, the unique impervious 2D structure of graphene imparts it with exceptional barrier properties toward all fluids and gases. The extremely small pores of its hexagonal lattice ensure minimal permeability even for the smallest atoms, i.e., He. Furthermore, the dense and delocalized electron cloud of the  $\pi$ -conjugated carbon network in graphene blocks the gap within its close packed aromatic rings and poses a repelling field to reactive atoms or molecules, thus providing a physical separation between the refined metal surface and environmental reactants. Hence, graphene can be understood as an impenetrable nanometric shield which can effectively isolate subjacent metal surfaces from invasive agents without altering their thermal conductivity and optical properties. By prolonging the infiltration path of corrosive media through the coating, graphene can greatly enhance its corrosion resistance and extend its service life.<sup>[12,200]</sup>

Let us take as an example the investigation carried out by Yu and coworkers<sup>[275]</sup> who exploited the impermeable nature of graphene to create a high-performance polymer/graphene sandwich-like anti-corrosive system. Given the paucity of reports on CVD-

**Table 6.** Nanoparticle-decorated graphene oxide dispersed in polymer matrices.

Anti-corrosion system	Polymer matrix	Substrate	Ref	Year
Nps/graphene-based nanofiller				
SiO <sub>2</sub> /graphene oxide	Epoxy resin	Steel	[234]	2016
SiO <sub>2</sub> /graphene oxide	Epoxy resin	Steel	[237]	2016
SiO <sub>2</sub> /graphene oxide	Epoxy resin	Steel	[247]	2017
Al <sub>2</sub> O <sub>3</sub> /graphene oxide	Epoxy resin	Steel	[274]	2015
Fe <sub>3</sub> O <sub>4</sub> /graphene oxide	Epoxy resin	Steel	[251]	2018
CaCO <sub>3</sub> /graphene oxide	Epoxy resin	Steel	[248]	2016
TiO <sub>2</sub> /graphene oxide	Epoxy resin	Steel	[249]	2015
□ -(2,3-epoxypropoxy)propyltrimethoxysilane (GPTMS)-modified TiO <sub>2</sub> /graphene oxide	Epoxy resin	Aluminum	[250]	2018
TiO <sub>2</sub> /graphene oxide	Epoxy resin	Steel	[238]	2016

grown graphene-based coatings able to provide long-term protection of metals, the authors aimed at developing a hybrid structure consisting of alternating SLG and PVB films on a commercial aerospace aluminum alloy (AA2024-T3). After comparing the effect of immersion in simulated seawater on uncoated AA2024, pure PVB-coated AA2024 and graphene/PVB-coated AA2024, the best electrochemical performance was assigned to the hybrid coating made up of two graphene layers sandwiched by three polymeric films (PVB/SLG/PVB/SLG/PVB). Such system entirely suppressed the deterioration of the aluminum substrate, the surface of which remained unaltered for up to 120 days of immersion in 3.5 wt% NaCl solution. In contrast, the graphene-free variants and the PVB/SLG/PVB system were able to provide corrosion protection only in the short-term (30 days), which clearly emphasized the dramatic improvement of the barrier properties of PVB coatings by inclusion of atomically thin graphene layers. Thus, Yu and his team managed to combine the adhesive and insulating properties of polymer films with the imperviousness of CVD-grown graphene sheets, while avoiding the latter's intrinsic drawbacks, such as poor adhesion and galvanic corrosion.

Fabricating impeccable, defect-free coatings is considered virtually impossible to achieve, since the formation of cracks is often unavoidable during their preparation. Such fissures pose menacing entry points for corrosive media to invade the metal, and once the aggressive species penetrate the metal, its corrosion resistance and structural integrity are jeopardized. If crack extension occurs, more vulnerable areas will be exposed, and severe localized corrosion may occur. In addition to its ability to hinder the penetration of corrosive agents through coatings due to its impermeable nature, graphene can effectively increase their fracture toughness, preventing crack propagation and the consequential ingress of threatening substances.<sup>[236,276,277]</sup> The mechanisms underpinning the effectiveness of graphene in hampering the expansion of existing cracks mainly involve the consumption of

the crack growth energy. When the crack reaches the graphene/matrix interface, the crack tip stress will cause interfacial debonding. Microcracks will be formed either around or in the graphene itself and will consume a significant amount of the original fracture energy. If external forces continue to intensify, crack deflection may occur through the deteriorated graphene. As the crack deviates from the original expansion direction and the propagation path is lengthened, the crack propagation resistance is increased. Moreover, the addition of graphene to crystalline and semicrystalline polymers can also affect their crystallization behavior, as shown by Zhang et al.<sup>[278]</sup> They prepared a transparent poly(lactic acid) (PLA) nanocomposite film reinforced with fully exfoliated octadecylamine-functionalized graphene (ODAG) as an effective nanofiller, by solution blending and casting method. Given the good compatibility between the two materials, ODAG could be uniformly dispersed in the PLA matrix and improved interfacial adhesion was achieved. In comparison with neat PLA, the obtained PLA/ODAG nanohybrid exhibited a 34% increase in tensile strength, 44% increase in Young's modulus, and 300% improvement in tensile toughness with the addition of only 0.4 wt% ODAG. The simultaneous improvement in mechanical strength and toughness could be attributed not only to the homogenous distribution of ODA-modified graphene across the PLA matrix, but also to the enhanced crystallization behavior of the thermoplastic polymer. The incorporation of ODAG facilitated the cold crystallization process of PLA and notably improved its crystallinity.

The effectiveness of corrosive-protective schemes relies heavily on the adhesion quality between the substrate and the deposited films and, therefore, it is imperative to ensure proper adhesion strength through the chemical bonds established between them. Apart from providing an effective barrier against the diffusion of water, oxygen and ions, functionalized graphene oxide can concurrently improve the adhesion strength between the organic coating

and the subjacent metal and, consequently, increase the degree of corrosion protection. Parhizkar et al.<sup>[279]</sup> used APTES to chemically alter the surface of graphene oxide and improve the adhesion and corrosion protection properties of an epoxy coating. Both were effectively enhanced by the deposition of a functionalized GO (fGO) film on the surface of steel prior to the application of the subsequent organic coating. Moreover, the cathodic delamination rate of the latter was decreased. The same group also studied the effect of 3-(Triethoxysilyl)propyl isocyanate (TEPI)- and APTES-functionalized GO nanofillers (IGO and AGO, respectively) embedded in sol-gel based silane films on the adhesion strength, corrosion protection and cathodic disbanding of the outermost epoxy coating applied on the silane-treated steel substrate.<sup>[280]</sup> While the incorporation of non-functionalized GO displayed no significant effect, the well-dispersed IGO and AGO inclusions significantly improved the adhesion quality and corrosion resistance of the topmost layer, due to their excellent barrier properties, good compatibility with the silane matrix and covalent bonds established with the epoxy coating.

In an example of the use of graphene-based materials to provide enhanced functionality to the anti-corrosion coating, Fan et al.<sup>[281]</sup> fabricated GO/Al<sub>2</sub>O<sub>3</sub> hybrids without the assistance of surfactants via two titration methods, wherein GO and Al<sub>2</sub>O<sub>3</sub> colloids were utilized as titrants for composites with low (1.23 to 1.92 wt.%) and high GO content (2.88 to 11.5 wt.%), respectively. After sintering by spark plasma sintering, FLG/Al<sub>2</sub>O<sub>3</sub> nanocomposites were obtained and GO was simultaneously reduced to rGO. A percolation threshold as low as 0.38 vol.% was achieved with a graphene content of 2.35 vol.%. Additionally, the electrical conductivity surpassed 10<sup>3</sup> S m<sup>-1</sup>. The most captivating finding, however, was related to the charge carrier type, which changed from p- to n-type with the increase in graphene content. Such conversion was attributed to the doping effect induced by the alumina matrix, which is thickness-dependent with respect to rGO.

The synergistic advantage of combining graphene derivatives and metal oxides was also explored by Song<sup>[282]</sup> and Jiao.<sup>[283]</sup> The former prepared Co<sub>3</sub>O<sub>4</sub>/rGO nanosheet composites through a facile hydrothermal route, by exploiting the electrostatic and coordination interaction between the individual negatively charged GO nanosheets and Co<sup>2+</sup> ions. The as-synthesized sheet-on-sheet nanohybrids exhibited good cyclic performance and coulomb efficiency with a specific capacitance over 402 F g<sup>-1</sup> at a current density of

0.5–2.0 A g<sup>-1</sup>, mainly as a result of the high porosity of the composite structure. In the latter case, a highly-ordered Fe<sub>3</sub>O<sub>4</sub>-graphite nanosheets/epoxy composite was obtained by tethering the magnetic nanoparticles onto the surface of graphite nanoplatelets, by wet-chemical precipitation method, and aligning the latter in the epoxy resin under a low magnetic field. The Fe<sub>3</sub>O<sub>4</sub>-modified graphite nanoplatelets were embedded in the EP matrix in such a highly oriented manner that its permeability dropped considerably and the gas barrier properties increased one order of magnitude compared to the blank EP and more than 65% compared to the randomly arranged graphite nanoplatelets/EP specimens.

### 4.3. Composites for active corrosion protection

The addition of chemically treated graphene to organic coatings can go beyond the mere improvement in adhesion and passive barrier properties. By intentionally altering graphene's structure with, for instance, corrosion inhibitors, highly efficient protective coatings can be developed. In order to overcome the presence of defects in epoxy coatings, metronidazole (MET)-modified graphene oxide nanocomposites (GME) were synthesized via a two-step method that involved grafting maleic anhydride (MA) on GO surface (GM),<sup>[232]</sup> followed by the covalent attachment of MET by the esterification mechanism. GME materials were shown to enhance epoxy films' corrosion protection performance at a low weight fraction of 0.2 wt%. Given that MET could be released from the GME hybrids and form an adsorption film, the scratched specimens were able to self-repair the damaged areas as a means to prolong the lifetime of the subjacent metallic structure.

The adsorptive behavior of *Urtica Dioica* (U.D) leaf extract on the graphene oxide nanosheets was examined by Nikpour et al.,<sup>[284]</sup> who investigated its influence on the corrosion inhibiting properties of an epoxy film. The achieved results revealed that the addition of GO-U.D and GO-U.D + Zn<sup>2+</sup> to the epoxy layer with an artificial defect improved the coating resistance to corrosion and decreased its delamination. It was also observed that the inhibition effect of GO-U.D sheets became more prominent in the presence of zinc cations. The chelation between the U.D molecules and Zn species led to the deposition of a protective film on the active anodic and cathodic sites of steel, and both electrochemical reactions were suppressed. The corrosion-inhibiting effect of green corrosion inhibitors (GIs) obtained from U.D leaves was

also explored by Ramezanzadeh and colleagues,<sup>[261]</sup> who utilized three-dimensional GO nanosheets as a platform to fabricate a protective system comprised of PANI nanofibers and the sustainable inhibiting agents. The GO-PANI-GI nanostructures were synthesized through a layer-by-layer assembly technique, and their anti-corrosive properties were analyzed in saline solutions on mild steel panels. The investigation confirmed that positively charged PANI strongly anchored to GO surface via physisorption mechanism, and GIs stabilized near protonated PANI through intermolecular H-bond interactions. This multilayered graphene-based nanocomposite demonstrated effective corrosion inhibition performance due to the adsorption of GI molecules on the anodic and cathodic sites and the passivation of steel surface in the presence of PANI fibers.

The corrosion resistance of aminoazobenzene- and diaminobenzene-functionalized graphene oxide composites (AAB-GO and DAB-GO, respectively) has also been examined, and it has been shown that both composites act as efficient corrosion-inhibiting agents by adsorbing on the mild steel surface and that their performance boosts with concentration.<sup>[285]</sup> It was also found that AAB-GO and DAB-GO act as mixed-type inhibitors, behaving predominantly in a cathodic manner. More recently, Sun and his team developed a facile CVD method to modify graphene nanosheets with molecular-sized polydimethylsiloxane.<sup>[269]</sup> The synthesized nanostructures were used to reinforce epoxy films, which displayed a coating resistance one order of magnitude higher than that of neat epoxy. PDMS-modified graphene nanosheets were able to enhance its performance at a loading as high as 5 wt%.

Qui et al.<sup>[243]</sup> synthesized FLG functionalized by poly (2-aminothiazole) (PAT) with free basal plane defects in organic solvent based on the  $\pi$ - $\pi$  interaction between them. In contrast to neat epoxy and PAT-based films, the coatings containing PAT/graphene hybrids displayed excellent corrosion performance and lower wear rate by dint of multifunctional graphene and passive effect of PAT, which acted both as a corrosion inhibitor and a lubricating agent.

Another strategy combining the passive barrier property of graphene and active inhibition functionality has been recently developed by Hou,<sup>[245]</sup> who proposed graphene oxide nanocontainers as a promising alternative to conventional capsule-based technologies, whose barrier effect is limited due to their spherical shape. The layer-by-layer self-assembled GO-based nanostructures, encapsulated with polymeric ionic

liquid (PIL), an environmentally friendly corrosion inhibitor, endowed the resulting container-impregnated epoxy composites with effective active inhibition function and superior barrier properties. While the embedded PIL could exert its corrosion-inhibiting effect at defected areas, the impermeable GO nanosheets provided passive protection by preventing the penetration of corrosive species through the coating.

Other functional integration approaches involve the modification of graphene to produce compounds able to react with the underlying metals to form chemical conversion layers. The investigations carried out by Taheri<sup>[262]</sup> and Ramezanzadeh<sup>[233]</sup> are cases in point. The authors modified negatively charged graphene oxide sheets with PANI nanofibers with zinc cations (GO-PANI-Zn) and cerium oxide (GO-PANI-CeO<sub>2</sub>), respectively, through a layer-by-layer assembly method. In the former case, zinc ions demonstrated electrostatic and cation- $\pi$  interactions with emeraldine base and salt forms of PANI. GO-PANI-Zn hybrids displayed improved thermal stability and active inhibition properties through adsorption of polyaniline as anodic and zinc cations as cathodic inhibitors, and consequent formation of a dense metal oxide passive layer. In addition, the results confirmed the high cation exchange capability of the synthesized nanostructures. Analogously, the excellent cation exchange ability of multifunctional GO-PANI-CeO<sub>2</sub> nanocomposites led to the creation of an adsorptive protective film on the metal surface and enhancement of barrier properties and corrosion inhibition performance of epoxy coatings.

The biomedical applications of graphene-based materials have also attracted ever-increasing interest, particularly the corrosion protection of metallic implants, such as Ti and its alloys, which can be deteriorated through wear and exposure to corrosive environments.<sup>[286]</sup> In this context, graphene-reinforced hydroxyapatite (HAp) biocomposites appear as a potential solution.<sup>[287,288]</sup> The incorporation of such materials as additives in HAp hybrids has been obtained through different approaches, namely biomimetic mineralization,<sup>[289,290]</sup> *in situ* synthesis,<sup>[291,292]</sup> electrospinning,<sup>[293]</sup> spark plasma sintering<sup>[294]</sup> and radio-frequency chemical vapor deposition.<sup>[295]</sup> Recent reports have investigated the potential of electrodeposited graphene-based HAp composites as improved protective schemes for Ti substrates.<sup>[287,288,296]</sup> These novel coatings exhibit not only enhanced mechanical performance and corrosion stability when compared to pure HAp films, but also superior bioactivity.

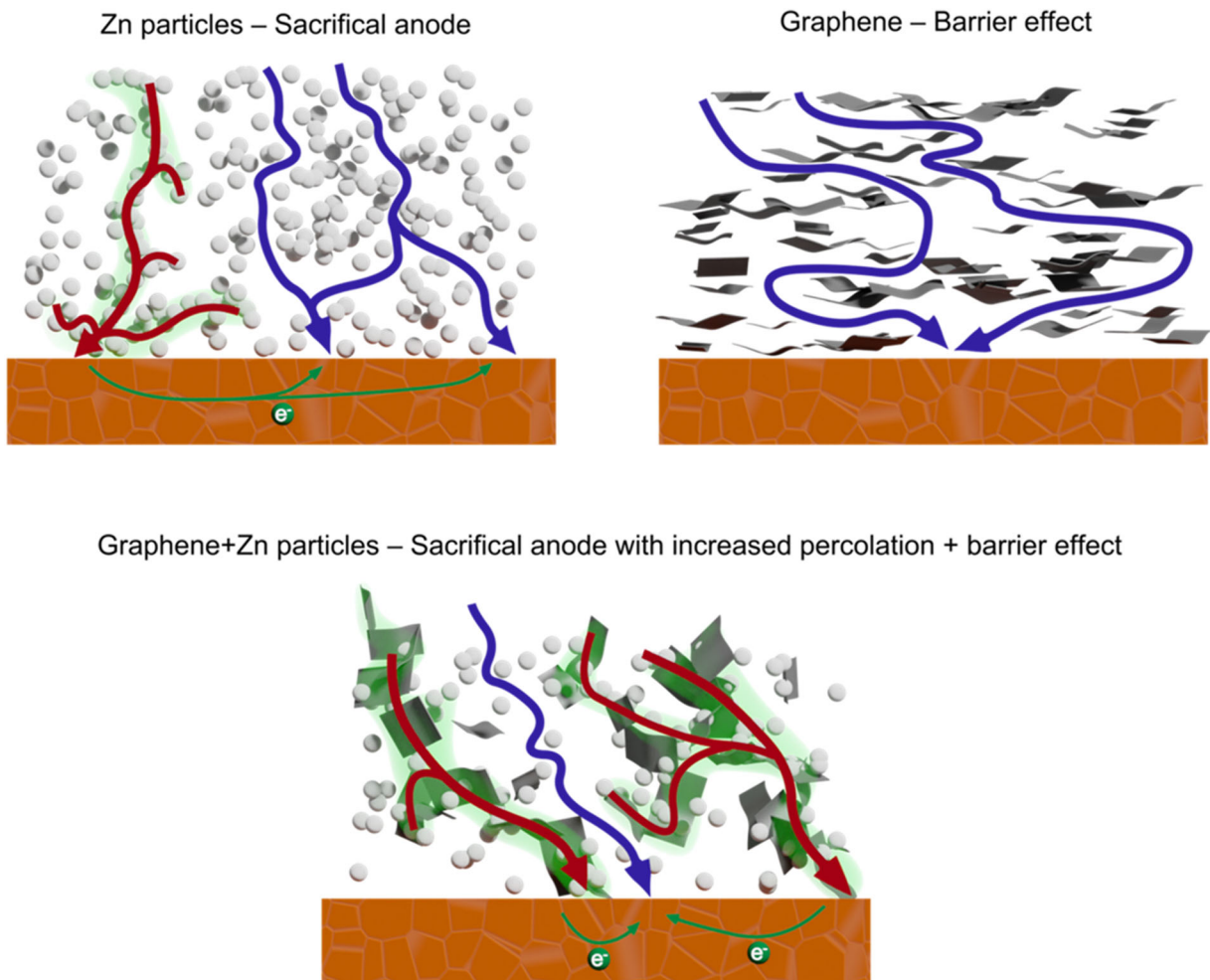


**Figure 10.** Schematic illustration of the enhancement of the sacrificial anode protection in zinc-rich coatings by graphene through increased percolation and the barrier effect.

Taking into consideration the fact that highly conductive graphene can aggravate localized corrosion at exposed metal-coating interfaces, several efforts have been made to suppress its undesired corrosion-promotion effect.<sup>[226,259,260,268]</sup> Contrarily, other authors have taken advantage of such feature to mitigate corrosion processes on metal surfaces by incorporating graphene-based conductive additives in organic coatings. Since the 1930s, zinc-rich coatings (ZRCs) have been extensively utilized for a multiplicity of industrial purposes under a wide range of hostile conditions. Such systems are able to protect metal substrates in the long term, even when slight mechanical damage occurs. Whilst the polymer matrix serves as a barrier toward corrosive agents, zinc particles provide cathodic protection by acting as sacrificial anodes. Given the electron pathway established between those particles and the underlying metal, a galvanic cell is formed, wherein the substrate behaves as cathode. Hence, the electron migration is suppressed, and corrosion processes are inhibited or retarded. Epoxy

binders stand out amongst the most commonly used binders for ZRCs by virtue of their remarkable mechanical and chemical resistance and high adhesive strength. Since such film-forming elements possess low electrical conductivity, a considerable load of zinc particles is required to ensure electric continuity and the occurrence of preferential galvanic corrosion of zinc. However, an overload of zinc powder may adversely affect the coating flexibility and adhesion to the substrate, and eventually compromise its performance. For this reason, the protective mechanisms of ZRCs strongly rely on the value of pigment volume concentration. On the other hand, when this value is lower than the critical pigment volume concentration, the barrier effect prevails over cathodic protection. In this regard, efforts have been made to enhance the electrical conductivity of ZRCs without it being necessary to increase the amount of zinc particles. An attractive option involves the utilization of carbon-based conductive fillers. The uniform distribution of graphene additives can greatly enhance both

percolation and barrier properties of ZRCs, when added in the proper amount. Several authors have focused on the impact of graphene and its derivatives on the corrosion resistance of ZRCs applied on steel<sup>[297–302]</sup> and iron<sup>[303]</sup> surfaces. The incorporation of graphene nanosheets into zinc-rich coatings can significantly enhance the role of the sacrificial anode (Figure 10). On one hand, the presence of graphene provides electrical continuity between zinc particles and the metallic substrate, thereby improving the percolation process with a lower amount of zinc pigments as compared with traditional ZRCs. On the other hand, graphene acts as a cathode and prevents the electrolyte from further permeating through the coating, seeking a cathodic counterpart for zinc powder particles. The resulting insoluble, non-conductive corrosion products effectively fill the permeation channel in the short term and, consequently, alleviate the diffusion of aggressive agents. Thus, the protective mechanism of zinc-rich epoxy coatings lies in the combination of barrier properties and cathodic protection.<sup>[12]</sup>

## 5. Critical analysis

In the previous sections different methods for production of graphene and graphene-based materials were presented and their application in the field of corrosion protection were described. In this final section, additional considerations are presented considering two main points: the availability and quality of graphene-based materials for the target application and what can be done further in terms of characterization to obtain additional information on the developed systems.

### 5.1. Production method vs. application

The development of practical graphene-based anti-corrosion solutions depends heavily on the ability to produce this material in an economically viable fashion, while possessing the required properties. For anti-corrosion coatings based on graphene films, CVD presents itself as the best option. Building on its ability to provide large area single- and few-layer graphene, the recent progress in regard to CVD has led to arbitrarily large films with a very low surface density of grain boundaries. This allows to address one of the main shortcomings of graphene film anti-corrosion coatings, which are the structural defects which make the underlying metal surface accessible to corrosive species from the surrounding environment.

However, CVD growth is mostly limited to transition metal substrates, most often in the form of a foil or a thin sheet. This limits its direct growth on other metals. A number of approaches to transfer graphene from the original transition metal to the desired substrate exist, but these tend to be rather laborious and incompatible with target substrates possessing a non-planar geometry, not to mention the associated concern of introducing cracks, tears and wrinkles in the graphene during the process. These would defeat the purpose of graphene as an impermeable barrier to the corrosive species.

As composite coatings with graphene are concerned, the most viable options seem to be the different types of high-throughput exfoliation. High shear stress exfoliation, for example, benefits from dispensing the use of intercalating agents, while requiring considerably less time to achieve the same amount of FLG as through sonication, also avoiding the introduction of basal plane defects often seen after ball milling. Electrochemical exfoliation has also seen a lot of progress and is perhaps one of the more easily scalable exfoliation techniques. However, all these approaches share some common shortcomings. The thickness (number of graphene layers) and the lateral dimensions of the obtained flakes are often hard to control. Besides, the use of appropriate solvents is usually required, either during or after the process, to aid in the exfoliation and to avoid re-aggregation, with the best suited ones being environmentally hazardous. Environmentally friendly alternatives are available, but further research is needed. One should also note that these exfoliation approaches are also adequate for anti-corrosion solutions based on non-composite coatings formed from graphene flake suspensions.

Composite coatings containing graphene-based materials such as GO or rGO, on the other hand, continue to rely on the Hummers method and its variations as the most commonly employed production approach. This type of material is particularly relevant when functionalization is required, as happens in the cases where the dispersibility of the graphene-based material in a polymeric matrix needs to be improved. There, GOs and rGOs benefit from the presence of oxygen containing groups on their surface. And even then, vigorous mechanical dispersion strategies need to be implemented.

This underlines one of the main issues concerning composite anti-corrosion coatings with graphene and graphene-based materials: the need for functionalization, particularly with the aim of improving its dispersibility in polymeric matrices. In this context, both covalent and non-covalent modification approaches have delivered some promising results, as have the

different strategies revolving around nanoparticle immobilization. It is worth pointing out, however, that most of these approaches use graphene oxide as the starting point, leaving plenty of room for further work in the development of reliable functionalization techniques of pristine graphene flakes.

One should also be aware that, independently of the type of the anti-corrosion coating, it is important that any future work in this field matches the employed graphene or graphene-based material to the role and characteristics that are expected from it, as there is a number of works which ascribe the properties of pristine graphene to other graphene-based materials, such as GO. Both categories of materials have a place in the field of anti-corrosion technology, but the requirements for each one of them can vary greatly. While certain applications may require, for example, an easily attainable functionalization of the graphene-based material, and, thus, the presence of oxygen containing groups can be beneficial, others can demand sufficient electrical conductivity, as in the case of zinc-rich coatings, where pristine graphene flakes may result in better anti-corrosion performance.

## **5.2. Challenges and guidelines for characterization of anti-corrosion coatings using graphene**

As described in sections 3 and 4, the contact between the graphene film and the metal substrate is of utmost importance for a long-lasting corrosion resistance. To achieve a maximal barrier effect under relevant service life conditions, a high-quality graphene film should fully cover the metal surface, despite their rough surfaces or curved shapes, while making it difficult for reactive agents such as oxygen and water to reach the metal surface. Therefore, a good adhesion between the graphene or graphene-based coating and the substrate, with high resistivity of this coating to wear and friction, is highly desirable.

The industry employs standardized methods to evaluate adhesion between coatings and substrates. As an example, the cross-cut tape test ASTM D3359 is widely used for ranking adhesion properties of coatings. Some works available in the literature have used this method to prove that organic coatings do not lose adhesion to the substrate upon modification by graphene-based materials.<sup>[304,305]</sup> Furthermore, evaluation of adhesion in laboratories is often carried out using pull-off tests following the ASTM D4541 standard. Parhizkar et al.<sup>[279,280]</sup> applied a pull-off method for testing adhesion properties of epoxy coatings deposited on the samples coated with a functionalized GO

film, with sol-gel coatings containing GO additives or functionalized GO having been used for adhesion promotion between the metal and the epoxy coating. The results demonstrated an improvement in adhesion strength of the coating systems containing GO modified with 3-(triethoxysilyl) propyl isocyanate and APTES silanes. These systems demonstrated cohesion failure at the modified GO-coating/epoxy interface, unlike the simple unmodified GO/epoxy system. This effect was attributed to NH<sub>2</sub> and NCO functional groups present in the modified GO that can create strong covalent bonding with the top epoxy coating.

Overall, in the circumstances where adhesion strength is in demand or may be compromised by the additives used in coating systems, an appropriate testing should be performed. Adhesion tests can reveal at which interface the adhesive failure occurs, thus indicating a potentially weak spot in the coating system. Proper measures can be developed afterwards in order to curb the weakness.

Another aspect lacking extensive coverage in the literature so far is the detailed analysis of diffusion in coatings modified with graphene and graphene-derived materials. Most of the works on coatings modified with graphene and its derivatives claim that the aforementioned additives offer protection against diffusion of corrosive species through the coating. In fact, methods such as EIS have been used for characterization of coated metals for decades. Impedance spectra taken from samples under immersion in different electrolytes contain valuable information concerning the properties of metal/polymer and metal/solution interfaces, as well as other properties of the coatings. Using an appropriate equivalent circuit model allows to extract different parameters and assess evolution of parameters in time. The capacitance of a coating can be easily extracted from impedance spectra,<sup>[306]</sup> and it depends on surface area, thickness and the dielectric constant of the coating. Moreover, the swelling of the coating can have an impact on the capacitance of the coating during immersion, as the latter will depend on the amount of water absorbed, due to it having a much larger dielectric constant than an organic coating.<sup>[307]</sup> A quantitative representation of water uptake by a coating was provided by the Brasher and Kingsbury equation,<sup>[308]</sup> which correlates water uptake to the coating's capacitance. Considering diffusion to be the main driving force for the water absorption, a particular solution of Fick's second law allows to obtain the diffusion coefficient.<sup>[309]</sup> Upon combining the Brasher and Kingsbury equation with the solution of Fick's second law a new equation is derived. It displays a linear dependence between the capacitance and the square root

of time during a short time of immersion when water uptake follows the Fickian diffusion. Diffusion coefficient of water is obtained from the slope of that dependence. Such an approach may be used to characterize organic coating systems containing graphene and its derivatives. However, this analysis is very demanding and requires careful impedance measurements and selection of correct equivalent circuit models for interpretation of EIS spectra.

In conclusion, like with any other type of material under scrutiny for industrial implementation, it is evident that graphene-like materials are not the only existing solution to address all the technological challenges in the field of protective coatings, especially in cases where more cost-effective additives exist and give similar performances.

However, it is undeniable that the studies available in the literature so far point to unique properties rendered by graphene and its derivatives which, together with the implementation of industrial processes to produce sufficient amounts of these nanostructured materials, will contribute to the generation of new solutions for corrosion protection in the forthcoming years.

## Acknowledgments

This work was developed within the scope of the projects: “GNESIS—Graphenest’s New Engineered System and its Implementation Solutions,” Project 33566 (POCI-01-0247-FEDER-033566), financed by the European Regional Development Fund (FEDER) through the Competitiveness and Internationalization Operational Program (POCI); and i3N Project (UIDB/50025/2020 & UIDP/50025/2020) and CICECO-Aveiro Institute of Materials (UIDB/50011/2020 & UIDP/50011/2020), both financed by national funds through the Portuguese Foundation for Science and Technology (Fundação para a Ciência e a Tecnologia, FCT I.P.) Bohdan Kulyk thanks Fundação para a Ciência e a Tecnologia (FCT I.P.) for the PhD grant SFRH/BD/141525/2018. Alexandre Carvalho thanks Fundação para a Ciência e a Tecnologia (FCT I.P.) for the PhD grant DAEPHYS-FCT PD/BD/114063/2015 and the funding from “Programa de Estímulo à Investigação 2016” from Fundação Calouste Gulbenkian. Kiryl Yasakau thanks Fundação para a Ciência e a Tecnologia (FCT I.P.) for the researcher grant IF/01284/2015. The authors also thank João França and Vitor Abrantes from Graphenest for their contribution in the framework of GNESIS project.

## Disclosure statement

The authors declare no conflict of interest.

## ORCID

Bohdan Kulyk  <http://orcid.org/0000-0002-0497-2216>

## References

- Novoselov, K. S.; Geim, A. K.; Morozov, S. V.; Jiang, D.; Zhang, Y.; Dubonos, S. V.; Grigorieva, I. V.; Firsov, A. A. Electric Field Effect in Atomically Thin Carbon Films. *Science* 2004, **306**, 666–669. doi:[10.1126/science.1102896](https://doi.org/10.1126/science.1102896)
- Bootlin, K. I.; Sikes, K. J.; Jiang, Z.; Klima, M.; Fudenberg, G.; Hone, J.; Kim, P.; Stormer, H. L. Ultrahigh Electron Mobility in Suspended Graphene. *Solid State Commun* 2008, **146**, 351–355. doi:[10.1016/j.ssc.2008.02.024](https://doi.org/10.1016/j.ssc.2008.02.024)
- Banszerus, L.; Schmitz, M.; Engels, S.; Dauber, J.; Oellers, M.; Haupt, F.; Watanabe, K.; Taniguchi, T.; Beschoten, B.; Stampfer, C. Ultrahigh-Mobility Graphene Devices from Chemical Vapor Deposition on Reusable Copper. *Sci. Adv.* 2015, **1**, e1500222. doi:[10.1126/sciadv.1500222](https://doi.org/10.1126/sciadv.1500222)
- Balandin, A. A.; Ghosh, S.; Bao, W.; Calizo, I.; Teweldebrhan, D.; Miao, F.; Lau, C. N. Superior Thermal Conductivity of Single-Layer Graphene. *Nano Lett.* 2008, **8**, 902–907. doi:[10.1021/nl0731872](https://doi.org/10.1021/nl0731872)
- Nika, D. L.; Balandin, A. A. Phonons and Thermal Transport in Graphene and Graphene-Based Materials. *Rep. Prog. Phys.* 2017, **80**, 036502. doi:[10.1088/1361-6633/80/3/036502](https://doi.org/10.1088/1361-6633/80/3/036502)
- Balandin, A. A. Phononics of Graphene and Related Materials. *ACS Nano*. 2020, **14**, 5170–5178. doi:[10.1021/acsnano.0c02718](https://doi.org/10.1021/acsnano.0c02718)
- Lee, C.; Wei, X.; Kysar, J. W.; Hone, J. Measurement of the Elastic Properties and Intrinsic Strength of Monolayer Graphene. *Science* 2008, **321**, 385–388. doi:[10.1126/science.1157996](https://doi.org/10.1126/science.1157996)
- Galvão, T. L. P.; Wilhelm, M.; Gomes, J. R. B.; Tedim, J. Emerging Trends in Smart Nanocontainers for Corrosion Applications. *Smart Nanocontainers* 2020, **163**, 385–398.
- Kozhukharov, S. V.; Samichkov, V. I.; Girginov, C. A.; Machkova, M. S. Actual Trends in the Elaboration of Advanced Multifunctional Coating Systems for the Efficient Protection of Lightweight Aircraft Alloys. *Corros. Rev.* 2017, **35**, 383–396. doi:[10.1515/corrrev-2017-0026](https://doi.org/10.1515/corrrev-2017-0026)
- Bunch, J. S.; Verbridge, S. S.; Alden, J. S.; van der Zande, A. M.; Parpia, J. M.; Craighead, H. G.; McEuen, P. L. Impermeable Atomic Membranes from Graphene Sheets. *Nano Lett.* 2008, **8**, 2458–2462. doi:[10.1021/nl801457b](https://doi.org/10.1021/nl801457b)
- Liu, L.; Ryu, S.; Tomaszik, M. R.; Stolyarova, E.; Jung, N.; Hybertsen, M. S.; Steigerwald, M. L.; Brus, L. E.; Flynn, G. W. Graphene Oxidation: Thickness-Dependent Etching and Strong Chemical Doping. *Nano Lett.* 2008, **8**, 1965–1970. doi:[10.1021/nl0808684](https://doi.org/10.1021/nl0808684)
- Cui, G.; Bi, Z.; Zhang, R.; Liu, J.; Yu, X.; Li, Z. A Comprehensive Review on Graphene-Based anti-Corrosive Coatings. *Chem. Eng. J.* 2019, **373**, 104–121. doi:[10.1016/j.cej.2019.05.034](https://doi.org/10.1016/j.cej.2019.05.034)
- Ding, R.; Li, W.; Wang, X.; Gui, T.; Li, B.; Han, P.; Tian, H.; Liu, A.; Wang, X.; Liu, X.; et al. A Brief Review of Corrosion Protective films and Coatings Based on Graphene and Graphene Oxide. *J. Alloys*

- Compd.* 2018, **764**, 1039–1055. doi:[10.1016/j.jallcom.2018.06.133](https://doi.org/10.1016/j.jallcom.2018.06.133)
14. Camilli, L.; Yu, F.; Cassidy, A.; Hornekaer, L.; Bøggild, P. Challenges for Continuous Graphene as a Corrosion Barrier. *2D Mater.* 2019, **6**, 022002. doi:[10.1088/2053-1583/ab04d4](https://doi.org/10.1088/2053-1583/ab04d4)
  15. Berger, C.; Song, Z.; Li, X.; Wu, X.; Brown, N.; Naud, C.; Mayou, D.; Li, T.; Hass, J.; Marchenkov, A. N.; et al. Electronic Confinement and Coherence in Patterned Epitaxial Graphene. *Science* 2006, **312**, 1191–1196. doi:[10.1126/science.1125925](https://doi.org/10.1126/science.1125925)
  16. Emtsev, K. V.; Bostwick, A.; Horn, K.; Jobst, J.; Kellogg, G. L.; Ley, L.; McChesney, J. L.; Ohta, T.; Reshanov, S. A.; Röhrl, J.; et al. Towards Wafer-Size Graphene Layers by Atmospheric Pressure Graphitization of Silicon Carbide. *Nat. Mater.* 2009, **8**, 203–207. doi:[10.1038/nmat2382](https://doi.org/10.1038/nmat2382)
  17. Emtsev, K. V.; Speck, F.; Seyller, T.; Ley, L.; Riley, J. D. Interaction, Growth, and Ordering of Epitaxial Graphene on SiC{0001} Surfaces: A Comparative Photoelectron Spectroscopy Study. *Phys. Rev. B* 2008, **77**, 1–10. doi:[10.1103/PhysRevB.77.155303](https://doi.org/10.1103/PhysRevB.77.155303)
  18. Hass, J.; Feng, R.; Li, T.; Li, X.; Zong, Z.; de Heer, W. A.; First, P. N.; Conrad, E. H.; Jeffrey, C. A.; Berger, C. Highly Ordered Graphene for Two Dimensional Electronics. *Appl. Phys. Lett.* 2006, **89**, 143106. doi:[10.1063/1.2358299](https://doi.org/10.1063/1.2358299)
  19. Ferrari, A. C.; Bonaccorso, F.; Fal'ko, V.; Novoselov, K. S.; Roche, S.; Bøggild, P.; Borini, S.; Koppens, F. H. L.; Palermo, V.; Pugno, N.; et al. Science and Technology Roadmap for Graphene, Related Two-Dimensional Crystals, and Hybrid Systems. *Nanoscale* 2015, **7**, 4598–4810. [Database] doi:[10.1039/c4nr01600a](https://doi.org/10.1039/c4nr01600a)
  20. Mishra, N.; Boeckl, J.; Motta, N.; Iacopi, F. Graphene Growth on Silicon Carbide: A Review. *Phys. Status Solidi A* 2016, **213**, 2277–2289. doi:[10.1002/pssa.201600091](https://doi.org/10.1002/pssa.201600091)
  21. Sutter, P. W.; Flege, J. I.; Sutter, E. A. Epitaxial Graphene on Ruthenium. *Nat. Mater.* 2008, **7**, 406–411. doi:[10.1038/nmat2166](https://doi.org/10.1038/nmat2166)
  22. Yu, Q.; Lian, J.; Siriponglert, S.; Li, H.; Chen, Y. P.; Pei, S.-S. Graphene Segregated on Ni Surfaces and Transferred to Insulators. *Appl. Phys. Lett.* 2008, **93**, 113103–113104. doi:[10.1063/1.2982585](https://doi.org/10.1063/1.2982585)
  23. Coraux, J.; N'Diaye, A. T.; Busse, C.; Michely, T. Structural Coherency of Graphene on Ir(111). *Nano Lett.* 2008, **8**, 565–570. doi:[10.1021/nl0728874](https://doi.org/10.1021/nl0728874)
  24. Li, X.; Cai, W.; An, J.; Kim, S.; Nah, J.; Yang, D.; Piner, R.; Velamakanni, A.; Jung, I.; Tutuc, E.; et al. Large-Area Synthesis of High-Quality and Uniform Graphene Films on Copper Foils. *Science* 2009, **324**, 1312–1314. doi:[10.1126/science.1171245](https://doi.org/10.1126/science.1171245)
  25. Kim, Y.; Song, W.; Lee, S. Y.; Jeon, C.; Jung, W.; Kim, M.; Park, C.-Y. Low-Temperature Synthesis of Large-Area Graphene-Based Transparent Conductive Films Using Surface Wave Plasma Chemical Vapor Deposition. *Appl. Phys. Lett.* 2011, **98**, 263106. doi:[10.1063/1.3561747](https://doi.org/10.1063/1.3561747)
  26. Kulyk, B.; Carvalho, A. F.; Fernandes, A. J. S.; Costa, F. M. Millimeter Sized Graphene Domains through in Situ Oxidation/Reduction Treatment of the Copper Substrate. *Carbon* 2020, **169**, 403–415. doi:[10.1016/j.carbon.2020.08.002](https://doi.org/10.1016/j.carbon.2020.08.002)
  27. Xu, X.; Zhang, Z.; Dong, J.; Yi, D.; Niu, J.; Wu, M.; Lin, L.; Yin, R.; Li, M.; Zhou, J.; et al. Ultrafast Epitaxial Growth of Metre-Sized Single-Crystal Graphene on Industrial Cu Foil. *Sci. Bull.* 2017, **62**, 1074–1080. doi:[10.1016/j.scib.2017.07.005](https://doi.org/10.1016/j.scib.2017.07.005)
  28. Muñoz, R.; Gómez-Aleixandre, C. Review of CVD Synthesis of Graphene. *Chem. Vap. Deposition* 2013, **19**, 297–322. doi:[10.1002/cvde.201300051](https://doi.org/10.1002/cvde.201300051)
  29. Suk, J. W.; Kitt, A.; Magnuson, C. W.; Hao, Y.; Ahmed, S.; An, J.; Swan, A. K.; Goldberg, B. B.; Ruoff, R. S. Transfer of CVD-Grown Monolayer Graphene onto Arbitrary Substrates. *ACS Nano* 2011, **5**, 6916–6924. doi:[10.1021/nn201207c](https://doi.org/10.1021/nn201207c)
  30. Li, X.; Zhu, Y.; Cai, W.; Borysiak, M.; Han, B.; Chen, D.; Piner, R. D.; Colombo, L.; Ruoff, R. S. Transfer of Large-Area Graphene Films for High-Performance Transparent Conductive Electrodes. *Nano Lett.* 2009, **9**, 4359–4363. doi:[10.1021/nl902623y](https://doi.org/10.1021/nl902623y)
  31. Wang, Y.; Zheng, Y.; Xu, X.; Dubuisson, E.; Bao, Q.; Lu, J.; Loh, K. P. Electrochemical Delamination of CVD Grown Graphene Film: Toward the Recyclable Use of Copper Catalyst SI. *ACS Nano* 2011, **5**, 9927–9910. doi:[10.1021/nn203700w](https://doi.org/10.1021/nn203700w)
  32. Banszerus, L.; Schmitz, M.; Engels, S.; Goldsche, M.; Watanabe, K.; Taniguchi, T.; Beschoten, B.; Stampfer, C. Ballistic Transport Exceeding 28 μm in CVD Grown Graphene. *Nano Lett.* 2016, **16**, 1387–1391. doi:[10.1021/acs.nanolett.5b04840](https://doi.org/10.1021/acs.nanolett.5b04840)
  33. Pirkle, A.; Chan, J.; Venugopal, A.; Hinojos, D.; Magnuson, C. W.; McDonnell, S.; Colombo, L.; Vogel, E. M.; Ruoff, R. S.; Wallace, R. M. The Effect of Chemical Residues on the Physical and Electrical Properties of Chemical Vapor Deposited Graphene Transferred to SiO<sub>2</sub>. *Appl. Phys. Lett.* 2011, **99**, 122108. doi:[10.1063/1.3643444](https://doi.org/10.1063/1.3643444)
  34. Chan, J.; Venugopal, A.; Pirkle, A.; McDonnell, S.; Hinojos, D.; Magnuson, C. W.; Ruoff, R. S.; Colombo, L.; Wallace, R. M.; Vogel, E. M. Reducing Extrinsic Performance-Limiting Factors in Graphene Grown by Chemical Vapor Deposition. *ACS Nano* 2012, **6**, 3224–3229. doi:[10.1021/nn300107f](https://doi.org/10.1021/nn300107f)
  35. Peltekis, N.; Kumar, S.; McEvoy, N.; Lee, K.; Weidlich, A.; Duesberg, G. S. The Effect of Downstream Plasma Treatments on Graphene Surfaces. *Carbon* 2012, **50**, 395–403. doi:[10.1016/j.carbon.2011.08.052](https://doi.org/10.1016/j.carbon.2011.08.052)
  36. Zhang, Z.; et al. Rosin-Enabled Ultraclean and Damage-Free Transfer of Graphene for Large-Area Flexible Organic Light-Emitting Diodes. *Nat. Commun.* 2017, **8**, 14560.
  37. Luo, D.; You, X.; Li, B.-W.; Chen, X.; Park, H. J.; Jung, M.; Ko, T. Y.; Wong, K.; Yousaf, M.; Chen, X.; et al. Role of Graphene in Water-Assisted Oxidation of Copper in Relation to Dry Transfer of Graphene. *Chem. Mater.* 2017, **29**, 4546–4556. doi:[10.1021/acs.chemmater.7b01276](https://doi.org/10.1021/acs.chemmater.7b01276)
  38. Hong, J.-Y.; Shin, Y. C.; Zubair, A.; Mao, Y.; Palacios, T.; Dresselhaus, M. S.; Kim, S. H.; Kong, J. A Rational Strategy for Graphene Transfer on

- Substrates with Rough Features. *Adv. Mater.* 2016, **28**, 2382–2392. doi:[10.1002/adma.201505527](https://doi.org/10.1002/adma.201505527)
39. Carvalho, A. F.; Fernandes, A. J. S.; Ben Hassine, M.; Ferreira, P.; Fortunato, E.; Costa, F. M. Millimeter-Sized Few-Layer Suspended Graphene Membranes. *Appl. Mater. Today* 2020, **21**, 100879. doi:[10.1016/j.apmt.2020.100879](https://doi.org/10.1016/j.apmt.2020.100879)
40. Ferrari, A. C.; Basko, D. M. Raman Spectroscopy as a Versatile Tool for Studying the Properties of Graphene. *Nat. Nanotechnol.* 2013, **8**, 235–246. doi:[10.1038/nnano.2013.46](https://doi.org/10.1038/nnano.2013.46)
41. Del Rio-Castillo, A. E.; Merino, C.; Díez-Barra, E.; Vázquez, E. Selective Suspension of Single Layer Graphene Mechanochemically Exfoliated from Carbon Nanofibres. *Nano Res.* 2014, **7**, 963–972. doi:[10.1007/s12274-014-0457-4](https://doi.org/10.1007/s12274-014-0457-4)
42. Jeon, I.-Y.; Choi, H.-J.; Jung, S.-M.; Seo, J.-M.; Kim, M.-J.; Dai, L.; Baek, J.-B. Large-Scale Production of Edge-Selectively Functionalized Graphene Nanoplatelets via Ball Milling and Their Use as Metal-Free Electrocatalysts for Oxygen Reduction Reaction. *J. Am. Chem. Soc.* 2013, **135**, 1386–1393. doi:[10.1021/ja3091643](https://doi.org/10.1021/ja3091643)
43. Yao, Y.; Lin, Z.; Li, Z.; Song, X.; Moon, K.-S.; Wong, C.-P. Large-Scale Production of Two-Dimensional Nanosheets. *J. Mater. Chem.* 2012, **22**, 13494–13499. doi:[10.1039/c2jm30587a](https://doi.org/10.1039/c2jm30587a)
44. Deng, S.; Qi, X.-d.; Zhu, Y.-l.; Zhou, H.-j.; Chen, F.; Fu, Q. A Facile Way to Large-Scale Production of Few-Layered Graphene via Planetary Ball Mill. *Chin. J. Polym. Sci.* 2016, **34**, 1270–1280. doi:[10.1007/s10118-016-1836-y](https://doi.org/10.1007/s10118-016-1836-y)
45. Al-Sherbini, A. S.; Bakr, M.; Ghoneim, I.; Saad, M. Exfoliation of Graphene Sheets via High Energy Wet Milling of Graphite in 2-Ethylhexanol and Kerosene. *J. Adv. Res.* 2017, **8**, 209–215. doi:[10.1016/j.jare.2017.01.004](https://doi.org/10.1016/j.jare.2017.01.004)
46. Li, X.; Shen, J.; Wu, C.; Wu, K. Ball-Mill-Exfoliated Graphene: Tunable Electrochemistry and Phenol Sensing. *Small* 2019, **15**, 1805567. doi:[10.1002/smll.201805567](https://doi.org/10.1002/smll.201805567)
47. Zhu, H.; Cao, Y.; Zhang, J.; Zhang, W.; Xu, Y.; Guo, J.; Yang, W.; Liu, J. One-Step Preparation of Graphene Nanosheets via Ball Milling of Graphite and the Application in Lithium-Ion Batteries. *J. Mater. Sci.* 2016, **51**, 3675–3683. doi:[10.1007/s10853-015-9655-z](https://doi.org/10.1007/s10853-015-9655-z)
48. Liu, L.; Xiong, Z.; Hu, D.; Wu, G.; Chen, P. Production of High Quality Single- or Few-Layered Graphene by Solid Exfoliation of Graphite in the Presence of Ammonia Borane. *Chem. Commun. (Camb.)* 2013, **49**, 7890–7892. doi:[10.1039/c3cc43670e](https://doi.org/10.1039/c3cc43670e)
49. Damm, C.; Nacken, T. J.; Peukert, W. Quantitative Evaluation of Delamination of Graphite by Wet Media Milling. *Carbon* 2015, **81**, 284–294. doi:[10.1016/j.carbon.2014.09.059](https://doi.org/10.1016/j.carbon.2014.09.059)
50. Knieke, C.; Berger, A.; Voigt, M.; Taylor, R. N. K.; Röhr, J.; Peukert, W. Scalable Production of Graphene Sheets by Mechanical Delamination. *Carbon* 2010, **48**, 3196–3204. doi:[10.1016/j.carbon.2010.05.003](https://doi.org/10.1016/j.carbon.2010.05.003)
51. Hernandez, Y.; Lotya, M.; Rickard, D.; Bergin, S. D.; Coleman, J. N. Measurement of Multicomponent Solubility Parameters for Graphene Facilitates Solvent Discovery. *Langmuir* 2010, **26**, 3208–3213. doi:[10.1021/la903188a](https://doi.org/10.1021/la903188a)
52. Suryanarayana, C. Mechanical Alloying and Milling. *Mech. Alloy. Milling* 2004, **46**, 1–472.
53. Xing, T.; Li, L. H.; Hou, L.; Hu, X.; Zhou, S.; Peter, R.; Petracic, M.; Chen, Y. Disorder in Ball-Milled Graphite Revealed by Raman Spectroscopy. *Carbon* 2013, **57**, 515–519. doi:[10.1016/j.carbon.2013.02.029](https://doi.org/10.1016/j.carbon.2013.02.029)
54. Welham, N. J.; Berbenni, V.; Chapman, P. G. Effect of Extended Ball Milling on Graphite. *J. Alloys Compd.* 2003, **349**, 255–263. doi:[10.1016/S0925-8388\(02\)00880-0](https://doi.org/10.1016/S0925-8388(02)00880-0)
55. Zhao, W.; Fang, M.; Wu, F.; Wu, H.; Wang, L.; Chen, G. Preparation of Graphene by Exfoliation of Graphite Using Wet Ball Milling. *J. Mater. Chem.* 2010, **20**, 5817–5819. doi:[10.1039/c0jm01354d](https://doi.org/10.1039/c0jm01354d)
56. Zhao, W.; Wu, F.; Wu, H.; Chen, G. Preparation of Colloidal Dispersions of Graphene Sheets in Organic Solvents by Using Ball Milling. *J. Nanomater.* 2010, **2010**, 1–5. doi:[10.1155/2010/528235](https://doi.org/10.1155/2010/528235)
57. Mao, M.; Chen, S.; He, P.; Zhang, H.; Liu, H. Facile and Economical Mass Production of Graphene Dispersions and Flakes. *J. Mater. Chem. A* 2014, **2**, 4132–4135. doi:[10.1039/C3TA14632D](https://doi.org/10.1039/C3TA14632D)
58. Kairi, M. I.; Dayou, S.; Kairi, N. I.; Bakar, S. A.; Vigolo, B.; Mohamed, A. R. Toward High Production of Graphene Flakes-a Review on Recent Developments in Their Synthesis Methods and Scalability. *J. Mater. Chem. A* 2018, **6**, 15010–15026. doi:[10.1039/C8TA04255A](https://doi.org/10.1039/C8TA04255A)
59. León, V.; Rodriguez, A. M.; Prieto, P.; Prato, M.; Vázquez, E. Exfoliation of Graphite with Triazine Derivatives under Ball-Milling Conditions: Preparation of Few-Layer Graphene via Selective Noncovalent Interactions. *ACS Nano.* 2014, **8**, 563–571. doi:[10.1021/nn405148t](https://doi.org/10.1021/nn405148t)
60. Yi, M.; Shen, Z. A Review on Mechanical Exfoliation for the Scalable Production of Graphene. *J. Mater. Chem. A* 2015, **3**, 11700–11715. doi:[10.1039/C5TA00252D](https://doi.org/10.1039/C5TA00252D)
61. Alinejad, B.; Mahmoodi, K. Synthesis of Graphene Nanoflakes by Grinding Natural Graphite Together with NaCl in a Planetary Ball Mill. *Funct. Mater. Lett.* 2017, **10**, 1750047. doi:[10.1142/S1793604717500473](https://doi.org/10.1142/S1793604717500473)
62. Lv, Y.; Yu, L.; Jiang, C.; Chen, S.; Nie, Z. Synthesis of Graphene Nanosheet Powder with Layer Number Control via a Soluble Salt-Assisted Route. *RSC Adv.* 2014, **4**, 13350–13354. doi:[10.1039/c3ra45060k](https://doi.org/10.1039/c3ra45060k)
63. Hernandez, Y.; Nicolosi, V.; Lotya, M.; Blighe, F. M.; Sun, Z.; De, S.; McGovern, I. T.; Holland, B.; Byrne, M.; Gun'Ko, Y. K.; et al. High-Yield Production of Graphene by Liquid-Phase Exfoliation of Graphite. *Nat. Nanotechnol.* 2008, **3**, 563–568. doi:[10.1038/nnano.2008.215](https://doi.org/10.1038/nnano.2008.215)
64. Khan, U.; O'Neill, A.; Lotya, M.; De, S.; Coleman, J. N. High-Concentration Solvent Exfoliation of Graphene. *Small* 2010, **6**, 864–871. doi:[10.1002/smll.200902066](https://doi.org/10.1002/smll.200902066)

65. Economopoulos, S. P.; Rotas, G.; Miyata, Y.; Shinohara, H.; Tagmatarchis, N. Exfoliation and Chemical Modification Using Microwave Irradiation Affording Highly Functionalized Graphene. *ACS Nano*. 2010, **4**, 7499–7507. doi:[10.1021/nn101735e](https://doi.org/10.1021/nn101735e)
66. Zhang, X.; Coleman, A. C.; Katsonis, N.; Browne, W. R.; van Wees, B. J.; Feringa, B. L. Dispersion of Graphene in Ethanol Using a Simple Solvent Exchange Method. *Chem. Commun. (Camb.)* 2010, **46**, 7539–7541. doi:[10.1039/c0cc02688c](https://doi.org/10.1039/c0cc02688c)
67. Hamilton, C. E.; Lomeda, J. R.; Sun, Z.; Tour, J. M.; Barron, A. R. High-Yield Organic Dispersions of Unfunctionalized Graphene. *Nano Lett.* 2009, **9**, 3460–3462. doi:[10.1021/nl9016623](https://doi.org/10.1021/nl9016623)
68. Hasan, T.; Torrisi, F.; Sun, Z.; Popa, D.; Nicolosi, V.; Privitera, G.; Bonaccorso, F.; Ferrari, A. C. Solution-Phase Exfoliation of Graphite for Ultrafast Photonics. *Phys. stat. sol. (b)* 2010, **247**, 2953–2957. doi:[10.1002/pssb.201000339](https://doi.org/10.1002/pssb.201000339)
69. Bourlinos, A. B.; Georgakilas, V.; Zboril, R.; Sterioti, T. A.; Stubos, A. K. Liquid-Phase Exfoliation of Graphite towards Solubilized Graphenes. *Small* 2009, **5**, 1841–1845. doi:[10.1002/smll.200900242](https://doi.org/10.1002/smll.200900242)
70. Zhang, M.; Parajuli, R. R.; Mastrogiovanni, D.; Dai, B.; Lo, P.; Cheung, W.; Brukh, R.; Chiu, P. L.; Zhou, T.; Liu, Z.; et al. Production of Graphene Sheets by Direct Dispersion with Aromatic Healing Agents. *Small* 2010, **6**, 1100–1107. doi:[10.1002/smll.200901978](https://doi.org/10.1002/smll.200901978)
71. An, X.; Simmons, T.; Shah, R.; Wolfe, C.; Lewis, K. M.; Washington, M.; Nayak, S. K.; Talapatra, S.; Kar, S. Stable Aqueous Dispersions of Noncovalently Functionalized Graphene from Graphite and Their Multifunctional High-Performance Applications. *Nano Lett.* 2010, **10**, 4295–4301. doi:[10.1021/nl903557p](https://doi.org/10.1021/nl903557p)
72. Bose, S.; Kuila, T.; Mishra, A. K.; Kim, N. H.; Lee, J. H. Preparation of Non-Covalently Functionalized Graphene Using 9-Anthracene Carboxylic Acid. *Nanotechnology* 2011, **22**, 405603. doi:[10.1088/0957-4484/22/40/405603](https://doi.org/10.1088/0957-4484/22/40/405603)
73. O'Neill, A.; Khan, U.; Nirmalraj, P. N.; Boland, J.; Coleman, J. N. Graphene Dispersion and Exfoliation in Low Boiling Point Solvents. *J. Phys. Chem. C* 2011, **115**, 5422–5428. doi:[10.1021/jp110942e](https://doi.org/10.1021/jp110942e)
74. Lotya, M.; Hernandez, Y.; King, P. J.; Smith, R. J.; Nicolosi, V.; Karlsson, L. S.; Blighe, F. M.; De, S.; Wang, Z.; McGovern, I. T.; et al. Liquid Phase Production of Graphene by Exfoliation of Graphite in Surfactant/Water Solutions. *J. Am. Chem. Soc.* 2009, **131**, 3611–3620. doi:[10.1021/ja807449u](https://doi.org/10.1021/ja807449u)
75. Maragó, O. M.; Bonaccorso, F.; Saija, R.; Privitera, G.; Gucciardi, P. G.; Iatì, M. A.; Calogero, G.; Jones, P. H.; Borghese, F.; Denti, P.; et al. Brownian Motion of Graphene. *ACS Nano*. 2010, **4**, 7515–7523. doi:[10.1021/nn1018126](https://doi.org/10.1021/nn1018126)
76. Guardia, L.; Fernández-Merino, M. J.; Paredes, J. I.; Solís-Fernández, P.; Villar-Rodil, S.; Martínez-Alonso, A.; Tascon, J. M. D. High-Throughput Production of Pristine Graphene in an Aqueous Dispersion Assisted by Non-Ionic Surfactants. *Carbon* 2011, **49**, 1653–1662. doi:[10.1016/j.carbon.2010.12.049](https://doi.org/10.1016/j.carbon.2010.12.049)
77. Nuvoli, D.; Valentini, L.; Alzari, V.; Scognamillo, S.; Bon, S. B.; Piccinini, M.; Illescas, J.; Mariani, A. High Concentration Few-Layer Graphene Sheets Obtained by Liquid Phase Exfoliation of Graphite in Ionic Liquid. *J. Mater. Chem.* 2011, **21**, 3428–3431. doi:[10.1039/C0JM02461A](https://doi.org/10.1039/C0JM02461A)
78. Green, A. A.; Hersam, M. C. Solution Phase Production of Graphene with Controlled Thickness via Density Differentiation. *Nano Lett.* 2009, **9**, 4031–4036. doi:[10.1021/nl902200b](https://doi.org/10.1021/nl902200b)
79. Zhuo, H.; Zhang, X.; Wang, L.; Lu, Q.; Kaplan, D. L. Sonication Exfoliation of Defect-Free Graphene in Aqueous Silk Nanofiber Solutions. *ACS Sustainable Chem. Eng.* 2018, **6**, 12261–12267. doi:[10.1021/acssuschemeng.8b02644](https://doi.org/10.1021/acssuschemeng.8b02644)
80. Sun, Z.; Huang, X.; Liu, F.; Yang, X.; Rösler, C.; Fischer, R. A.; Muhrer, M.; Schuhmann, W. Amine-Based Solvents for Exfoliating Graphite to Graphene Outperform the Dispersing Capacity of N-Methyl-Pyrrolidone and Surfactants. *Chem. Commun. (Camb.)* 2014, **50**, 10382–10385. doi:[10.1039/c4cc03923h](https://doi.org/10.1039/c4cc03923h)
81. Dong, X.; Shi, Y.; Zhao, Y.; Chen, D.; Ye, J.; Yao, Y.; Gao, F.; Ni, Z.; Yu, T.; Shen, Z.; et al. Symmetry Breaking of Graphene Monolayers by Molecular Decoration. *Phys. Rev. Lett.* 2009, **102**, 1–4. doi:[10.1103/PhysRevLett.102.135501](https://doi.org/10.1103/PhysRevLett.102.135501)
82. Notley, S. M. Highly Concentrated Aqueous Suspensions of Graphene through Ultrasonic Exfoliation with Continuous Surfactant Addition. *Langmuir* 2012, **28**, 14110–14113. doi:[10.1021/la302750e](https://doi.org/10.1021/la302750e)
83. Zheng, X.; Xu, Q.; Li, J.; Li, L.; Wei, J. High-Throughput, Direct Exfoliation of Graphite to Graphene via a Cooperation of Supercritical CO<sub>2</sub> and Pyrene-Polymers. *RSC Adv.* 2012, **2**, 10632–10638. doi:[10.1039/c2ra21316h](https://doi.org/10.1039/c2ra21316h)
84. Sampath, S.; Basuray, A. N.; Hartlieb, K. J.; Aytun, T.; Stupp, S. I.; Stoddart, J. F. Direct Exfoliation of Graphite to Graphene in Aqueous Media with Diazaperopyrenium Dications. *Adv. Mater.* 2013, **25**, 2740–2745. doi:[10.1002/adma.201205157](https://doi.org/10.1002/adma.201205157)
85. Englert, J. M.; Röhrl, J.; Schmidt, C. D.; Graupner, R.; Hundhausen, M.; Hauke, F.; Hirsch, A. Soluble Graphene: Generation of Aqueous Graphene Solutions Aided by a Perylenebisimide-Based Bolaamphiphile. *Adv. Mater.* 2009, **21**, 4265–4269. doi:[10.1002/adma.200901578](https://doi.org/10.1002/adma.200901578)
86. Štengl, V. Preparation of Graphene by Using an Intense Cavitation Field in a Pressurized Ultrasonic Reactor. *Chem. Eur. J.* 2012, **18**, 14047–14054. doi:[10.1002/chem.201201411](https://doi.org/10.1002/chem.201201411)
87. Bang, G. S.; So, H. M.; Lee, M. J.; Ahn, C. W. Preparation of Graphene with Few Defects Using Expanded Graphite and Rose Bengal. *J. Mater. Chem.* 2012, **22**, 4806–4810. doi:[10.1039/c2jm14205h](https://doi.org/10.1039/c2jm14205h)
88. Bourlinos, A. B.; Georgakilas, V.; Zboril, R.; Steriotis, T. A.; Stubos, A. K.; Trapalis, C. Aqueous-Phase Exfoliation of Graphite in the Presence of Polyvinylpyrrolidone for the Production of Water-

- Soluble Graphenes. *Solid State Commun.* 2009, **149**, 2172–2176. doi:[10.1016/j.ssc.2009.09.018](https://doi.org/10.1016/j.ssc.2009.09.018)
89. Liang, Y. T.; Hersam, M. C. Highly Concentrated Graphene Solutions via Polymer Enhanced Solvent Exfoliation and Iterative Solvent Exchange. *J. Am. Chem. Soc.* 2010, **132**, 17661–17663. doi:[10.1021/ja107661g](https://doi.org/10.1021/ja107661g)
90. Liu, W.; Zhou, R.; Zhou, D.; Ding, G.; Soah, J. M.; Yue, C. Y.; Lu, X. Lignin-Assisted Direct Exfoliation of Graphite to Graphene in Aqueous Media and Its Application in Polymer Composites. *Carbon* 2015, **83**, 188–197. doi:[10.1016/j.carbon.2014.11.036](https://doi.org/10.1016/j.carbon.2014.11.036)
91. Chen, X.; Dobson, J. F.; Raston, C. L. Vortex Fluidic Exfoliation of Graphite and Boron Nitride. *Chem. Commun. (Camb.)* 2012, **48**, 3703–3705. doi:[10.1039/c2cc17611d](https://doi.org/10.1039/c2cc17611d)
92. Wahid, M. H.; Eroglu, E.; Chen, X.; Smith, S. M.; Raston, C. L. Functional Multi-Layer Graphene-Algae Hybrid Material Formed Using Vortex Fluidics. *Green Chem.* 2013, **15**, 650–655. doi:[10.1039/c2gc36892g](https://doi.org/10.1039/c2gc36892g)
93. Liang, S.; Yi, M.; Shen, Z.; Liu, L.; Zhang, X.; Ma, S. One-Step Green Synthesis of Graphene Nanomesh by Fluid-Based Method. *RSC Adv.* 2014, **4**, 16127–16131. doi:[10.1039/C4RA01250J](https://doi.org/10.1039/C4RA01250J)
94. Yi, M.; Shen, Z.; Zhang, W.; Zhu, J.; Liu, L.; Liang, S.; Zhang, X.; Ma, S. Hydrodynamics-Assisted Scalable Production of Boron Nitride Nanosheets and Their Application in Improving Oxygen-Atom Erosion Resistance of Polymeric Composites. *Nanoscale* 2013, **5**, 10660–10667. doi:[10.1039/c3nr03714b](https://doi.org/10.1039/c3nr03714b)
95. Blomquist, N.; et al. Effects of Geometry on Large-Scale Tube-Shear Exfoliation of Graphite to Multilayer Graphene and Nanographite in Water. *Sci. Rep.* 2019, **9**, 1–8.
96. Zhang, K.; Tang, J.; Yuan, J.; Li, J.; Sun, Y.; Matsuba, Y.; Zhu, D.-M.; Qin, L.-C. Production of Few-Layer Graphene via Enhanced High-Pressure Shear Exfoliation in Liquid for Supercapacitor Applications. *ACS Appl. Nano Mater.* 2018, **1**, 2877–2884. doi:[10.1021/acsanm.8b00515](https://doi.org/10.1021/acsanm.8b00515)
97. Zhang, Z.; Jin, H.; Miao, X.; Ju, T.; Li, Y.; Ji, J. Gas-Driven Exfoliation for Producing High-Quality Graphene. *Chem. Commun. (Camb.)* 2019, **55**, 7749–7751. doi:[10.1039/c9cc03159f](https://doi.org/10.1039/c9cc03159f)
98. Paton, K. R.; Varrla, E.; Backes, C.; Smith, R. J.; Khan, U.; O'Neill, A.; Boland, C.; Lotya, M.; Istrate, O. M.; King, P.; et al. Scalable Production of Large Quantities of Defect-Free Few-Layer Graphene by Shear Exfoliation in Liquids. *Nat. Mater.* 2014, **13**, 624–630. doi:[10.1038/nmat3944](https://doi.org/10.1038/nmat3944)
99. Xu, Y.; Cao, H.; Xue, Y.; Li, B.; Cai, W. Liquid-Phase Exfoliation of Graphene: An Overview on Exfoliation Media, Techniques, and Challenges. *Nanomaterials* 2018, **8**, 942. doi:[10.3390/nano8110942](https://doi.org/10.3390/nano8110942)
100. Tian, J.; Guo, L.; Yin, X.; Wu, W. The Liquid-Phase Preparation of Graphene by Shear Exfoliation with Graphite Oxide as a Dispersant. *Mater. Chem. Phys.* 2019, **223**, 1–8. doi:[10.1016/j.matchemphys.2018.10.039](https://doi.org/10.1016/j.matchemphys.2018.10.039)
101. Yi, M.; Shen, Z. Kitchen Blender for Producing High-Quality Few-Layer Graphene. *Carbon* 2014, **78**, 622–626. doi:[10.1016/j.carbon.2014.07.035](https://doi.org/10.1016/j.carbon.2014.07.035)
102. Varrla, E.; Paton, K. R.; Backes, C.; Harvey, A.; Smith, R. J.; McCauley, J.; Coleman, J. N. Turbulence-Assisted Shear Exfoliation of Graphene Using Household Detergent and a Kitchen Blender. *Nanoscale* 2014, **6**, 11810–11819. doi:[10.1039/c4nr03560g](https://doi.org/10.1039/c4nr03560g)
103. Liu, L.; Shen, Z.; Yi, M.; Zhang, X.; Ma, S. A Green, Rapid and Size-Controlled Production of High-Quality Graphene Sheets by Hydrodynamic Forces. *RSC Adv.* 2014, **4**, 36464–36470. doi:[10.1039/C4RA05635C](https://doi.org/10.1039/C4RA05635C)
104. Ismail, Z.; Kassim, N. F. A.; Abdullah, A. H.; Abidin, A. S. Z.; Ismail, F. S.; Yusoh, K. Black Tea Assisted Exfoliation Using a Kitchen Mixer Allowing One-Step Production of Graphene. *Mater. Res. Express* 2017, **4**, 075607. doi:[10.1088/2053-1591/aa7ae2](https://doi.org/10.1088/2053-1591/aa7ae2)
105. Tran, T. S.; Park, S. J.; Yoo, S. S.; Lee, T. R.; Kim, T. Y. High Shear-Induced Exfoliation of Graphite into High Quality Graphene by Taylor-Couette Flow. *RSC Adv.* 2016, **6**, 12003–12008. doi:[10.1039/C5RA22273G](https://doi.org/10.1039/C5RA22273G)
106. Bjerglund, E. T.; Kristensen, M. E. P.; Stambula, S.; Botton, G. A.; Pedersen, S. U.; Daasbjerg, K. Efficient Graphene Production by Combined Bipolar Electrochemical Intercalation and High-Shear Exfoliation. *ACS Omega* 2017, **2**, 6492–6499. doi:[10.1021/acsomega.7b01057](https://doi.org/10.1021/acsomega.7b01057)
107. Phiri, J.; Gane, P.; Maloney, T. C. High-Concentration Shear-Exfoliated Colloidal Dispersion of Surfactant-Polymer-Stabilized Few-Layer Graphene Sheets. *J. Mater. Sci.* 2017, **52**, 8321–8337. doi:[10.1007/s10853-017-1049-y](https://doi.org/10.1007/s10853-017-1049-y)
108. Ding, J.; Zhao, H.; Zheng, Y.; Wang, Q.; Chen, H.; Dou, H.; Yu, H. Efficient Exfoliation of Layered Materials by Waste Liquor. *Nanotechnology* 2018, **29**, 095603. doi:[10.1088/1361-6528/aaa05f](https://doi.org/10.1088/1361-6528/aaa05f)
109. Lotya, M.; King, P. J.; Khan, U.; De, S.; Coleman, J. N. High-Concentration, Surfactant-Stabilized Graphene Dispersions. *ACS Nano* 2010, **4**, 3155–3162. doi:[10.1021/nn1005304](https://doi.org/10.1021/nn1005304)
110. Diasio, M. A.; Green, D. L. The Effect of Solvent Viscosity on Production of Few-Layer Graphene from Liquid-Phase Exfoliation of Graphite. *MRS Adv.* 2019, **4**, 241–247. doi:[10.1557/adv.2019.13](https://doi.org/10.1557/adv.2019.13)
111. Tubon Usca, G.; Vacacela Gomez, C.; Guevara, M.; Tene, T.; Hernandez, J.; Molina, R.; Tavolaro, A.; Miriello, D.; Caputi, L. S. Zeolite-Assisted Shear Exfoliation of Graphite into Few-Layer Graphene. *Crystals* 2019, **9**, 377. doi:[10.3390/crust9080377](https://doi.org/10.3390/crust9080377)
112. Yoon, H.-J.; Lee, J. Y.; Yoon, T.-H. Millstone Exfoliation: A True Shear Exfoliation for Large-Size Few-Layer Graphene Oxide. *Nanoscale Res. Lett.* 2018, **13**, 186.
113. Li, L.; Wang, M.; Guo, J.; Cao, M.; Qiu, H.; Dai, L.; Yang, Z. Regulation of Radicals from Electrochemical Exfoliation of a Double-Graphite Electrode to Fabricate High-Quality Graphene. *J. Mater. Chem. C* 2018, **6**, 6257–6263. doi:[10.1039/C8TC01565A](https://doi.org/10.1039/C8TC01565A)

114. Yang, S.; Ricciardulli, A. G.; Liu, S.; Dong, R.; Lohe, M. R.; Becker, A.; Squillaci, M. A.; Samorì, P.; Müllen, K.; Feng, X. Ultrafast Delamination of Graphite into High-Quality Graphene Using Alternating Currents. *Angew. Chem. Int. Ed. Engl.* 2017, **56**, 6669–6675. doi:[10.1002/anie.201702076](https://doi.org/10.1002/anie.201702076)
115. Zhang, Y.; Xu, Y. Simultaneous Electrochemical Dual-Electrode Exfoliation of Graphite toward Scalable Production of High-Quality Graphene. *Adv. Funct. Mater.* 2019, **29**, 1902171. doi:[10.1002/adfm.201902171](https://doi.org/10.1002/adfm.201902171)
116. Achee, T. C.; et al. High-Yield Scalable Graphene Nanosheet Production from Compressed Graphite Using Electrochemical Exfoliation. *Sci. Rep.* 2018, **8**, 1–8.
117. Abdelkader, A. M.; Cooper, A. J.; Dryfe, R. A. W.; Kinloch, I. A. How to Get between the Sheets: A Review of Recent Works on the Electrochemical Exfoliation of Graphene Materials from Bulk Graphite. *Nanoscale* 2015, **7**, 6944–6956. doi:[10.1039/c4nr06942k](https://doi.org/10.1039/c4nr06942k)
118. Morales, G. M.; Schifani, P.; Ellis, G.; Ballesteros, C.; Martínez, G.; Barbero, C.; Salavagione, H. J. High-Quality Few Layer Graphene Produced by Electrochemical Intercalation and Microwave-Assisted Expansion of Graphite. *Carbon* 2011, **49**, 2809–2816. doi:[10.1016/j.carbon.2011.03.008](https://doi.org/10.1016/j.carbon.2011.03.008)
119. Alanyaloğlu, M.; Segura, J. J.; Oró-Solè, J.; Casañ-Pastor, N. The Synthesis of Graphene Sheets with Controlled Thickness and Order Using Surfactant-Assisted Electrochemical Processes. *Carbon* 2012, **50**, 142–152. doi:[10.1016/j.carbon.2011.07.064](https://doi.org/10.1016/j.carbon.2011.07.064)
120. Cooper, A. J.; Wilson, N. R.; Kinloch, I. A.; Dryfe, R. A. W. Single Stage Electrochemical Exfoliation Method for the Production of Few-Layer Graphene via Intercalation of Tetraalkylammonium Cations. *Carbon* 2014, **66**, 340–350. doi:[10.1016/j.carbon.2013.09.009](https://doi.org/10.1016/j.carbon.2013.09.009)
121. Zhou, M.; Tang, J.; Cheng, Q.; Xu, G.; Cui, P.; Qin, L.-C. Few-Layer Graphene Obtained by Electrochemical Exfoliation of Graphite Cathode. *Chem. Phys. Lett.* 2013, **572**, 61–65. doi:[10.1016/j.cplett.2013.04.013](https://doi.org/10.1016/j.cplett.2013.04.013)
122. Shinde, D. B.; Brenker, J.; Easton, C. D.; Tabor, R. F.; Neild, A.; Majumder, M. Shear Assisted Electrochemical Exfoliation of Graphite to Graphene. *Langmuir* 2016, **32**, 3552–3559. doi:[10.1021/acs.langmuir.5b04209](https://doi.org/10.1021/acs.langmuir.5b04209)
123. Rao, K. S.; Senthilnathan, J.; Liu, Y. F.; Yoshimura, M. Role of Peroxide Ions in Formation of Graphene Nanosheets by Electrochemical Exfoliation of Graphite. *Sci. Rep.* 2014, **4**, 4237.
124. Narayan, R.; Kim, S. O. Surfactant Mediated Liquid Phase Exfoliation of Graphene. *Nano Converg.* 2015, **2**, 20. doi:[10.1186/s40580-015-0050-x](https://doi.org/10.1186/s40580-015-0050-x)
125. Liu, F.; Wang, C.; Sui, X.; Riaz, M. A.; Xu, M.; Wei, L.; Chen, Y. Synthesis of Graphene Materials by Electrochemical Exfoliation: Recent Progress and Future Potential. *Carbon Energy* cey2 2019, **1**, 173–199. doi:[10.1002/cey2.14](https://doi.org/10.1002/cey2.14)
126. Munuera, J. M.; Paredes, J. I.; Villar-Rodil, S.; Castro-Muñiz, A.; Martínez-Alonso, A.; Tascón, J. M. D. High Quality, Low-Oxidized Graphene via Anodic Exfoliation with Table Salt as an Efficient Oxidation-Preventing co-Electrolyte for Water/Oil Remediation and Capacitive Energy Storage Applications. *Appl. Mater. Today* 2018, **11**, 246–254. doi:[10.1016/j.apmt.2018.03.002](https://doi.org/10.1016/j.apmt.2018.03.002)
127. Chen, D.; Wang, F.; Li, Y.; Wang, W.-W.; Huang, T.-X.; Li, J.-F.; Novoselov, K. S.; Tian, Z.-Q.; Zhan, D. Programmed Electrochemical Exfoliation of Graphite to High Quality graphene. *Chem. Commun. (Camb.)* 2019, **55**, 3379–3382. doi:[10.1039/c9cc00393b](https://doi.org/10.1039/c9cc00393b)
128. Liu, Z.; Wu, Z.-S.; Yang, S.; Dong, R.; Feng, X.; Müllen, K. Ultraflexible in-Plane Micro-Supercapacitors by Direct Printing of Solution-Processable Electrochemically Exfoliated Graphene. *Adv. Mater.* 2016, **28**, 2217–2222. doi:[10.1002/adma.201505304](https://doi.org/10.1002/adma.201505304)
129. Mir, A.; Shukla, A. Bilayer-Rich Graphene Suspension from Electrochemical Exfoliation of Graphite. *Mater. Des.* 2018, **156**, 62–70. doi:[10.1016/j.matdes.2018.06.035](https://doi.org/10.1016/j.matdes.2018.06.035)
130. Wang, G.; Wang, B.; Park, J.; Wang, Y.; Sun, B.; Yao, J. Highly Efficient and Large-Scale Synthesis of Graphene by Electrolytic Exfoliation. *Carbon* 2009, **47**, 3242–3246. doi:[10.1016/j.carbon.2009.07.040](https://doi.org/10.1016/j.carbon.2009.07.040)
131. Moradi, M.; Aghazadeh, J.; Mansouri Tehrani, A. The Synthesis of Graphene Sheets Using Sodium Dodecyl Sulfate (SDS) as a Surfactant; an Electrochemical Process. *AMR* 2013, **829**, 456–460. doi:[10.4028/www.scientific.net/AMR.829.456](https://doi.org/10.4028/www.scientific.net/AMR.829.456)
132. Niu, L.; Li, M.; Tao, X.; Xie, Z.; Zhou, X.; Raju, A. P. A.; Young, R. J.; Zheng, Z. Salt-Assisted Direct Exfoliation of Graphite into High-Quality, Large-Size, Few-Layer Graphene Sheets. *Nanoscale* 2013, **5**, 7202–7208. doi:[10.1039/c3nr02173d](https://doi.org/10.1039/c3nr02173d)
133. Lei, H.; Tu, J.; Yu, Z.; Jiao, S. Exfoliation Mechanism of Graphite Cathode in Ionic Liquids. *ACS Appl. Mater. Interfaces* 2017, **9**, 36702–36707. doi:[10.1021/acsami.7b03306](https://doi.org/10.1021/acsami.7b03306)
134. Wei, P.; Shen, J.; Wu, K.; Yang, N. Defect-Dependent Electrochemistry of Exfoliated Graphene Layers. *Carbon* 2019, **154**, 125–131. doi:[10.1016/j.carbon.2019.07.100](https://doi.org/10.1016/j.carbon.2019.07.100)
135. Li, J.; Yan, H.; Dang, D.; Wei, W.; Meng, L. Salt and Water co-Assisted Exfoliation of Graphite in Organic Solvent for Efficient and Large Scale Production of High-Quality Graphene. *J. Colloid Interface Sci.* 2019, **535**, 92–99. doi:[10.1016/j.jcis.2018.09.094](https://doi.org/10.1016/j.jcis.2018.09.094)
136. Joo, E. H.; Kuila, T.; Kim, N. H.; Lee, J. H.; Kim, S. A.; Park, E. G.; Lee, U. H. Electrochemically Preparation of Functionalized Graphene Using Sodium Dodecyl Benzene Sulfonate(SDBS). *AMR* 2013, **747**, 246–249. doi:[10.4028/www.scientific.net/AMR.747.246](https://doi.org/10.4028/www.scientific.net/AMR.747.246)
137. Parvez, K.; Wu, Z.-S.; Li, R.; Liu, X.; Graf, R.; Feng, X.; Müllen, K. Exfoliation of Graphite into Graphene in Aqueous Solutions of Inorganic Salts. *J. Am. Chem. Soc.* 2014, **136**, 6083–6091. doi:[10.1021/ja5017156](https://doi.org/10.1021/ja5017156)

138. Su, C.-Y.; Lu, A.-Y.; Xu, Y.; Chen, F.-R.; Khlobystov, A. N.; Li, L.-J. High-Quality Thin Graphene Films from Fast Electrochemical Exfoliation. *ACS Nano*. 2011, **5**, 2332–2339. doi:[10.1021/nn200025p](https://doi.org/10.1021/nn200025p)
139. Rao, K. S.; Senthilnathan, J.; Cho, H.-W.; Wu, J.-J.; Yoshimura, M. Soft Processing of Graphene Nanosheets by Glycine-Bisulfate Ionic-Complex-Assisted Electrochemical Exfoliation of Graphite for Reduction Catalysis. *Adv. Funct. Mater.* 2015, **25**, 298–305. doi:[10.1002/adfm.201402621](https://doi.org/10.1002/adfm.201402621)
140. Ejigu, A.; Fujisawa, K.; Spencer, B. F.; Wang, B.; Terrones, M.; Kinloch, I. A.; Dryfe, R. A. W. On the Role of Transition Metal Salts during Electrochemical Exfoliation of Graphite: Antioxidants or Metal Oxide Decorators for Energy Storage Applications. *Adv. Funct. Mater.* 2018, **28**, 1804357. doi:[10.1002/adfm.201804357](https://doi.org/10.1002/adfm.201804357)
141. Huang, X.; Li, S.; Qi, Z.; Zhang, W.; Ye, W.; Fang, Y. Low Defect Concentration Few-Layer Graphene Using a Two-Step Electrochemical Exfoliation. *Nanotechnology* 2015, **26**, 105602. doi:[10.1088/0957-4484/26/10/105602](https://doi.org/10.1088/0957-4484/26/10/105602)
142. Munuera, J. M.; Paredes, J. I.; Villar-Rodil, S.; Ayán-Varela, M.; Pagán, A.; Aznar-Cervantes, S. D.; Cenis, J. L.; Martínez-Alonso, A.; Tascón, J. M. D. High Quality, Low Oxygen Content and Biocompatible Graphene Nanosheets Obtained by Anodic Exfoliation of Different Graphite Types. *Carbon* 2015, **94**, 729–739. doi:[10.1016/j.carbon.2015.07.053](https://doi.org/10.1016/j.carbon.2015.07.053)
143. Munuera, J. M.; Paredes, J. I.; Enterriá, M.; Pagán, A.; Villar-Rodil, S.; Pereira, M. F. R.; Martins, J. I.; Figueiredo, J. L.; Cenis, J. L.; Martínez-Alonso, A.; Tascón, J. M. D. Electrochemical Exfoliation of Graphite in Aqueous Sodium Halide Electrolytes toward Low Oxygen Content Graphene for Energy and Environmental Applications. *ACS Appl. Mater. Interfaces* 2017, **9**, 24085–24099. doi:[10.1021/acsami.7b04802](https://doi.org/10.1021/acsami.7b04802)
144. Marković, Z. M.; Budimir, M. D.; Kepić, D. P.; Holclajtner-Antunović, I. D.; Marinović-Cincović, M. T.; Dramišanin, M. D.; Spasojević, V. D.; Peruško, D. B.; Špitalský, Z.; Mičušik, M.; et al. Semi-Transparent, Conductive Thin Films of Electrochemical Exfoliated Graphene. *RSC Adv.* 2016, **6**, 39275–39283. doi:[10.1039/C6RA04250C](https://doi.org/10.1039/C6RA04250C)
145. Wu, L.; Li, W.; Li, P.; Liao, S.; Qiu, S.; Chen, M.; Guo, Y.; Li, Q.; Zhu, C.; Liu, L. Powder, Paper and Foam of Few-Layer Graphene Prepared in High Yield by Electrochemical Intercalation Exfoliation of Expanded Graphite. *Small* 2014, **10**, 1421–1429. doi:[10.1002/smll.201302730](https://doi.org/10.1002/smll.201302730)
146. Tripathi, P.; Prakash Patel, C. R.; Dixit, A.; Singh, A. P.; Kumar, P.; Shaz, M. A.; Srivastava, R.; Gupta, G.; Dhawan, S. K.; Gupta, B. K.; et al. High Yield Synthesis of Electrolyte Heating Assisted Electrochemically Exfoliated Graphene for Electromagnetic Interference Shielding Applications. *RSC Adv.* 2015, **5**, 19074–19081. doi:[10.1039/C4RA17230B](https://doi.org/10.1039/C4RA17230B)
147. Sevilla, M.; Ferrero, G. A.; Fuertes, A. B. Aqueous Dispersions of Graphene from Electrochemically Exfoliated Graphite. *Chemistry* 2016, **22**, 17351–17358. doi:[10.1002/chem.201603321](https://doi.org/10.1002/chem.201603321)
148. Chen, C. H.; Yang, S. W.; Chuang, M. C.; Woon, W. Y.; Su, C. Y. Towards the Continuous Production of High Crystallinity Graphene via Electrochemical Exfoliation with Molecular in Situ Encapsulation. *Nanoscale* 2015, **7**, 15362–15373. doi:[10.1039/C5NR03669K](https://doi.org/10.1039/C5NR03669K)
149. Najafabadi, A. T.; Gyenge, E. Synergistic Production of Graphene Microsheets by Simultaneous Anodic and Cathodic Electro-Exfoliation of Graphitic Electrodes in Aprotic Ionic Liquids. *Carbon* 2015, **84**, 449–459. doi:[10.1016/j.carbon.2014.12.041](https://doi.org/10.1016/j.carbon.2014.12.041)
150. Gong, Y.; Ping, Y.; Li, D.; Luo, C.; Ruan, X.; Fu, Q.; Pan, C. Preparation of High-Quality Graphene via Electrochemical Exfoliation & Spark Plasma Sintering and Its Applications. *Appl. Surf. Sci.* 2017, **397**, 213–219. doi:[10.1016/j.apsusc.2016.11.153](https://doi.org/10.1016/j.apsusc.2016.11.153)
151. Yang, Y.; Lu, F.; Zhou, Z.; Song, W.; Chen, Q.; Ji, X. Electrochemically Cathodic Exfoliation of Graphene Sheets in Room Temperature Ionic Liquids N-Butyl, Methylpyrrolidinium Bis(Trifluoromethylsulfonyl)Imide and Their Electrochemical Properties. *Electrochim. Acta* 2013, **113**, 9–16. doi:[10.1016/j.electacta.2013.09.031](https://doi.org/10.1016/j.electacta.2013.09.031)
152. Abdelkader, A. M.; Kinloch, I. A.; Dryfe, R. A. W. Continuous Electrochemical Exfoliation of Micrometer-Sized Graphene Using Synergistic Ion Intercalations and Organic Solvents. *ACS Appl. Mater. Interfaces* 2014, **6**, 1632–1639. doi:[10.1021/am404497n](https://doi.org/10.1021/am404497n)
153. Wang, J.; Manga, K. K.; Bao, Q.; Loh, K. P. High-Yield Synthesis of Few-Layer Graphene Flakes through Electrochemical Expansion of Graphite in Propylene Carbonate Electrolyte. *J. Am. Chem. Soc.* 2011, **133**, 8888–8891. doi:[10.1021/ja203725d](https://doi.org/10.1021/ja203725d)
154. Huang, H.; Xia, Y.; Tao, X.; Du, J.; Fang, J.; Gan, Y.; Zhang, W. Highly Efficient Electrolytic Exfoliation of Graphite into Graphene Sheets Based on Li Ions Intercalation-Expansion-Microexplosion Mechanism. *J. Mater. Chem.* 2012, **22**, 10452–10456. doi:[10.1039/c2jm0092j](https://doi.org/10.1039/c2jm0092j)
155. Mensing, J. P.; Kerdcharoen, T.; Sriprachuabwong, C.; Wisitsoraat, A.; Phokharatkul, D.; Lomas, T.; Tuantranont, A. Facile Preparation of Graphene-Metal Phthalocyanine Hybrid Material by Electrolytic Exfoliation. *J. Mater. Chem.* 2012, **22**, 17094–17099. doi:[10.1039/c2jm32588h](https://doi.org/10.1039/c2jm32588h)
156. Parvez, K.; Li, R.; Puniredd, S. R.; Hernandez, Y.; Hinkel, F.; Wang, S.; Feng, X.; Müllen, K. Electrochemically Exfoliated Graphene as Solution-Processable, Highly Conductive Electrodes for Organic Electronics. *ACS Nano*. 2013, **7**, 3598–3606. doi:[10.1021/nn400576v](https://doi.org/10.1021/nn400576v)
157. Liu, J.; Yang, H.; Zhen, S. G.; Poh, C. K.; Chaurasia, A.; Luo, J.; Wu, X.; Yeow, E. K. L.; Sahoo, N. G.; Lin, J.; Shen, Z. A Green Approach to the Synthesis of High-Quality Graphene Oxide Flakes via Electrochemical Exfoliation of Pencil Core. *RSC Adv.* 2013, **3**, 11745–11750. doi:[10.1039/c3ra41366g](https://doi.org/10.1039/c3ra41366g)
158. Yang, S.; Brüller, S.; Wu, Z.-S.; Liu, Z.; Parvez, K.; Dong, R.; Richard, F.; Samorì, P.; Feng, X.; Müllen,

- K. Organic Radical-Assisted Electrochemical Exfoliation for the Scalable Production of High-Quality Graphene. *J. Am. Chem. Soc.* 2015, **137**, 13927–13932. doi:[10.1021/jacs.5b09000](https://doi.org/10.1021/jacs.5b09000)
159. Guo, H.-L.; Wang, X.-F.; Qian, Q.-Y.; Wang, F.-B.; Xia, X.-H. A Green Approach to the Synthesis of Graphene Nanosheets. *ACS Nano.* 2009, **3**, 2653–2659. doi:[10.1021/nn900227d](https://doi.org/10.1021/nn900227d)
160. Ambrosi, A.; Chua, C. K.; Latiff, N. M.; Loo, A. H.; Wong, C. H. A.; Eng, A. Y. S.; Bonanni, A.; Pumera, M. Graphene and Its electrochemistry—An Update. *Chem. Soc. Rev.* 2016, **45**, 2458–2493. doi:[10.1039/c6cs00136j](https://doi.org/10.1039/c6cs00136j)
161. Zhong, Y. L.; Swager, T. M. Enhanced Electrochemical Expansion of Graphite for in Situ Electrochemical Functionalization. *J. Am. Chem. Soc.* 2012, **134**, 17896–17899. doi:[10.1021/ja309023f](https://doi.org/10.1021/ja309023f)
162. Brodie, Xiii, B. C. On the Atomic Weight of Graphite. *Philos. Trans. R. Soc. London* 1859, **149**, 249–259.
163. Staudenmaier, L. Verfahren Zur Darstellung Der Graphitsäure. *Ber. Dtsch. Chem. Ges.* 1898, **31**, 1481–1487. doi:[10.1002/cber.18980310237](https://doi.org/10.1002/cber.18980310237)
164. Hummers, W. S.; Offeman, R. E. Preparation of Graphitic Oxide. *J. Am. Chem. Soc.* 1958, **80**, 1339–1339. doi:[10.1021/ja01539a017](https://doi.org/10.1021/ja01539a017)
165. Hofmann, U.; König, E. Untersuchungen Über Graphitoxyd. *Z. Anorg. Allg. Chem.* 1937, **234**, 311–336. doi:[10.1002/zaac.19372340405](https://doi.org/10.1002/zaac.19372340405)
166. Marcano, D. C.; Kosynkin, D. V.; Berlin, J. M.; Sinitskii, A.; Sun, Z.; Slesarev, A.; Alemany, L. B.; Lu, W.; Tour, J. M. Improved Synthesis of Graphene Oxide. *ACS Nano.* 2010, **4**, 4806–4814. doi:[10.1021/nn1006368](https://doi.org/10.1021/nn1006368)
167. Dreyer, D. R.; Todd, A. D.; Bielawski, C. W. Harnessing the Chemistry of Graphene Oxide. *Chem. Soc. Rev.* 2014, **43**, 5288–5301. doi:[10.1039/c4cs00060a](https://doi.org/10.1039/c4cs00060a)
168. Wissler, M. Graphite and Carbon Powders for Electrochemical Applications. *J. Power Sources* 2006, **156**, 142–150. doi:[10.1016/j.jpowsour.2006.02.064](https://doi.org/10.1016/j.jpowsour.2006.02.064)
169. Buchsteiner, A.; Lerf, A.; Pieper, J. Water Dynamics in Graphite Oxide Investigated with Neutron Scattering. *J. Phys. Chem. B.* 2006, **110**, 22328–22338. doi:[10.1021/jp0641132](https://doi.org/10.1021/jp0641132)
170. Ke, Q.; Wang, J. Graphene-Based Materials for Supercapacitor Electrodes—A Review. *J. Mater.* 2016, **2**, 37–54. doi:[10.1016/j.jmat.2016.01.001](https://doi.org/10.1016/j.jmat.2016.01.001)
171. Chen, J.; Yao, B.; Li, C.; Shi, G. An Improved Hummers Method for Eco-Friendly Synthesis of Graphene Oxide. *Carbon* 2013, **64**, 225–229. doi:[10.1016/j.carbon.2013.07.055](https://doi.org/10.1016/j.carbon.2013.07.055)
172. Wang, G.; Qian, F.; Saltikov, C. W.; Jiao, Y.; Li, Y. Microbial Reduction of Graphene Oxide by Shewanella. *Nano Res.* 2011, **4**, 563–570. doi:[10.1007/s12274-011-0112-2](https://doi.org/10.1007/s12274-011-0112-2)
173. Hossain, M. Z.; Johns, J. E.; Bevan, K. H.; Karmel, H. J.; Liang, Y. T.; Yoshimoto, S.; Mukai, K.; Koitaya, T.; Yoshinobu, J.; Kawai, M.; et al. Chemically Homogeneous and Thermally Reversible Oxidation of Epitaxial Graphene. *Nat. Chem.* 2012, **4**, 305–309. doi:[10.1038/nchem.1269](https://doi.org/10.1038/nchem.1269)
174. Zhao, S.; Surwade, S. P.; Li, Z.; Liu, H. Photochemical Oxidation of CVD-Grown Single Layer Graphene. *Nanotechnology* 2012, **23**, 355703. doi:[10.1088/0957-4484/23/35/355703](https://doi.org/10.1088/0957-4484/23/35/355703)
175. Ramesh, P.; Itkis, M. E.; Bekyarova, E.; Wang, F.; Niyogi, S.; Chi, X.; Berger, C.; de Heer, W.; Haddon, R. C. Electro-Oxidized Epitaxial Graphene Channel Field-Effect Transistors with Single-Walled Carbon Nanotube Thin Film Gate Electrode. *J. Am. Chem. Soc.* 2010, **132**, 14429–14436. doi:[10.1021/ja101706j](https://doi.org/10.1021/ja101706j)
176. Kim, M. C.; Hwang, G. S.; Ruoff, R. S. Epoxide Reduction with Hydrazine on Graphene: A First Principles Study. *J. Chem. Phys.* 2009, **131**, 064704. doi:[10.1063/1.3197007](https://doi.org/10.1063/1.3197007)
177. Yang, D.; Velamakanni, A.; Bozoklu, G.; Park, S.; Stoller, M.; Piner, R. D.; Stankovich, S.; Jung, I.; Field, D. A.; Ventrice, C. A.; et al. Chemical Analysis of Graphene Oxide Films after Heat and Chemical Treatments by X-Ray Photoelectron and Micro-Raman Spectroscopy. *Carbon* 2009, **47**, 145–152. doi:[10.1016/j.carbon.2008.09.045](https://doi.org/10.1016/j.carbon.2008.09.045)
178. Renteria, J. D.; Ramirez, S.; Malekpour, H.; Alonso, B.; Centeno, A.; Zurutuza, A.; Cocemasov, A. I.; Nika, D. L.; Balandin, A. A. Strongly Anisotropic Thermal Conductivity of Free-Standing Reduced Graphene Oxide Films Annealed at High Temperature. *Adv. Funct. Mater.* 2015, **25**, 4664–4672. doi:[10.1002/adfm.201501429](https://doi.org/10.1002/adfm.201501429)
179. Toh, S. Y.; Loh, K. S.; Kamarudin, S. K.; Daud, W. R. W. Graphene Production via Electrochemical Reduction of Graphene Oxide: Synthesis and Characterisation. *Chem. Eng. J.* 2014, **251**, 422–434. doi:[10.1016/j.cej.2014.04.004](https://doi.org/10.1016/j.cej.2014.04.004)
180. Nair, R. R.; Wu, H. A.; Jayaram, P. N.; Grigorieva, I. V.; Geim, A. K. Unimpeded Permeation of Water through Helium-Leak-Tight Graphene-Based Membranes. *Science* 2012, **335**, 442–444. doi:[10.1126/science.1211694](https://doi.org/10.1126/science.1211694)
181. Lyu, J.; Wen, X.; Kumar, U.; You, Y.; Chen, V.; Joshi, R. K. Separation and Purification Using GO and r-GO Membranes. *RSC Adv.* 2018, **8**, 23130–23151. doi:[10.1039/C8RA03156H](https://doi.org/10.1039/C8RA03156H)
182. Dato, A.; Radmilovic, V.; Lee, Z.; Phillips, J.; Frenklach, M. Substrate-Free Gas-Phase Synthesis of Graphene Sheets. *Nano Lett.* 2008, **8**, 2012–2016. doi:[10.1021/nl8011566](https://doi.org/10.1021/nl8011566)
183. Dato, A. Graphene Synthesized in Atmospheric Plasmas—A Review. *J. Mater. Res.* 2019, **34**, 214–230. doi:[10.1557/jmr.2018.470](https://doi.org/10.1557/jmr.2018.470)
184. Tatarova, E.; Dias, A.; Henriques, J.; Abrashev, M.; Bundaleska, N.; Kovacevic, E.; Bundaleski, N.; Cvelbar, U.; Valcheva, E.; Arnaudov, B.; et al. Towards Large-Scale in Free-Standing Graphene and N-Graphene Sheets. *Sci. Rep.* 2017, **7**, 10175. doi:[10.1038/s41598-017-10810-3](https://doi.org/10.1038/s41598-017-10810-3)
185. Melero, C.; Rincón, R.; Muñoz, J.; Zhang, G.; Sun, S.; Perez, A.; Royuela, O.; González-Gago, C.; Calzada, M. D. Scalable Graphene Production from Ethanol Decomposition by Microwave Argon Plasma Torch. *Plasma Phys. Control. Fusion* 2018, **60**, 014009. doi:[10.1088/1361-6587/aa8480](https://doi.org/10.1088/1361-6587/aa8480)

186. Tatarova, E.; Dias, A.; Henriques, J.; Botelho do Rego, A. M.; Ferraria, A. M.; Abrashev, M. V.; Luhrs, C. C.; Phillips, J.; Dias, F. M.; Ferreira, C. M. Microwave Plasmas Applied for the Synthesis of Free Standing Graphene Sheets. *J. Phys. D: Appl. Phys.* 2014, **47**, 385501. doi:[10.1088/0022-3727/47/38/385501](https://doi.org/10.1088/0022-3727/47/38/385501)
187. Münzer, A.; Xiao, L.; Sehlleier, Y. H.; Schulz, C.; Wiggers, H. All Gas-Phase Synthesis of Graphene: Characterization and Its Utilization for Silicon-Based Lithium-Ion Batteries. *Electrochim. Acta* 2018, **272**, 52–59. doi:[10.1016/j.electacta.2018.03.137](https://doi.org/10.1016/j.electacta.2018.03.137)
188. Lin, J.; et al. Laser-Induced Porous Graphene Films from Commercial Polymers. *Nat. Commun.* 2014, **5**, 1–8.
189. Wang, F.; Wang, K.; Zheng, B.; Dong, X.; Mei, X.; Lv, J.; Duan, W.; Wang, W. Laser-Induced Graphene: preparation, Functionalization and Applications. *Mater. Technol.* 2018, **33**, 340–356. doi:[10.1080/10667857.2018.1447265](https://doi.org/10.1080/10667857.2018.1447265)
190. Carvalho, A. F.; Fernandes, A. J. S.; Leitão, C.; Deuermeier, J.; Marques, A. C.; Martins, R.; Fortunato, E.; Costa, F. M. Laser-Induced Graphene Strain Sensors Produced by Ultraviolet Irradiation of Polyimide. *Adv. Funct. Mater.* 2018, **28**, 1805271–1805278. doi:[10.1002/adfm.201805271](https://doi.org/10.1002/adfm.201805271)
191. Zhang, Z.; Song, M.; Hao, J.; Wu, K.; Li, C.; Hu, C. Visible Light Laser-Induced Graphene from Phenolic Resin: A New Approach for Directly Writing Graphene-Based Electrochemical Devices on Various Substrates. *Carbon* 2018, **127**, 287–296. doi:[10.1016/j.carbon.2017.11.014](https://doi.org/10.1016/j.carbon.2017.11.014)
192. Ye, R.; James, D. K.; Tour, J. M. Laser-Induced Graphene. *Acc. Chem. Res.* 2018, **51**, 1609–1620. doi:[10.1021/acs.accounts.8b00084](https://doi.org/10.1021/acs.accounts.8b00084)
193. Carvalho, A. F.; Fernandes, A. J. S.; Martins, R.; Fortunato, E.; Costa, F. M. Laser-Induced Graphene Piezoresistive Sensors Synthesized Directly on Cork Insoles for Gait Analysis. *Adv. Mater. Technol.* 2020, **5**, 2000630. doi:[10.1002/admt.202000630](https://doi.org/10.1002/admt.202000630)
194. Cardoso, A. R.; Marques, A. C.; Santos, L.; Carvalho, A. F.; Costa, F. M.; Martins, R.; Sales, M. G. F.; Fortunato, E. Molecularly-Imprinted Chloramphenicol Sensor with Laser-Induced Graphene Electrodes. *Biosens. Bioelectron.* 2019, **124–125**, 167–175. doi:[10.1016/j.bios.2018.10.015](https://doi.org/10.1016/j.bios.2018.10.015)
195. Xu, G.; Jarjes, Z. A.; Desprez, V.; Kilmartin, P. A.; Travas-Sejdic, J. Sensitive, Selective, Disposable Electrochemical Dopamine Sensor Based on PEDOT-Modified Laser Scribed Graphene. *Biosens. Bioelectron.* 2018, **107**, 184–191. doi:[10.1016/j.bios.2018.02.031](https://doi.org/10.1016/j.bios.2018.02.031)
196. Luong, D. X.; Subramanian, A. K.; Silva, G. A. L.; Yoon, J.; Cofer, S.; Yang, K.; Owuor, P. S.; Wang, T.; Wang, Z.; Lou, J.; et al. Laminated Object Manufacturing of 3D-Printed Laser-Induced Graphene Foams. *Adv. Mater.* 2018, **30**, 1707416–1707416. doi:[10.1002/adma.201707416](https://doi.org/10.1002/adma.201707416)
197. Luo, S.; Hoang, P. T.; Liu, T. Direct Laser Writing for Creating Porous Graphitic Structures and Their Use for Flexible and Highly Sensitive Sensor and Sensor Arrays. *Carbon* 2016, **96**, 522–531. doi:[10.1016/j.carbon.2015.09.076](https://doi.org/10.1016/j.carbon.2015.09.076)
198. Ye, X.; Long, J.; Lin, Z.; Zhang, H.; Zhu, H.; Zhong, M. Direct Laser Fabrication of Large-Area and Patterned Graphene at Room Temperature. *Carbon* 2014, **68**, 784–790. doi:[10.1016/j.carbon.2013.11.069](https://doi.org/10.1016/j.carbon.2013.11.069)
199. Luong, D. X.; Bets, K. V.; Algozeeb, W. A.; Stanford, M. G.; Kittrell, C.; Chen, W.; Salvatierra, R. V.; Ren, M.; McHugh, E. A.; Advincula, P. A.; et al. Gram-Scale Bottom-up Flash Graphene Synthesis. *Nature* 2020, **577**, 647–651. doi:[10.1038/s41586-020-1938-0](https://doi.org/10.1038/s41586-020-1938-0)
200. Nine, M. J.; Cole, M. A.; Tran, D. N. H.; Lasic, D. Graphene: A Multipurpose Material for Protective Coatings. *J. Mater. Chem. A* 2015, **3**, 12580–12602. doi:[10.1039/C5TA01010A](https://doi.org/10.1039/C5TA01010A)
201. Singh Raman, R. K.; Tiwari, A. Graphene: The Thinnest Known Coating for Corrosion Protection. *JOM* 2014, **66**, 637–642. doi:[10.1007/s11837-014-0921-3](https://doi.org/10.1007/s11837-014-0921-3)
202. Gergely, A.; Kristóf, T. Corrosion Protection with Ultrathin Graphene Coatings: A Review. *Hungarian J. Ind. Chem.* 2013, **41**, 83–108.
203. Chen, S.; Brown, L.; Levendorf, M.; Cai, W.; Ju, S.-Y.; Edgeworth, J.; Li, X.; Magnuson, C. W.; Velamakanni, A.; Piner, R. D.; et al. Oxidation Resistance of Graphene-Coated Cu and Cu/Ni Alloy. *ACS Nano* 2011, **5**, 1321–1327. doi:[10.1021/nn103028d](https://doi.org/10.1021/nn103028d)
204. Tong, Y.; Bohm, S.; Song, M. Graphene Based Materials and Their Composites as Coatings. *Austin J. Nanomed. Nanotechnol.* 2014, **1**, 1–16.
205. Nayak, P. K.; Hsu, C. J.; Wang, S. C.; Sung, J. C.; Huang, J. L. Graphene Coated Ni Films: A Protective Coating. *Thin Solid Films* 2013, **529**, 312–316. doi:[10.1016/j.tsf.2012.03.067](https://doi.org/10.1016/j.tsf.2012.03.067)
206. Kiran, N. U.; Dey, S.; Singh, B. P.; Besra, L. Graphene Coating on Copper by Electrophoretic Deposition for Corrosion Prevention. *Coatings* 2017, **7**, 214.
207. Pu, N.-W.; Shi, G.-N.; Liu, Y.-M.; Sun, X.; Chang, J.-K.; Sun, C.-L.; Ger, M.-D.; Chen, C.-Y.; Wang, P.-C.; Peng, Y.-Y.; et al. Graphene Grown on Stainless Steel as a High-Performance and Ecofriendly anti-Corrosion Coating for Polymer Electrolyte Membrane Fuel Cell Bipolar Plates. *J. Power Sources* 2015, **282**, 248–256. doi:[10.1016/j.jpowsour.2015.02.055](https://doi.org/10.1016/j.jpowsour.2015.02.055)
208. Giovannetti, G.; Khomyakov, P. A.; Brocks, G.; Karpan, V. M.; van den Brink, J.; Kelly, P. J. Doping Graphene with Metal Contacts. *Phys. Rev. Lett.* 2008, **101**, 026803. doi:[10.1103/PhysRevLett.101.026803](https://doi.org/10.1103/PhysRevLett.101.026803)
209. Anisur, M. R.; Chakraborty Banerjee, P.; Easton, C. D.; Singh Raman, R. K. Controlling Hydrogen Environment and Cooling during CVD Graphene Growth on Nickel for Improved Corrosion Resistance. *Carbon* 2018, **127**, 131–140. doi:[10.1016/j.carbon.2017.10.079](https://doi.org/10.1016/j.carbon.2017.10.079)
210. Ye, X.; Lin, Z.; Zhang, H.; Zhu, H.; Liu, Z.; Zhong, M. Protecting Carbon Steel from Corrosion by Laser in Situ Grown Graphene Films. *Carbon* 2015, **94**, 326–334. doi:[10.1016/j.carbon.2015.06.080](https://doi.org/10.1016/j.carbon.2015.06.080)

211. Quezada-Rentería, J. A.; Cházaro-Ruiz, L. F.; Rangel-Mendez, J. R. Synthesis of Reduced Graphene Oxide (rGO) Films onto Carbon Steel by Cathodic Electrophoretic Deposition: Anticorrosive Coating. *Carbon* 2017, **122**, 266–275. doi:[10.1016/j.carbon.2017.06.074](https://doi.org/10.1016/j.carbon.2017.06.074)
212. Tiwari, A.; Singh Raman, R. Durable Corrosion Resistance of Copper Due to Multi-Layer Graphene. *Materials* 2017, **10**, 1112. doi:[10.3390/ma10101112](https://doi.org/10.3390/ma10101112)
213. Raza, M. A.; Rehman, Z. U.; Ghauri, F. A.; Ahmad, A.; Ahmad, R.; Raffi, M. Corrosion Study of Electrophoretically Deposited Graphene Oxide Coatings on Copper Metal. *Thin Solid Films* 2016, **620**, 150–159. doi:[10.1016/j.tsf.2016.09.036](https://doi.org/10.1016/j.tsf.2016.09.036)
214. Hsieh, Y.-P.; Hofmann, M.; Chang, K.-W.; Jhu, J. G.; Li, Y.-Y.; Chen, K. Y.; Yang, C. C.; Chang, W.-S.; Chen, L.-C. Complete Corrosion Inhibition through Graphene Defect Passivation. *ACS Nano* 2014, **8**, 443–445. doi:[10.1021/nn404756q](https://doi.org/10.1021/nn404756q)
215. Zhou, F.; Li, Z.; Shenoy, G. J.; Li, L.; Liu, H. Enhanced Room-Temperature Corrosion of Copper in the Presence of Graphene. *ACS Nano*. 2013, **7**, 6939–6947. doi:[10.1021/nn402150t](https://doi.org/10.1021/nn402150t)
216. Wlasny, I.; Dabrowski, P.; Rogala, M.; Kowalczyk, P. J.; Pasternak, I.; Strupinski, W.; Baranowski, J. M.; Klusek, Z. Role of Graphene Defects in Corrosion of Graphene-Coated Cu(111) Surface. *Appl. Phys. Lett.* 2013, **102**, 111601. doi:[10.1063/1.4795861](https://doi.org/10.1063/1.4795861)
217. Zhang, Y. H.; Zhang, H. R.; Wang, B.; Chen, Z. Y.; Zhang, Y. Q.; Wang, B.; Sui, Y. P.; Zhu, B.; Tang, C. M.; Li, X. L.; et al. Role of Wrinkles in the Corrosion of Graphene Domain-Coated Cu Surfaces. *Appl. Phys. Lett.* 2014, **104**, 143110. doi:[10.1063/1.4871000](https://doi.org/10.1063/1.4871000)
218. Schriver, M.; Regan, W.; Gannett, W. J.; Zaniewski, A. M.; Crommie, M. F.; Zettl, A. Graphene as a Long-Term Metal Oxidation Barrier: Worse than Nothing. *ACS Nano*. 2013, **7**, 5763–5768. doi:[10.1021/nn4014356](https://doi.org/10.1021/nn4014356)
219. Chang, C.-H.; Huang, T.-C.; Peng, C.-W.; Yeh, T.-C.; Lu, H.-I.; Hung, W.-I.; Weng, C.-J.; Yang, T.-I.; Yeh, J.-M. Novel Anticorrosion Coatings Prepared from Polyaniline/Graphene Composites. *Carbon* 2012, **50**, 5044–5051. doi:[10.1016/j.carbon.2012.06.043](https://doi.org/10.1016/j.carbon.2012.06.043)
220. Malekpour, H.; Chang, K.-H.; Chen, J.-C.; Lu, C.-Y.; Nika, D. L.; Novoselov, K. S.; Balandin, A. A. Thermal Conductivity of Graphene Laminate. *Nano Lett.* 2014, **14**, 5155–5161. doi:[10.1021/nl501996v](https://doi.org/10.1021/nl501996v)
221. Kargar, F.; Barani, Z.; Balinskii, M.; Magana, A. S.; Lewis, J. S.; Balandin, A. A. Dual-Functional Graphene Composites for Electromagnetic Shielding and Thermal Management. *Adv. Electron. Mater.* 2019, **5**, 1800558. doi:[10.1002/aem.201800558](https://doi.org/10.1002/aem.201800558)
222. Barani, Z.; Kargar, F.; Godziszewski, K.; Rehman, A.; Yashchyshyn, Y.; Rumyantsev, S.; Cywiński, G.; Knap, W.; Balandin, A. A. Graphene Epoxy-Based Composites as Efficient Electromagnetic Absorbers in the Extremely High-Frequency Band. *ACS Appl. Mater. Interfaces* 2020, **12**, 28635–28644. doi:[10.1021/acsami.0c06729](https://doi.org/10.1021/acsami.0c06729)
223. Chang, K.-C.; Hsu, M.-H.; Lu, H.-I.; Lai, M.-C.; Liu, P.-J.; Hsu, C.-H.; Ji, W.-F.; Chuang, T.-L.; Wei, Y.; Yeh, J.-M.; Liu, W.-R. Room-Temperature Cured Hydrophobic Epoxy/Graphene Composites as Corrosion Inhibitor for Cold-Rolled Steel. *Carbon* 2014, **66**, 144–153. doi:[10.1016/j.carbon.2013.08.052](https://doi.org/10.1016/j.carbon.2013.08.052)
224. Liu, S.; Gu, L.; Zhao, H.; Chen, J.; Yu, H. Corrosion Resistance of Graphene-Reinforced Waterborne Epoxy Coatings. *J. Mater. Sci. Technol.* 2016, **32**, 425–431. doi:[10.1016/j.jmst.2015.12.017](https://doi.org/10.1016/j.jmst.2015.12.017)
225. Hu, H.; He, Y.; Long, Z.; Zhan, Y. Synergistic Effect of Functional Carbon Nanotubes and Graphene Oxide on the Anti-Corrosion Performance of Epoxy Coating. *Polym. Adv. Technol.* 2017, **28**, 754–762. doi:[10.1002/pat.3977](https://doi.org/10.1002/pat.3977)
226. Ding, J.; Zhao, H.-R.; Zheng, Y.; Zhao, X.; Yu, H. A Long-Term Anticorrosive Coating through Graphene Passivation. *Carbon* 2018, **138**, 197–206. doi:[10.1016/j.carbon.2018.06.018](https://doi.org/10.1016/j.carbon.2018.06.018)
227. Hayatgheib, Y.; Ramezanadeh, B.; Kardar, P.; Mahdavian, M. A Comparative Study on Fabrication of a Highly Effective Corrosion Protective System Based on Graphene Oxide-Polyaniline Nanofibers/Epoxy Composite. *Corros. Sci.* 2018, **133**, 358–373. doi:[10.1016/j.corsci.2018.01.046](https://doi.org/10.1016/j.corsci.2018.01.046)
228. Ding, J.; Rahman, O.; Peng, W.; Dou, H.; Yu, H. A Novel Hydroxyl Epoxy Phosphate Monomer Enhancing the Anticorrosive Performance of Waterborne Graphene/Epoxy Coatings. *Appl. Surf. Sci.* 2018, **427**, 981–991. doi:[10.1016/j.apsusc.2017.08.224](https://doi.org/10.1016/j.apsusc.2017.08.224)
229. Cui, M.; Ren, S.; Zhao, H.; Xue, Q.; Wang, L. Polydopamine Coated Graphene Oxide for Anticorrosive Reinforcement of Water-Borne Epoxy Coating. *Chem. Eng. J.* 2018, **335**, 255–266. doi:[10.1016/j.cej.2017.10.172](https://doi.org/10.1016/j.cej.2017.10.172)
230. Ramezanadeh, B.; Bahlakeh, G.; Mohamadzadeh Moghadam, M. H.; Mirafatab, R. Impact of Size-Controlled p-Phenylenediamine (PPDA)-Functionalized Graphene Oxide Nanosheets on the GO-PPDA/Epoxy anti-Corrosion, Interfacial Interactions and Mechanical Properties Enhancement: Experimental and Quantum Mechanics Investigations. *Chem. Eng. J.* 2018, **335**, 737–755. doi:[10.1016/j.cej.2017.11.019](https://doi.org/10.1016/j.cej.2017.11.019)
231. Ramezanadeh, B.; Niroumandrad, S.; Ahmadi, A.; Mahdavian, M.; Moghadam, M. H. M. Enhancement of Barrier and Corrosion Protection Performance of an Epoxy Coating through Wet Transfer of Amino Functionalized Graphene Oxide. *Corros. Sci.* 2016, **103**, 283–304. doi:[10.1016/j.corsci.2015.11.033](https://doi.org/10.1016/j.corsci.2015.11.033)
232. Yu, Z.; Lv, L.; Ma, Y.; Di, H.; He, Y. Covalent Modification of Graphene Oxide by Metronidazole for Reinforced anti-Corrosion Properties of Epoxy Coatings. *RSC Adv.* 2016, **6**, 18217–18226. doi:[10.1039/C5RA23595B](https://doi.org/10.1039/C5RA23595B)
233. Ramezanadeh, B.; Bahlakeh, G.; Ramezanadeh, M. Polyaniline-Cerium Oxide (PAni-CeO<sub>2</sub>) Coated Graphene Oxide for Enhancement of Epoxy Coating Corrosion Protection Performance on Mild Steel. *Corros. Sci.* 2018, **137**, 111–126. doi:[10.1016/j.corsci.2018.03.038](https://doi.org/10.1016/j.corsci.2018.03.038)

234. Ramezanzadeh, B.; Haeri, Z.; Ramezanzadeh, M. A Facile Route of Making Silica Nanoparticles-Covered Graphene Oxide Nanohybrids ( $\text{SiO}_2\text{-GO}$ ); Fabrication of  $\text{SiO}_2\text{-GO}/\text{Epoxy}$  Composite Coating with Superior Barrier and Corrosion Protection Performance. *Chem. Eng. J.* 2016, **303**, 511–528. doi:10.1016/j.cej.2016.06.028
235. Rajabi, M.; Rashed, G. R.; Zaarei, D. Assessment of Graphene Oxide/Epoxy Nanocomposite as Corrosion Resistance Coating on Carbon Steel. *Corros. Eng. Sci. Technol.* 2015, **50**, 509–516. doi:10.1179/1743278214Y.0000000232
236. Yu, K.; Wang, M.; Qian, K.; Lu, X.; Sun, J. The Synergy Effect of Graphene/ $\text{SiO}_2$  Hybrid Materials on Reinforcing and Toughening Epoxy Resin. *Fibers Polym.* 2016, **17**, 453–459. doi:10.1007/s12221-016-5862-8
237. Ma, Y.; Di, H.; Yu, Z.; Liang, L.; Lv, L.; Pan, Y.; Zhang, Y.; Yin, D. Fabrication of Silica-Decorated Graphene Oxide Nanohybrids and the Properties of Composite Epoxy Coatings Research. *Appl. Surf. Sci.* 2016, **360**, 936–945. doi:10.1016/j.apsusc.2015.11.088
238. Kumar, A.; Anant, R.; Kumar, K.; Chauhan, S. S.; Kumar, S.; Kumar, R. Anticorrosive and Electromagnetic Shielding Response of a Graphene/ $\text{TiO}_2$ -Epoxy Nanocomposite with Enhanced Mechanical Properties. *RSC Adv.* 2016, **6**, 113405–113414. doi:10.1039/C6RA15273B
239. Pourhashem, S.; Vaezi, M. R.; Rashidi, A.; Bagherzadeh, M. R. Distinctive Roles of Silane Coupling Agents on the Corrosion Inhibition Performance of Graphene Oxide in Epoxy Coatings. *Prog. Org. Coatings* 2017, **111**, 47–56. doi:10.1016/j.porgcoat.2017.05.008
240. Pourhashem, S.; Ghasemy, E.; Rashidi, A.; Vaezi, M. R. Corrosion Protection Properties of Novel Epoxy Nanocomposite Coatings Containing Silane Functionalized Graphene Quantum Dots. *J. Alloys Compd.* 2018, **731**, 1112–1118. doi:10.1016/j.jallcom.2017.10.150
241. Chen, C.; Qiu, S.; Cui, M.; Qin, S.; Yan, G.; Zhao, H.; Wang, L.; Xue, Q. Achieving High Performance Corrosion and Wear Resistant Epoxy Coatings via Incorporation of Noncovalent Functionalized Graphene. *Carbon* 2017, **114**, 356–366. doi:10.1016/j.carbon.2016.12.044
242. Liu, C.; Qiu, S.; Du, P.; Zhao, H.; Wang, L. An Ionic Liquid-Graphene Oxide Hybrid Nanomaterial: Synthesis and Anticorrosive Applications. *Nanoscale* 2018, **10**, 8115–8124. doi:10.1039/c8nr01890a
243. Qiu, S.; Liu, G.; Li, W.; Zhao, H.; Wang, L. Noncovalent Exfoliation of Graphene and Its Multifunctional Composite Coating with Enhanced Anticorrosion and Tribological Performance. *J. Alloys Compd.* 2018, **747**, 60–70. doi:10.1016/j.jallcom.2018.03.007
244. He, Y.; Chen, C.; Xiao, G.; Zhong, F.; Wu, Y.; He, Z. Improved Corrosion Protection of Waterborne Epoxy/Graphene Coating by Combining Non-Covalent and Covalent Bonds. *React. Funct. Polym.* 2019, **137**, 104–115. doi:10.1016/j.reactfunctpolym.2019.02.001
245. Hou, P. Layer-by-Layer Self-Assembled Graphene Oxide Nanocontainers for Active Anticorrosion Application. *Int. J. Electrochem. Sci.* 2019, **14**, 3055–3069. doi:10.20964/2019.03.34
246. Pourhashem, S.; Rashidi, A.; Reza, M.; Reza, M. Excellent Corrosion Protection Performance of Epoxy Composite Coatings Filled with Amino-Silane Functionalized Graphene Oxide. *Surf. Coat. Technol.* 2017, **317**, 1–9. doi:10.1016/j.surfcoat.2017.03.050
247. Pourhashem, S.; Reza, M.; Rashidi, A. Investigating the Effect of  $\text{SiO}_2$ -Graphene Oxide Hybrid as Inorganic Nanofiller on Corrosion Protection Properties of Epoxy Coatings. *Surf. Coat. Technol.* 2017, **311**, 282–294. doi:10.1016/j.surfcoat.2017.01.013
248. Di, H.; Yu, Z.; Ma, Y.; Pan, Y.; Shi, H.; Lv, L.; Li, F.; Wang, C.; Long, T.; He, Y. Anchoring Calcium Carbonate on Graphene Oxide Reinforced with Anticorrosive Properties of Composite Epoxy Coatings. *Polym. Adv. Technol.* 2016, **27**, 915–921. doi:10.1002/pat.3748
249. Yu, Z.; Di, H.; Ma, Y.; He, Y.; Liang, L.; Lv, L.; Ran, X.; Pan, Y.; Luo, Z. Preparation of Graphene Oxide Modified by Titanium Dioxide to Enhance the anti-Corrosion Performance of Epoxy Coatings. *Surf. Coat. Technol.* 2015, **276**, 471–478. doi:10.1016/j.surfcoat.2015.06.027
250. Liu, J.; Yu, Q.; Yu, M.; Li, S.; Zhao, K.; Xue, B.; Zu, H. Silane Modification of Titanium Dioxide-Decorated Graphene Oxide Nanocomposite for Enhancing Anticorrosion Performance of Epoxy Coatings on AA-2024. *J. Alloys Compd.* 2018, **744**, 728–739. doi:10.1016/j.jallcom.2018.01.267
251. Zhan, Y.; Zhang, J.; Wan, X.; Long, Z.; He, S.; He, Y. Epoxy Composites Coating with  $\text{Fe}_3\text{O}_4$  Decorated Graphene Oxide: Modified Bio-Inspired Surface Chemistry, Synergistic Effect and Improved anti-Corrosion Performance. *Appl. Surf. Sci.* 2018, **436**, 756–767. doi:10.1016/j.apsusc.2017.12.095
252. Xia, W.; Xue, H.; Wang, J.; Wang, T.; Song, L.; Guo, H.; Fan, X.; Gong, H.; He, J. Functionized Graphene Serving as Free Radical Scavenger and Corrosion Protection in Gamma-Irradiated Epoxy Composites. *Carbon* 2016, **101**, 315–323. doi:10.1016/j.carbon.2016.02.004
253. Zhang, Z.; Zhang, W.; Li, D.; Sun, Y.; Wang, Z.; Hou, C.; Chen, L.; Cao, Y.; Liu, Y. Mechanical and Anticorrosive Properties of Graphene/Epoxy Resin Composites Coating Prepared by in-Situ Method. *Int. J. Mol. Sci.* 2015, **16**, 2239–2251. doi:10.3390/ijms16012239
254. Christopher, G.; Kulandainathan, M. A.; Harichandran, G. Comparative Study of Effect of Corrosion on Mild Steel with Waterborne Polyurethane Dispersion Containing Graphene Oxide versus Carbon Black Nanocomposites. *Prog. Org. Coatings* 2015, **89**, 199–211. doi:10.1016/j.porgcoat.2015.09.022
255. Li, Y.; Yang, Z.; Qiu, H.; Dai, Y.; Zheng, Q.; Li, J.; Yang, J. Self-Aligned Graphene as Anticorrosive Barrier in Waterborne Polyurethane Composite

- Coatings. *J. Mater. Chem. A* 2014, **2**, 14139–14145. doi:[10.1039/C4TA02262A](https://doi.org/10.1039/C4TA02262A)
256. Mo, M.; Zhao, W.; Chen, Z.; Yu, Q.; Zeng, Z.; Wu, X.; Xue, Q. Excellent Tribological and anti-Corrosion Performance of Polyurethane Composite Coatings Reinforced with Functionalized Graphene and Graphene Oxide Nanosheets. *RSC Adv.* 2015, **5**, 56486–56497. doi:[10.1039/C5RA10494G](https://doi.org/10.1039/C5RA10494G)
257. Mo, M.; Zhao, W.; Chen, Z.; Liu, E.; Xue, Q. Corrosion Inhibition of Functional Graphene Reinforced Polyurethane Nanocomposite Coatings with Regular Textures. *RSC Adv.* 2016, **6**, 7780–7790. doi:[10.1039/C5RA24823J](https://doi.org/10.1039/C5RA24823J)
258. Ramezanzadeh, B.; Ghasemi, E.; Mahdavian, M.; Changizi, E.; Mohamadzadeh Moghadam, M. H. Covalently-Grafted Graphene Oxide Nanosheets to Improve Barrier and Corrosion Protection Properties of Polyurethane Coatings. *Carbon* 2015, **93**, 555–573. doi:[10.1016/j.carbon.2015.05.094](https://doi.org/10.1016/j.carbon.2015.05.094)
259. Ding, J.; Zhao, H.; Ji, D.; Xu, B.; Zhao, X.; Wang, Z.; Wang, D.; Zhou, Q.; Yu, H. Achieving Long-Term Anticorrosion via the Inhibition of Graphene's Electrical Activity. *J. Mater. Chem. A* 2019, **7**, 2864–2874. doi:[10.1039/C8TA10337B](https://doi.org/10.1039/C8TA10337B)
260. Sun, W.; Wang, L.; Wu, T.; Pan, Y.; Liu, G. Synthesis of Low-Electrical-Conductivity Graphene/Pernigraniline Composites and Their Application in Corrosion Protection. *Carbon* 2014, **79**, 605–614. doi:[10.1016/j.carbon.2014.08.021](https://doi.org/10.1016/j.carbon.2014.08.021)
261. Ramezanzadeh, B.; Kardar, P.; Bahlakeh, G.; Hayatgheib, Y.; Mahdavian, M. Fabrication of a Highly Tunable Graphene Oxide Composite through Layer-by-Layer Assembly of Highly Crystalline Polyaniline Nano fibers and Green Corrosion Inhibitors: Complementary Experimental and First-Principles Quantum-Mechanics Modeling Approaches. *J. Phys. Chem. C* 2017, **121**, 20433–20450. doi:[10.1021/acs.jpcc.7b04323](https://doi.org/10.1021/acs.jpcc.7b04323)
262. Taheri, N. N.; Ramezanzadeh, B.; Mahdavian, M.; Bahlakeh, G. In-Situ Synthesis of Zn Doped Polyaniline on Graphene Oxide for Inhibition of Mild Steel Corrosion in 3.5 wt.% Chloride Solution. *J. Ind. Eng. Chem.* 2018, **63**, 322–339. doi:[10.1016/j.jiec.2018.02.033](https://doi.org/10.1016/j.jiec.2018.02.033)
263. Krishnamoorthy, K.; Jeyasubramanian, K.; Premanathan, M.; Subbiah, G.; Shin, H. S.; Kim, S. J. Graphene Oxide Nanopaint. *Carbon* 2014, **72**, 328–337. doi:[10.1016/j.carbon.2014.02.013](https://doi.org/10.1016/j.carbon.2014.02.013)
264. Yu, Y.-H.; Lin, Y.-Y.; Lin, C.-H.; Chan, C.-C.; Huang, Y.-C. High-Performance Polystyrene/Graphene-Based Nanocomposites with Excellent anti-Corrosion Properties. *Polym. Chem.* 2014, **5**, 535–550. doi:[10.1039/C3PY00825H](https://doi.org/10.1039/C3PY00825H)
265. Qi, K.; Sun, Y.; Duan, H.; Guo, X. A Corrosion-Protective Coating Based on a Solution-Processable Polymer-Grafted Graphene Oxide Nanocomposite. *Corros. Sci.* 2015, **98**, 500–506. doi:[10.1016/j.corsci.2015.05.056](https://doi.org/10.1016/j.corsci.2015.05.056)
266. Chang, K. C.; Ji, W. F.; Li, C. W.; Chang, C. H.; Peng, Y. Y.; Yeh, J. M.; Liu, W. R. The Effect of Varying Carboxylic-Group Content in Reduced Graphene Oxides on the Anticorrosive Properties of PMMA/Reduced Graphene Oxide Composites. *Express Polym. Lett.* 2014, **8**, 908–919. doi:[10.3144/expresspolymlett.2014.92](https://doi.org/10.3144/expresspolymlett.2014.92)
267. Chaudhry, A. U.; Mittal, V.; Mishra, B. Inhibition and Promotion of Electrochemical Reactions by Graphene in Organic Coatings. *RSC Adv.* 2015, **5**, 80365–80368. doi:[10.1039/C5RA12988E](https://doi.org/10.1039/C5RA12988E)
268. Sun, W.; Wang, L.; Wu, T.; Pan, Y.; Liu, G. Inhibited Corrosion-Promotion Activity of Graphene Encapsulated in Nanosized Silicon Oxide. *J. Mater. Chem. A* 2015, **3**, 16843–16848. doi:[10.1039/C5TA04236D](https://doi.org/10.1039/C5TA04236D)
269. Sun, W.; Wang, L.; Yang, Z.; Zhu, T.; Wu, T.; Dong, C.; Liu, G. A Facile Method for the Modification of Graphene Nanosheets as Promising Anticorrosion Pigments. *Mater. Lett.* 2018, **228**, 152–156. doi:[10.1016/j.matlet.2018.05.105](https://doi.org/10.1016/j.matlet.2018.05.105)
270. Verdejo, R.; Bernal, M. M.; Romasanta, L. J.; Lopez-Manchado, M. A. Graphene Filled Polymer Nanocomposites. *J. Mater. Chem.* 2011, **21**, 3301–3310. doi:[10.1039/C0JM02708A](https://doi.org/10.1039/C0JM02708A)
271. Ding, R.; Chen, S.; Lv, J.; Zhang, W.; Zhao, X.-d.; Liu, J.; Wang, X.; Gui, T.-j.; Li, B.-j.; Tang, Y.-z.; Li, W.-H. Study on Graphene Modified Organic anti-Corrosion Coatings: A Comprehensive Review. *J. Alloys Compd.* 2019, **806**, 611–635. doi:[10.1016/j.jallcom.2019.07.256](https://doi.org/10.1016/j.jallcom.2019.07.256)
272. Elias, D. C.; Nair, R. R.; Mohiuddin, T. M. G.; Morozov, S. V.; Blake, P.; Halsall, M. P.; Ferrari, A. C.; Boukhvalov, D. W.; Katsnelson, M. I.; Geim, A. K.; Novoselov, K. S. Control of Graphene's Properties by Reversible Hydrogenation: Evidence for Graphane. *Science* 2009, **323**, 610–613. doi:[10.1126/science.1167130](https://doi.org/10.1126/science.1167130)
273. Lu, N.; Li, Z.; Yang, J. Electronic Structure Engineering via on-Plane Chemical Functionalization: A Comparison Study on Two-Dimensional Polysilane and Graphane. *J. Phys. Chem. C* 2009, **113**, 16741–16746. doi:[10.1021/jp904208g](https://doi.org/10.1021/jp904208g)
274. Yu, Z.; Di, H.; Ma, Y.; Lv, L.; Pan, Y.; Zhang, C.; He, Y. Fabrication of Graphene Oxide-Alumina Hybrids to Reinforce the anti-Corrosion Performance of Composite Epoxy Coatings. *Appl. Surf. Sci.* 2015, **351**, 986–996. doi:[10.1016/j.apsusc.2015.06.026](https://doi.org/10.1016/j.apsusc.2015.06.026)
275. Yu, F.; Camilli, L.; Wang, T.; Mackenzie, D. M. A.; Curioni, M.; Akid, R.; Bøggild, P. Complete Long-Term Corrosion Protection with Chemical Vapor Deposited Graphene. *Carbon* 2018, **132**, 78–84. doi:[10.1016/j.carbon.2018.02.035](https://doi.org/10.1016/j.carbon.2018.02.035)
276. Wang, X.; Jin, J.; Song, M. An Investigation of the Mechanism of Graphene Toughening Epoxy. *Carbon* 2013, **65**, 324–333. doi:[10.1016/j.carbon.2013.08.032](https://doi.org/10.1016/j.carbon.2013.08.032)
277. Atif, R.; Shyha, I.; Inam, F. Mechanical, Thermal, and Electrical Properties of Graphene-Epoxy Nanocomposites—A Review. *Polymers (Basel)* 2016, **8**, 281. doi:[10.3390/polym8080281](https://doi.org/10.3390/polym8080281)
278. Zhang, L.; Li, Y.; Wang, H.; Qiao, Y.; Chen, J.; Cao, S. Strong and Ductile Poly(Lactic Acid) Nanocomposite Films Reinforced with Alkylated Graphene Nanosheets. *Chem. Eng. J.* 2015, **264**, 538–546. doi:[10.1016/j.cej.2014.11.066](https://doi.org/10.1016/j.cej.2014.11.066)

279. Parhizkar, N.; Shahrabi, T.; Ramezanzadeh, B. A New Approach for Enhancement of the Corrosion Protection Properties and Interfacial Adhesion Bonds between the Epoxy Coating and Steel Substrate through Surface Treatment by Covalently Modified Amino Functionalized Graphene Oxide Film. *Corros. Sci.* 2017, **123**, 55–75. doi:[10.1016/j.corsci.2017.04.011](https://doi.org/10.1016/j.corsci.2017.04.011)
280. Parhizkar, N.; Ramezanzadeh, B.; Shahrabi, T. Corrosion Protection and Adhesion Properties of the Epoxy Coating Applied on the Steel Substrate Pre-Treated by a Sol-Gel Based Silane Coating Filled with Amino and Isocyanate Silane Functionalized Graphene Oxide Nanosheets. *Appl. Surf. Sci.* 2018, **439**, 45–59. doi:[10.1016/j.apsusc.2017.12.240](https://doi.org/10.1016/j.apsusc.2017.12.240)
281. Fan, Y.; Jiang, W.; Kawasaki, A. Highly Conductive Few-Layer Graphene/Al<sub>2</sub>O<sub>3</sub> Nanocomposites with Tunable Charge Carrier Type. *Adv. Funct. Mater.* 2012, **22**, 3882–3889. doi:[10.1002/adfm.201200632](https://doi.org/10.1002/adfm.201200632)
282. Song, Z.; Zhang, Y.; Liu, W.; Zhang, S.; Liu, G.; Chen, H.; Qiu, J. Hydrothermal Synthesis and Electrochemical Performance of Co<sub>3</sub>O<sub>4</sub>/Reduced Graphene Oxide Nanosheet Composites for Supercapacitors. *Electrochim. Acta* 2013, **112**, 120–126. doi:[10.1016/j.electacta.2013.08.155](https://doi.org/10.1016/j.electacta.2013.08.155)
283. Jiao, W.; Shioya, M.; Wang, R.; Yang, F.; Hao, L.; Niu, Y.; Liu, W.; Zheng, L.; Yuan, F.; Wan, L.; He, X. Improving the Gas Barrier Properties of Fe<sub>3</sub>O<sub>4</sub>/Graphite Nanoplatelet Reinforced Nanocomposites by a Low Magnetic Field Induced Alignment. *Compos. Sci. Technol.* 2014, **99**, 124–130. doi:[10.1016/j.compscitech.2014.05.022](https://doi.org/10.1016/j.compscitech.2014.05.022)
284. Nikpour, B.; Ramezanzadeh, B.; Bahlakeh, G.; Mahdavian, M. Synthesis of Graphene Oxide Nanosheets Functionalized by Green Corrosion Inhibitive Compounds to Fabricate a Protective System. *Corros. Sci.* 2017, **127**, 240–259. doi:[10.1016/j.corsci.2017.08.029](https://doi.org/10.1016/j.corsci.2017.08.029)
285. Gupta, R. K.; Malviya, M.; Verma, C.; Quraishi, M. A. Aminoazobenzene and Diaminoazobenzene Functionalized Graphene Oxides as Novel Class of Corrosion Inhibitors for Mild Steel: Experimental and DFT Studies. *Mater. Chem. Phys.* 2017, **198**, 360–373. doi:[10.1016/j.matchemphys.2017.06.030](https://doi.org/10.1016/j.matchemphys.2017.06.030)
286. Souza, J. C. M. Wear and Corrosion Interactions on Titanium in Oral Environment: Literature Review. *J. Bio-Tribol-Corrosion* 2015, **1**, 13.
287. Li, M.; Liu, Q.; Jia, Z.; Xu, X.; Shi, Y.; Cheng, Y.; Zheng, Y.; Xi, T.; Wei, S. Electrophoretic Deposition and Electrochemical Behavior of Novel Graphene Oxide-Hyaluronic Acid-Hydroxyapatite Nanocomposite Coatings. *Appl. Surf. Sci.* 2013, **284**, 804–810. doi:[10.1016/j.apsusc.2013.08.012](https://doi.org/10.1016/j.apsusc.2013.08.012)
288. Janković, A.; Eraković, S.; Mitrić, M.; Matić, I. Z.; Juranić, Z. D.; Tsui, G. C. P.; Tang, C-y.; Mišković-Stanković, V.; Rhee, K. Y.; Park, S. J. Bioactive Hydroxyapatite/Graphene Composite Coating and Its Corrosion Stability in Simulated Body Fluid. *J. Alloys Compd.* 2015, **624**, 148–157. doi:[10.1016/j.jallcom.2014.11.078](https://doi.org/10.1016/j.jallcom.2014.11.078)
289. Kim, S.; Ku, S. H.; Lim, S. Y.; Kim, J. H.; Park, C. B. Graphene-Biomineral Hybrid Materials. *Adv. Mater.* 2011, **23**, 2009–2014. doi:[10.1002/adma.201100010](https://doi.org/10.1002/adma.201100010)
290. Liu, H.; Xi, P.; Xie, G.; Shi, Y.; Hou, F.; Huang, L.; Chen, F.; Zeng, Z.; Shao, C.; Wang, J. Simultaneous Reduction and Surface Functionalization of Graphene Oxide for Hydroxyapatite Mineralization. *J. Phys. Chem. C* 2012, **116**, 3334–3341. doi:[10.1021/jp2102226](https://doi.org/10.1021/jp2102226)
291. Li, M.; Wang, Y.; Liu, Q.; Li, Q.; Cheng, Y.; Zheng, Y.; Xi, T.; Wei, S. In Situ Synthesis and Biocompatibility of Nano Hydroxyapatite on Pristine and Chitosan Functionalized Graphene Oxide. *J. Mater. Chem. B* 2013, **1**, 475–484. doi:[10.1039/c2tb00053a](https://doi.org/10.1039/c2tb00053a)
292. Neelgund, G. M.; Oki, A.; Luo, Z. In-Situ Deposition of Hydroxyapatite on Graphene Nanosheets. *Mater. Res. Bull.* 2013, **48**, 175–179. doi:[10.1016/j.materresbull.2012.08.077](https://doi.org/10.1016/j.materresbull.2012.08.077)
293. Ma, H. B.; Su, W. X.; Tai, Z. X.; Sun, D. F.; Yan, X. B.; Liu, B.; Xue, Q. J. Preparation and Cytocompatibility of Polylactic Acid/Hydroxyapatite/Graphene Oxide Nanocomposite Fibrous Membrane. *Chin. Sci. Bull.* 2012, **57**, 3051–3058. doi:[10.1007/s11434-012-5336-3](https://doi.org/10.1007/s11434-012-5336-3)
294. Zhu, J.; Wong, H. M.; Yeung, K. W. K.; Tjong, S. C. Spark Plasma Sintered Hydroxyapatite/Graphite Nanosheet and Hydroxyapatite/Multiwalled Carbon Nanotube Composites: Mechanical and in Vitro Cellular Properties. *Adv. Eng. Mater.* 2011, **13**, 336–341. doi:[10.1002/adem.201000300](https://doi.org/10.1002/adem.201000300)
295. Biris, A. R.; Mahmood, M.; Lazar, M. D.; Dervishi, E.; Watanabe, F.; Mustafa, T.; Baciuț, G.; Baciuț, M.; Bran, S.; Ali, S.; Biris, A. S. Novel Multicomponent and Biocompatible Nanocomposite Materials Based on Few-Layer Graphenes Synthesized on a Gold/Hydroxyapatite Catalytic System with Applications in Bone Regeneration. *J. Phys. Chem. C* 2011, **115**, 18967–18976. doi:[10.1021/jp203474y](https://doi.org/10.1021/jp203474y)
296. Shi, Y. Y.; Li, M.; Liu, Q.; Jia, Z. J.; Xu, X. C.; Cheng, Y.; Zheng, Y. F. Electrophoretic Deposition of Graphene Oxide Reinforced Chitosan-Hydroxyapatite Nanocomposite Coatings on Ti Substrate. *J. Mater. Sci. Mater. Med.* 2016, **27**, 48. doi:[10.1007/s10856-015-5634-9](https://doi.org/10.1007/s10856-015-5634-9)
297. Hayatdavoudi, H.; Rahsepar, M. A Mechanistic Study of the Enhanced Cathodic Protection Performance of Graphene-Reinforced Zinc Rich Nanocomposite Coating for Corrosion Protection of Carbon Steel Substrate. *J. Alloys Compd.* 2017, **727**, 1148–1156. doi:[10.1016/j.jallcom.2017.08.250](https://doi.org/10.1016/j.jallcom.2017.08.250)
298. Ramezanzadeh, B.; Moghadam, M. H. M.; Shohani, N.; Mahdavian, M. Effects of Highly Crystalline and Conductive Polyaniline/Graphene Oxide Composites on the Corrosion Protection Performance of a Zinc-Rich Epoxy Coating. *Chem. Eng. J.* 2017, **320**, 363–375. doi:[10.1016/j.cej.2017.03.061](https://doi.org/10.1016/j.cej.2017.03.061)
299. Teng, S.; Gao, Y.; Cao, F.; Kong, D.; Zheng, X.; Ma, X.; Zhi, L. Zinc-Reduced Graphene Oxide for Enhanced Corrosion Protection of Zinc-Rich Epoxy Coatings. *Prog. Org. Coatings* 2018, **123**, 185–189. doi:[10.1016/j.porgcoat.2018.07.012](https://doi.org/10.1016/j.porgcoat.2018.07.012)

300. Ding, R.; Zheng, Y.; Yu, H.; Li, W.; Wang, X.; Gui, T. Study of Water Permeation Dynamics and anti-Corrosion Mechanism of Graphene/Zinc Coatings. *J. Alloys Compd.* 2018, **748**, 481–495. doi:[10.1016/j.jallcom.2018.03.160](https://doi.org/10.1016/j.jallcom.2018.03.160)
301. Mohammadi, S.; Roohi, H. Influence of Functionalized Multi-Layer Graphene on Adhesion Improvement and Corrosion Resistance Performance of Zinc-Rich Epoxy Primer. *Corros. Eng. Sci. Technol.* 2018, 1–9. doi:[10.1080/1478422X.2018.1495679](https://doi.org/10.1080/1478422X.2018.1495679)
302. Cheng, L.; Liu, C.; Han, D.; Ma, S.; Guo, W.; Cai, H.; Wang, X. Effect of Graphene on Corrosion Resistance of Waterborne Inorganic Zinc-Rich Coatings. *J. Alloys Compd.* 2019, **774**, 255–264. doi:[10.1016/j.jallcom.2018.09.315](https://doi.org/10.1016/j.jallcom.2018.09.315)
303. Ding, R.; Wang, X.; Jiang, J.; Gui, T.; Li, W. Study on Evolution of Coating State and Role of Graphene in Graphene Modified Low-Zinc Waterborne Epoxy Anticorrosion Coating by Electrochemical Impedance Spectroscopy. *J. Mater. Eng. Perform.* 2017, **26**, 3319–3335. doi:[10.1007/s11665-017-2790-8](https://doi.org/10.1007/s11665-017-2790-8)
304. Tsai, P. Y.; Chen, T. E.; Lee, Y. L. Development and Characterization of Anticorrosion and Antifriction Properties for High Performance Polyurethane/Graphene Composite Coatings. *Coatings* 2018, **8**, 250. doi:[10.3390/coatings8070250](https://doi.org/10.3390/coatings8070250)
305. Monetta, T.; Acuesta, A.; Carangelo, A.; Bellucci, F. The Effect of Graphene on the Protective Properties of Water-Based Epoxy Coatings on Al2024-T3. *Int. J. Corros.* 2017, **2017**, 1–9. doi:[10.1155/2017/1541267](https://doi.org/10.1155/2017/1541267)
306. Hsu, C. H.; Mansfeld, F. Technical Note: Concerning the Conversion of the Constant Phase Element Parameter Y<sub>0</sub> into a Capacitance. *Corrosion* 2001, **57**, 747–748. doi:[10.5006/1.3280607](https://doi.org/10.5006/1.3280607)
307. Bellucci, F.; Nicodemo, L. Water Transport in Organic Coatings. *Corrosion* 1993, **49**, 235–247. doi:[10.5006/1.3316044](https://doi.org/10.5006/1.3316044)
308. Brasher, D. M.; Kingsbury, A. H. Electrical Measurements in the Study of Immersed Paint Coatings on Metal. I. Comparison between Capacitance and Gravimetric Methods of Estimating Water-Uptake. *J. Appl. Chem.* 2007, **4**, 62–72. doi:[10.1002/jctb.5010040202](https://doi.org/10.1002/jctb.5010040202)
309. Perez, C.; Collazo, A.; Izquierdo, M.; Merino, P.; Novoa, X. R. Characterisation of the Barrier Properties of Different Paint Systems. *Prog. Org. Coatings* 1999, **36**, 102–108. doi:[10.1016/S0300-9440\(99\)00030-2](https://doi.org/10.1016/S0300-9440(99)00030-2)